Jara María Moya Pérez

# Computational techniques to simulate food processing and safety. Application to domestic meat cooking

Director/es

Calvo  Calzada, María Begoña
Grasa Orus, Jorge

# Universidad Zaragoza
1542

Tesis Doctoral

# COMPUTATIONAL TECHNIQUES TO SIMULATE FOOD PROCESSING AND SAFETY. APPLICATION TO DOMESTIC MEAT COOKING

Autor

## Jara María Moya Pérez

Director/es

Calvo  Calzada, María Begoña
Grasa Orus, Jorge

**UNIVERSIDAD DE ZARAGOZA**
**Escuela de Doctorado**

Programa de Doctorado en Ingeniería Mecánica

## 2022

# Universidad Zaragoza

1542

# Computational techniques to simulate food processing and safety. Application to domestic meat cooking

Thesis by

Jara Mª Moya Pérez

Faculty advisors

Begoña Calvo Calzada

Jorge Grasa Orús

Doctoral Degree in Mechanical Engineering
June 2022

# AGRADECIMIENTOS

Esta tesis es el punto final de una de las etapas más importantes de mi vida. Quien bien me conoce sabe que estos tres años han sido una montaña rusa: he tenido momentos buenos, momentos malos o no tan buenos, momentos en los que tomar decisiones cruciales y momentos en los que dejarse llevar... pero, al fin y al cabo, siempre me han encantado las montañas rusas. Y más aún si en los asientos contiguos hay tanta gente que me apoya y me quiere. Estas líneas están dedicadas a esas personas que han estado a mi lado desde el comienzo, pero también a las que se han ido, y a las que han llegado para iluminar el camino.

En primer lugar, me gustaría agradecer a mis directores de tesis, Begoña Calvo y Jorge Grasa, que me dieron la oportunidad hace mucho tiempo de conocer el mundo de la investigación y han procurado siempre guiarme lo mejor posible en todas las decisiones que he ido tomando. Gracias, porque sé que este último año no ha sido el mejor, pero habéis sido pacientes conmigo cuando yo no lo era ni conmigo misma. Gracias también a Miguel Ángel Martínez, que, aunque no conste como director, siempre ha sido un equipo junto a ellos. A los tres, os debo mucho.

No puedo olvidarme también de Sergio Lorente y del equipo de BSH con el que hemos colaborado estos años. Han enriquecido este proyecto y, por tanto, también mi crecimiento profesional. A todos vosotros, muchas gracias.

Continuo con el grupo T07-24R de Alimentos de Origen Vegetal, dirigido por Marisa Salvador, y con el grupo A03-17R de Nuevas Tecnologías de Procesado de Alimentos, dirigido por Ignacio Álvarez, de la universidad de Zaragoza. Sin vuestra colaboración no hubiese sido posible la elaboración de esta tesis. Gracias por siempre mostraros tan atentos y cooperativos.

Siguiendo a nivel universidad, esta tesis también me ha brindado la oportunidad de conocer a gente que ya considero amigos: Belén, Nico, Alberto, Diego, Itziar, Iulen, Bea... Gracias por tantas risas en la sala de becarios durante los dos primeros años, gracias por los consejos y por la ayuda, y gracias por continuar a mi lado fuera de la universidad. Sois increíbles.

Fuera ya del mundo ingenieril, se encuentran mis tres mejores amigas: Estela, Nuria y Maicas. Han estado presentes en las etapas de mi desarrollo más importantes, mi

adolescencia, y ahora en ésta. Estela, cuando la vida viene como un alud, que sepas que tú también eres mi luz, hasta el infinito y más allá. Nuria, gracias por mimarme tanto, por ser chispa en mi vida y por estar siempre tan orgullosa de mí, me impulsas. Maicas, gracias por las locuras, por entenderme, por defenderme siempre y por estar ahí pase el tiempo que pase. Os quiero.

Continúo con más amigos que, aunque no desde hace tanto tiempo, han llegado a ser fundamentales en mi vida. Juan, entrenar contigo a las seis de la mañana es casi tan guay como saber que siempre puedo contar contigo. Carmen, no me faltes nunca, porque no podría vivir sin tantas fotos de atardeceres en el móvil, y porque sería una pena perder a una persona tan maravillosa como tú. María, mi hogar no es un lugar si no un puñado de personas, y tú estás en ese puñadito. Por nuestras charlas sanadoras y por sentirnos tan comprendidas la una con la otra, gracias. Paola, Silvia gracias a vosotras también, por todas esas tardes de salvar el mundo. A todos vosotros, que los años sigan pasando, y sigáis ahí.

Tampoco quiero olvidar a otras personas que estuvieron conmigo durante gran parte de mi doctorado y que me han dejado tantas lecciones. Ruíz, Blanca, Ibarzo, Nuric, durante la pandemia, el barrio ha sido el mejor sitio del mundo gracias a vosotros.

Ya casi acabando, gracias a mi familia: a mi madre, a mi padre, a Bea, a mi hermano Diego, a Sara y a mis abuelos. Sois la mejor familia que podría tener, y no sólo lo digo yo, lo dice mucha gente. Soy quién soy gracias a vosotros y siempre os he dicho que todos mis éxitos son vuestros, así que, aquí tenéis otro más. Mamá, papá, Bea: sois la mezcla perfecta de la cual he podido aprender sobre todos los aspectos de la vida. Sois mis máximos referentes, y por supuesto, siempre hogar. Gracias por todo el esfuerzo en construirme y por quererme tan bien, os quiero mucho.

Y ya por fin, termino los agradecimientos con quién quiero que empiece la siguiente etapa de mi vida. Leyre, nada que añadir, nada que quitar. Llegaste para tantas cosas... entre ellas, para darme el empujón que necesitaba con esto. Iluminaste todo cuando apareciste, y desde entonces tengo claro qué es lo que quiero. Me has ayudado a alumbrar mis sombras, me has enseñado a relativizar, me has tranquilizado tantas veces, me has hecho disfrutar de los pequeños placeres del día a día. A ti, mi compañera de todo, el "gracias", se queda corto.

Esta tesis tiene un trocito de todos, la carne se hubiera cocinado algo peor sin vosotros.

Zaragoza a 20 de Febrero de 2022.

# ABSTRACT

The work presented in this Thesis focuses on the simulation of food processing techniques to transform raw or fresh foods into other safe forms suitable for consumption by humans. The first part of this Thesis focuses on the simulation of food treatments by ohmic heating, specifically by means of high intensity pulsed electric fields (PEF), with the aim of optimizing these processes and achieving the bacterial inactivation of the microorganisms existing in the food. The second part deals with the development of a numerical methodology that allows the simulation of food cooking processes based on heat treatments in order to predict its behavior when cooked in a domestic environment.

Regarding the simulation of PEF systems for the heat treatment of solid food, an axisymmetric finite element model has been experimentally validated. This model reproduces the PEF treatment in a cylindrical chamber which contain agar. With this model it has been possible to know the evolution of the temperature in the sample, as well as the inactivation level of Salmonella Typhimitium 878. Once this tool had been validated, the option of thermostating the electrodes of the simulated chamber was explored, with the aim of achieving greater homogeneity in the temperature reached and therefore also in the inactivation. A sensitivity analysis of the main operating parameters of the chamber has been carried out to determine the optimal combination that results in a better homogenization of the inactivation of bacteria as well as shorter treatment times.

Related to the cooking processes in a domestic environment, this work was focused on the cooking of beef meat, specifically of pieces extracted from the *longissimus dorsi* muscles from the heifers, on an induction hob with a pan. A 3D finite element model has been developed to reproduce this cooking procedure and it has been experimentally validated, The model is capable of predicting the heating of the meat and its weight loss evolution along the cooking process. The model includes the physics of heat transfer as well as the processes of water dripping and its evaporation. Furthermore, the model considers the turning over process of the meat too for different thicknesses of the meat and for different cooking degrees. Subsequently, the kinetics of color has been implemented into the model, to know the evolution of the color of the meat as a function of the temperature that it acquires during the process of cooking. By means of this implementation, it has been possible to obtain the color profiles along the thickness of the pieces of meat, in order to obtain the optimum turn over time that would give an equal degree of cooking on both sides of the meat.

# RESUMEN

El trabajo presentado en esta Tesis se centra en la simulación de técnicas de procesamiento de alimentos para transformarlos de productos crudos o frescos, en productos seguros y adecuados para el consumo humano. La primera parte de esta Tesis se centra en la simulación de tratamientos por calentamiento óhmico en alimentos sólidos, concretamente mediante pulsos eléctricos de alta intensidad (PEF), con el objetivo de optimizar estos procesos y lograr la inactivación de los microorganismos existentes en estos alimentos. La segunda parte trata el desarrollo de una metodología numérica que permite la simulación de procesos de cocinado de alimentos mediante tratamientos térmicos, concretamente el cocinado de carne de ternera a la plancha, con el fin de predecir su comportamiento al cocinarse en un entorno doméstico.

En cuanto a la simulación de sistemas PEF para el tratamiento de alimentos sólidos, se ha validado experimentalmente un modelo axisimétrico de elementos finitos que simula este tratamiento en una cámara cilíndrica de pulsos PEF que contiene agar. Con este modelo ha sido posible conocer la evolución de la temperatura en la muestra, así como la inactivación de la Salmonella Typhimitium 878. Una vez validada esta herramienta, se ha explorado la opción de termostatar los electrodos de la cámara simulada, con el objetivo de conseguir una mayor homogeneidad en la temperatura alcanzada y por tanto también en la inactivación. Se ha llevado a cabo un análisis de sensibilidad de los principales parámetros de funcionamiento de la cámara para conocer la combinación óptima que de lugar a una mejor homegenización de la inactivacion de bacterias así como tiempos más cortos de tratamiento.

En el caso de la simulación de carne de ternera a la plancha, se ha desarrollado un modelo 3D de elementos finitos que ha sido validado experimentalmente, capaz de reproducir el calentamiento de la carne y su pérdida de peso debido a este calentamiento, incluyendo el momento de darle la vuelta a los trozos de carne. El modelo incluye la física de transferencia de calor así como los procesos de goteo de agua y su evaporación, y el momento de darle la vuelta a la carne. Se ha comprobado que el modelo es valido para distintos espesores de carne y para distintos grados de cocinado. Posteriormente, a este modelo se le ha implementado la cinética del color, para conocer la evolución del color de la carne en función de la temperatura que esta adquiere durante el proceso. Mediante esta implementación se han podido obtener los

perfiles de color a lo largo del espesor de los trozos de carne para así poder obtener el tiempo de vuelta de la carne óptimo que daría un grado de cocinado igual por ambos lados de la carne.

**Palabras clave** Cocinado, modelo cocinado de comida, carne de ternera, retracción, puntos de cocinado, elementos finitos, calentamiento óhmico, PEF, comida sólida, cinética del color, inactivación microbiana.

# Contents

# List of Figures

# List of Tables

# Chapter 1

# Introduction

This thesis is framed in the context of the ARQUE project (Nuevas Tecnologías de Calentamiento y Control Aplicado a Electrodomésticos, RTC-2017-5965-6), a collaboration between the BSH Home Appliances Group and the University of Zaragoza, specifically with AMB group. BSH has in Zaragoza the most important research, development and manufacturing center worldwide for induction hobs. In fact, thanks to the collaborative work carried out since the 1980s between BSH Spain and the University of Zaragoza, it has become the technological benchmark related to this product, which reflects the figure of 500 patent applications in the field of induction hobs. BSH proposes several lines of research with which induction cookers (including containers and accessories) approach to a more autonomous behavior, more efficient and offering a better user experience. The line of research of this project in which this Thesis is focused is the automatic cooking. It includes both, the monitoring and simulation of the food transformation process and the guidance of the cooking process using sensors and external and internal parameters of the worktop itself. Subsequently, these data are processed to be used by the smart kitchen to reproduce the results during real cooking.

In this context of industrial digitalization and the advent of the Internet of Things (IoT) the concept of the Digital Twin (DT) has recently emerged as a virtual replica of the real process operation, which is connected to the real world by sensor data and advanced big data analytical tools (Defraeye et al., 2021). For food applications, a digital twin requires: i) sensor networks that measure essential variables and properties of the product and the process; ii) a platform to connect the sensors, actuators with cloud-based data storage and high performance computing, big data analytics, and applications to be used by relevant users within and across enterprises, which is conveniently provided by the Internet of Things (IoT); iii) a

DT simulation platform with computer models that use the data from the platform as inputs to perform computations for testing, design, optimization and control and providing output for improved data analysis, process performance and product quality, and therefore provide decision support. Is in this last part where the research is focused: the computational models which simulate and obtain the cooking processes and their relevant information. The modeling of food cooking processes has experienced a great evolution since the development of multiscale, multiphase and multi-physics approaches (Datta, 2016). Several comprehensive numerical tools and software platforms for improving insights, optimizing designs and cooking processes have emerged in recent years (Datta, 2007a, Dhall and Datta, 2011, Rabeler and Feyissa, 2018b, Datta, 2016). The computer model has been formulated as the computer analog of a physical reality, describing the real phenomena in terms of their mathematical description. Models have improved the understanding of the physical phenomena such fluid flow, heat and mass transfer and mechanical deformation that occur during food processing, and have been used for designing new or optimizing existing food processes. Depending on the complexity, different modeling approaches are used that can range from being completely observation-based to completely physics-based. The success of food process modeling comes with the development of efficient numerical techniques to solve coupled systems of spatio-temporal differential equations. Particularly the finite element and finite volume techniques have led to the emerging software for implementing and solving the model equations in a computer aided design (CAD) framework (Erdogdu et al., 2017).

The DT can integrate the computer simulation techniques to reproduce accurately and realistically all relevant processes. In addition, the DT also should be connected to the real-world product and processes by sensor data and analytical tools. In this manner, the model should run and update allowing results to be implemented by operational devices and/or personnel smoothly. As a result, the DT can elucidate important aspects of the ongoing process and product under development, just-in-time during real operation. The DT should also predict future product quality and safety, and improve product and process designs and control (Fig. 1.1).

In this context and for this reason, this Thesis pursues the aim of formulating a numerical methodology that allows addressing the main physical phenomena that occur in food products as a result of heat treatments during domestic and industrial cooking. Specifically, this work tries to define a methodology that provides information of the behavior of the meat during pan cooking by an induction hob.

In addition, in the same way that the design of computational models can be used
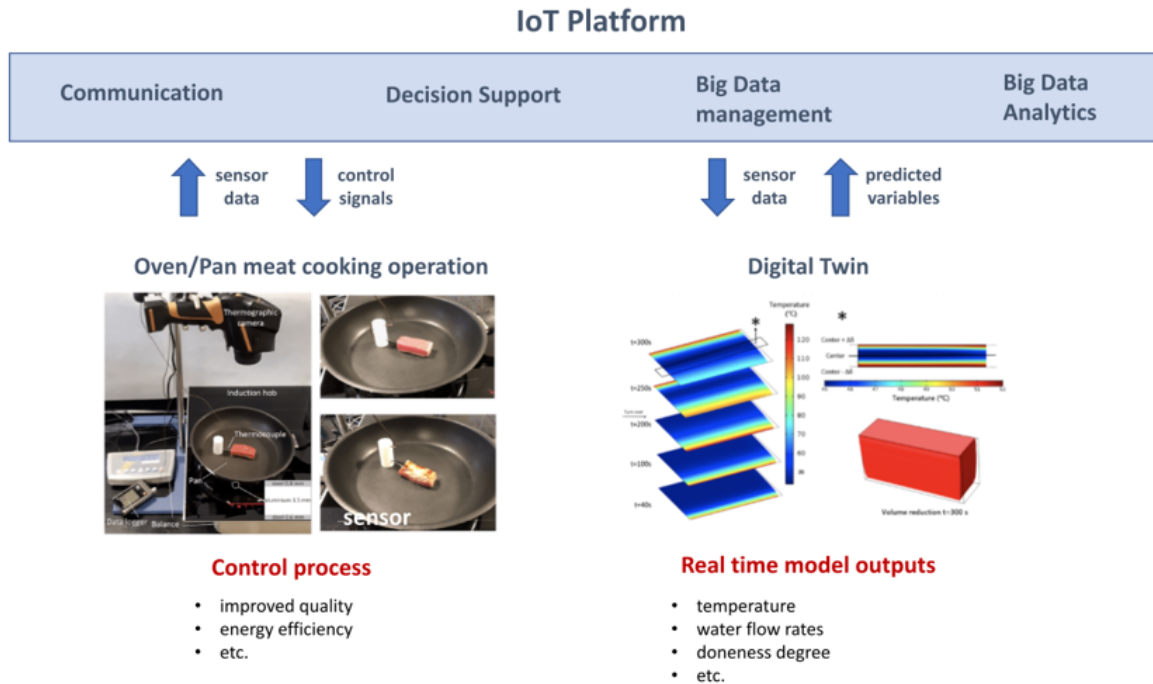
Figura 1.1: The use of the Internet of Things (IoT), specifically Digital Twins (DT), to help users during meat cooking.

to know how the food behaves during different cooking processes, these simulations can be used to study other heating techniques, fundamentally applicable to food industrial treatments, such as Pulsed Electric Field (PEF). This thesis includes an initial chapter in which the finite element methodology is used for the industrial application of PEF in food. The aim of this application is to obtain good quality food, without microorganisms harmful to humans, in a first thermal treatment prior to selling the product and then cooking it in different ways. This shows that FE methodology could be used for both areas, one of thermal treatments of industrial nature, and the cooking processes themselves.

To fully understand the implications of this Thesis, a general vision of the biological and physics aspects involved is required, as well as a description of past and current works developed on these areas, commonly known as the state of art. This Chapter includes this information, together with a brief description of the techniques and numerical methods used throughout the fulfillment of this Thesis.

## 1.1. Nature of meat and internal structure

Based on its final degree of cooking and the processes that have place inside itself, food can be classified into three groups: wet food with a gummy texture, foods

with lower water content and brittle texture and finally an intermediate typology between each of them (Dhall and Datta, 2011). In this regard, meat is composed of approximately 70 % -75 % of water by weight. Thus, it belongs to the first group, but it can lose up to half of this content during cooking. The volumetric variation during the cooking of the meat is due mainly to the loss of water. The rest of the components of the meat depend on the type and around the values shown in Fig. 1.2.

Regarding proteins of the meat, these can be classified into three large groups. Myobrilar proteins are those which make up the muscle tissue and therefore the main structure of the meat. Of these, the most relevant are the actin and myosin. Stromal proteins are those which make up the connective tissue between the different fibers and the main one is the collagen. Finally, sarcoplasmic proteins, which are present in the blood, such as myoglobin, are responsible for the reddish color of the meat, but they are nevertheless not relevant from the structural point of view. Focusing on the first two, the configuration of the protein structure of the muscles that make up the meat can be understood. Myofibrillar proteins make up the internal structure of the muscle, and are what provide the consistency and texture of the product. Within this structure is retained the intracellular serum associated with proteins and composed mainly of water, and to a lesser extent, by salts and non-protein substances soluble in water. The stromal proteins form an epithelium which groups some fibers with others. Extracellular serum is distributed in the pores between these structures, also called capillary (Gerhard, 2011). In Fig. 1.3 the structure of the muscle is shown with a cross section enlarging the area taken by the water content.
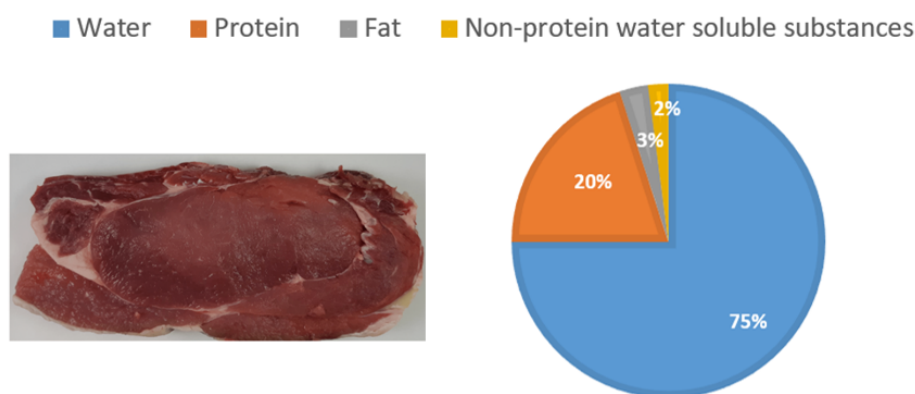


Figura 1.2: Percentages by weight of the components of the beef meat.
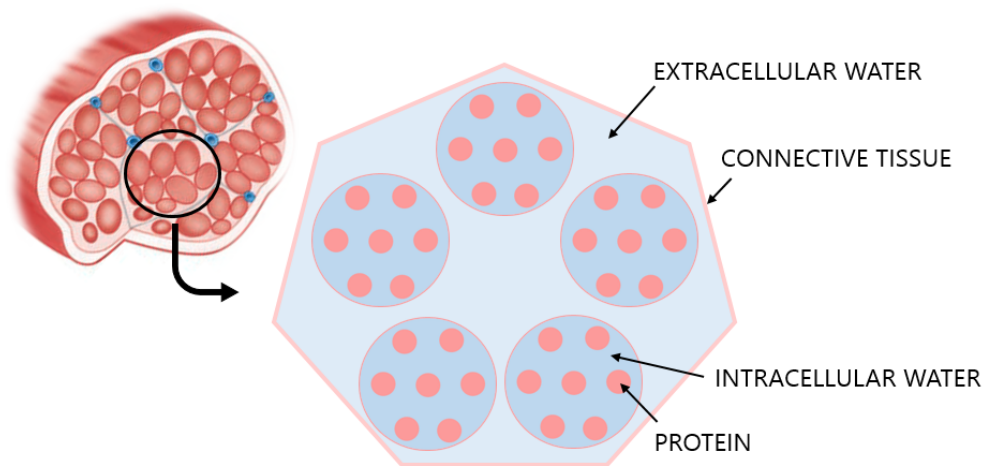
Figura 1.3: Distribution of extracellular an intracellular water (enlarged) along the cross section of the muscle.

The protein structure of the muscle is three-dimensional. When it is under a heating process, the protein is said to suffer a process of denaturation, in which the structure takes on a two-dimensional shape (secondary structure). These changes in the shape of the protein also affect the taste, the texture and more visually, the shrinkage of the meat. Depending on the origin of the meat, it contains some types of protein or others and in different proportions. Each protein begins to denature at a different temperature, which plays a crucial role in the cooking result (Tornberg, 2005).

This Thesis is particularized above all on the cooking of *longissimus dorsi* from beef meat. In this kind of meat, the denaturing process begins at about 35 °C with the transverse retraction of the fibers that make up the protein structure, but intensifies in the range of 40–60 °C, when the area of the fiber's section decreases and intracellular serum is released. At 60–70 °C the connective tissue shrinks longitudinally, and the extacellular serum is expelled into the environment. At temperatures above 90 °C, the remaining water content in the meat remains in it, since this percentage of moisture, around half of the initial content, is associated with proteins (Barbera and Tassone, 2006). Fig. 1.4 shows the thermal scale where this denaturation takes place, comparing different cooking degrees of beef meat.

The meat also undergoes a color change due to the protein denaturation process according to the increase of temperature (Fig. 1.4). Above a certain temperature value, hemoglobin and myoglobin are denatured, leading to color changes. In addition, through the impact of heat appear the sulphur-containing amino acids cysteine and methionine, which leads to an increase in palatability (Gerhard, 2011).
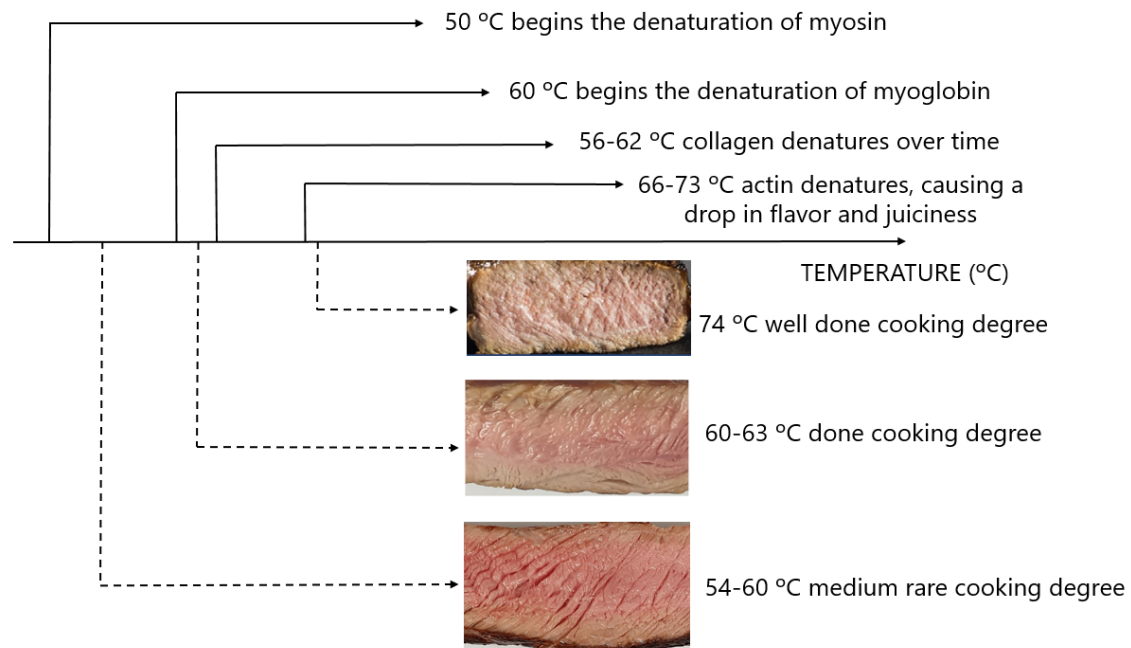
Figura 1.4: Thermal scale where denaturation temperatures of the proteins are compared with different cooking degrees of *longissimus dorsi* from beef meat.

## 1.2. Physics of meat pan cooking

This work focuses on beef pan cooking on an induction hob. In this cooking process, heat is transmitted from the surface of the pan to the inside of the meat by direct contact. This heating causes changes in meat properties.

As mentioned in the previous section, when the meat increases its temperature, protein denaturation occurs, changing its structure and properties. This denaturation consists mainly in the loss of the helical structure of proteins and changes in the hydrophobicity of its surface, provoking the release of retained water. It also takes place the contraction of the fibers of collagen which make up the connective tissue of the muscle and a longitudinal of the fibers (Tornberg, 2005).

The water with free movement within the meat once the protein denaturation has occurred, tends to move according to the pressure gradient created when the connective tissue retracts, being expelled towards the surface of the piece of meat. At 100 °C, the water of the surface goes to the vapor state, mixing with the ambient air. Since the heating of the meat occurs more quickly on its surface, the water hold capacity can decrease faster than the loss of moisture by evaporation on the surface; in this case, a part of the water would be lost by dripping in liquid state (Dhall and Datta, 2011).

Other relevant changes that occur during cooking in addition to the shrinkage of

the muscle, are the variations in texture and color, also caused by the temperature rise. These are the main indicators used by the users to easily assess the quality of cooked food, since it is not able to quantify at first sight parameters such as the temperature of the piece of meat. The color variation is related to the phenomenon of protein denaturation: hemoglobin and myoglobin are denature when reaching certain temperature values, changing its color (they become lighter) (Rabeler and Feyissa, 2018b). Furthermore, at high temperature Maillard reactions take place, which cause the characteristic brown color of the cooked meat. In Fig. 1.5 it can be perceived different shades of color in the meat depending on the degree of cooking.



Figura 1.5: Evolution of the color of the meat according to the degree of cooking.

Taking into account all these effects, we can summarized that the increase of temperature lead to the denaturation of the proteins with the consequent release of water, movement and its loss, provoking changes in the structure and color. Therefore, the physics involved in this process would be the heat transfer, the mass transfer, solid mechanics and color kinetics. Due to that, we can affirm that the meat pan cooking is a multiphysical and multiphase problem which is governed by different equations and their coupling. The frameworks that can be used to model multiphysical and multiphase processes were summarized by Datta (2016) and are shown in Fig. 1.6 . Framework one corresponds to the most common set of transport equations, with a continuum medium of a single phase. Framework two and three correspond to a multiphase problem in a porous medium but rigid. The difference between framework 2 and 3 is the magnitude of the pores, since framework 2 is for larger pores. This Thesis focuses on framework 4, using multiphase, deformable porous media continuum equations. This equations are the Darcy equation for the transport of species, the energy equation and the solid mechanics equations for small or large deformations providing solid velocity. In Fig. 1.7 an scheme where food is treated as a deformable porous medium is shown, and the transport of various components and phases due to their respective driving forces appear. Individual phases of water, vapor and air, and energy are tracked using their conservation equations (Dhall and Datta, 2011). The fluxes of the different species are written using Darcy's law in terms of swelling pressure, gas pressure or capillary

pressure, depending on the phase of the water. All these fluxes are combined with a velocity of the solid skeleton that comes from deformation obtained from solid mechanical analysis. There are very few empirical factors in this framework and a significant aspect of the formulations is that it is readily implementable in standard commercial software. With the developed models by this software, quality and safety models can be obtained by relating quality parameters such as color or texture with the temperature or the moisture or the volume change obtained in the first ones.

This study has focused specifically on the color of the meat as a measure of quality of the cooked meat. Users usually associate the final color that the meat acquires with its quality. In this case, the measured coordinates which determines the color of the meat, are defined using the scale cieLab, which consists of three parameters: $L^*$, which indicates the luminance of the color (the value 0 corresponds to white and 100 to black), $a^*$, which gives information on a scale from green (negative values) to red (positive values) and $b^*$ from blue to yellow (a negative value indicates blue and positive color, yellow). For the specific case of beef, only the values $L^*$ and $a^*$ are relevant, since during cooking meat changes its reddish hue and the clarity of its color.
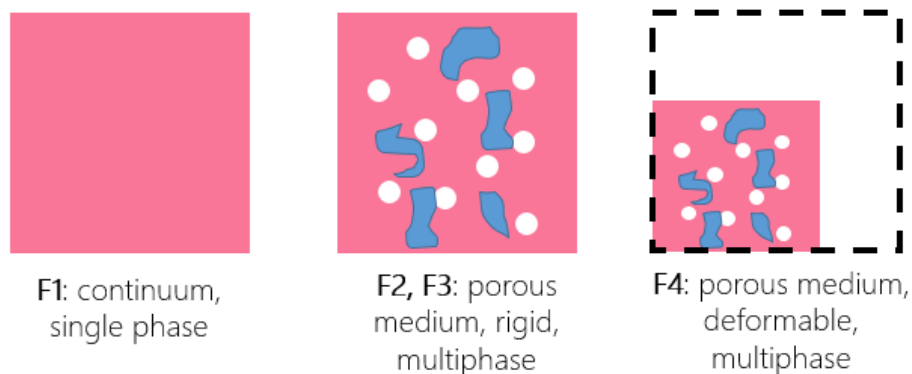


Figura 1.6: Schemes of the different frameworks and its suitable formulations for the food cooking problem.
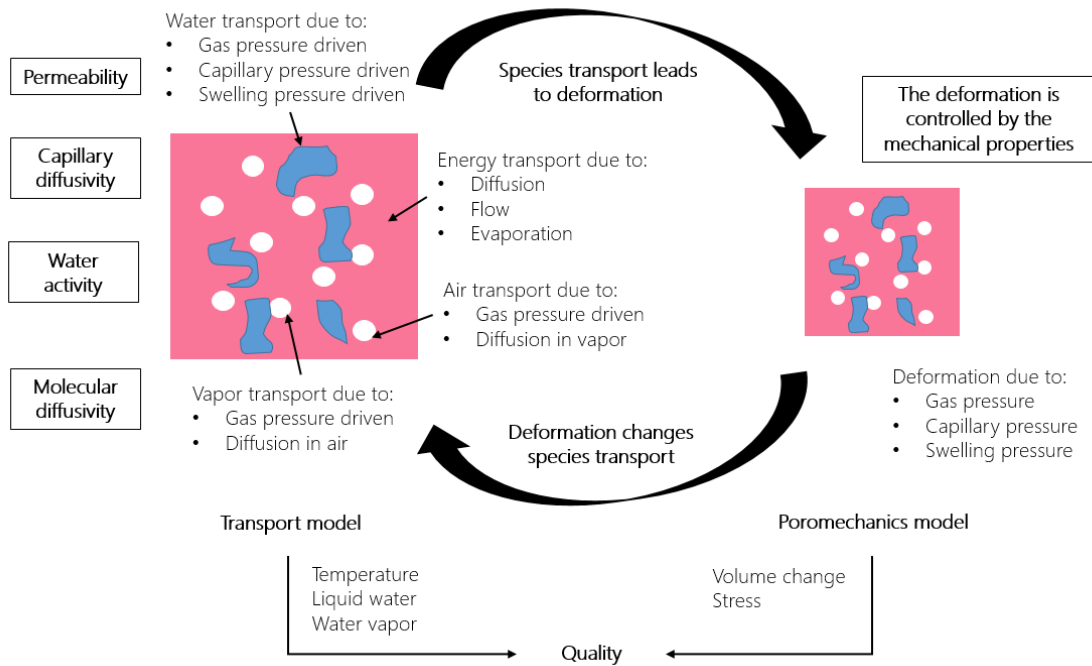
Figura 1.7: Schematic showing food as a deformable porous medium with the transport of various components and phases due to their respective driving forces.

The main hypotheses used in this work are:

- Meat is considered as a continuum biphasic (liquid-solid) porous material.

- The moisture flow due to the pressure gradient caused by the shrinking connective tissue follows Darcy's law.

- No internal heat generation and no evaporation occur inside of the piece of meat, so that the water inside the meat only appears in liquid state.

- The initial temperature and water concentration distribution are uniform.

- Both the solid matrix and the liquid water at each point have the same temperature.

- Meat is considered as a hyper-elastic material in which the total volume change is equal to the volume of moisture loss and consequently the solid matrix remains saturated.

- An isotropic Neo-Hookean formulation is used to represent the meat constitutive behavior.

The full development of the physics involved will be carried out in the next chapters.

## 1.3. PEF-ohmic system for microbial inactivation

In the last years, there is a growing demand for novel thermal processing technologies in the Food Industry, such as ohmic heating, dielectric heating and inductive heating. Some advantajes about the first one, ohmic heating, is that larger food can be treated, because of a higher penetration capacity, provoking in this way a more uniform heating (Ramaswamy et al., 2014). The fundamental principle of ohmic heating is that when electrical current flows through a conductor, molecules or atoms of the material suffer an agitation due to the motion of charges whithin the product, which results in an increase of temperature. In metallic conductors, the moving charges are electrons, but in food, the charges are usually ions or other charged molecules such as proteins. Theses charges move to the electrode of opposite polarity (Ramaswamy et al., 2014). Ohmic heating has multiple advantages:

- It offers greater heating uniformity than with other techniques. With conventional heating techniques heat is transferred from an external medium through heat exchange walls (Ramaswamy et al., 2014). In this way, with the application of these methods can appear cold spots in some locations of the product.

- Ohmic heating involves internal energy generation, and may achieve temperatures much higher than other methods. Therefore, it may be used to heat a product faster.

- The rate of heat generation may be altered by altering electric field strength (Ramaswamy et al., 2014). Field strength can be modified by altering voltage or frequency, parameters which can be motorize in order to make intelligent process decisions.

- The cost of ohmic heater has decreased in recent years.

- It offers a great energy efficiency since nearly all the generated energy in the food is used.

- There are a wide variety of ohmic heaters and their design is a very broad field of study.

- Bacterial spores in food show increased inactivation during ohmic heating in comparison to purely thermal treatments at the same temperature (Somavat et al., 2012, Pereira et al., 2007).

Within the ohmic heating techniques, Pulse Electric Fields (PEF) is a technology

which consists of applying to a product high intensity electric fields (0.5-50 kV/cm) in a intermittently way for periods of time of the order of microseconds. The product is placed between two electrodes and the heating occurs from the inside to the outside of the food. PEF is an energy-efficient system because it allows to reach high temperatures in the product in a short period of time, as it has been mentioned above. In addition, the high intensity electric fields induce the formation of pores in the cell membranes of the product (electroporation) affecting microorganisms that can be present in the product. As a result of this phenomenon, material from the inside of the cell is expelled to the outside environment leading to cell death (Figure 1.8).
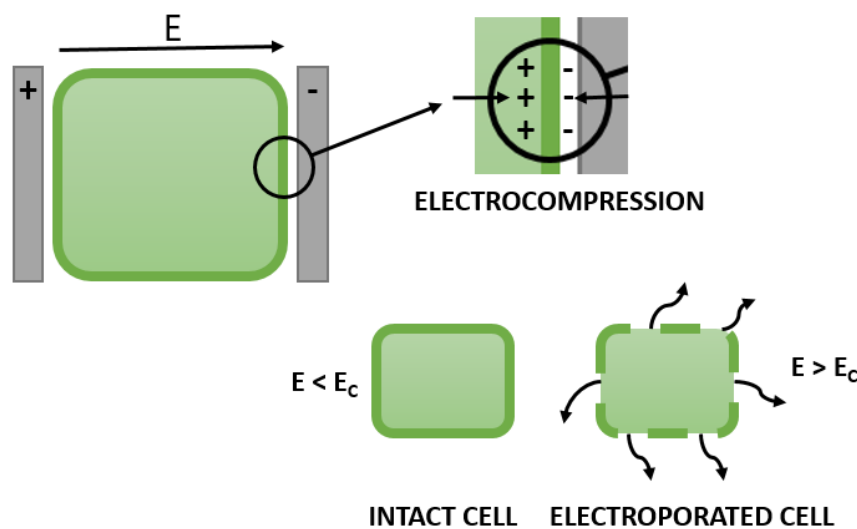


Figura 1.8: Electric field effect on a cell, where $E_c$ is the limit electric field and E is the current electric field.

Thus, PEFs are used in different fields of study since it allows the destruction of microorganisms. With its use in Food Industry, safe and stable food during storage can be obtain, but also in Pharmaceuticals or Medicine it can be use for inactivation of tumour cells for the treatment of cancer, or electroporation of eukaryotic cells can be used for obtaining compounds from the interior of the cell with high nutritional and biological value such as polyphenols, natural colourings, etc (Raso and Heinz, 2006).

In the Food Industry field, PEFs are not only being considered as a strategy to destroy microorganisms present in food, but also to modify textures (Kaur and Singh, 2016). This method offers a higher quality of the treated product than conventional thermal pasteurization methods, since it does not affect the properties of the food to a large degree.

The fact that PEF does not greatly modify the properties of the food is due to the required effects in the product are achieved without greatly increasing the temperature

of it, since only a small amount of energy is transmitted. The generation of heat in this type of system is based on the Joule Effect described by the Equation 1.1:

$$W = \int_0^\infty \chi(T) \cdot \Xi^2 dt \qquad (1.1)$$

where $\chi$ is the electric conductivity of the treated medium or product in S/m, $\Xi$ is the electric field applied strength in V/m and dt is the time diferential during which the electric field is applied in s (Sastry and Li, 1996).

In this manner, with the application of a potential difference between the electrodes separated by a certain distance where is placed the product, the heating of it would be reached. Looking at this equation, the electric field strength has a great importance in the transferred energy to the treated product, as slight modifications square this transmission. This electric field would depend on the voltage applied but also on the frequency of the pulses.

However, a limitation of this technology is that since heating occurs from the inside to the outside, this heating is not strictly isotropic (Ariza-Gracia et al., 2020, Icier and Ilicali, 2005, Marra, 2014, Shim et al., 2010). Cold points in the corners between the electrodes and the product could appear, while the hottest points would be located at the centre of the food. To achieve a high temperature even at the surface of the sample, the temperature on its center should therefore be increased, thus unwanted alterations in the properties of the product in these zones could take place. This represents a limitation of the technology, since , in principle, in the central points of the product is guaranteed the safety of food while the cold points do not receive the required minimum treatment to achieve the desired microbial inactivation, compromising the safety of the entire product. On the other hand, if cold areas are treated until reaching the required temperature, central area would be over-treated.

## 1.4.   Motivation

The main motivation of this Thesis lies in the necessity of widen the knowledge about the behaviour of food when it is subjected to heating, both domestically and industrially, using numerical models.

In the field of domestic cooking, this Thesis focuses on numerical modeling of beef meat pan cooking on an induction hob, as part of the ARQUE project in collaboration with BSH. If the behavior of meat when cooking is known, it is possible to create guided

cooking systems based on product response to heating, being this the main objective of this project.

The great advance of technology in recent years has allowed it to be included in many aspects of everyday life. An example would be mobile phones. Because of this, companies seek to develop systems which connect these devices with everything that surrounds us, including in the domestic environment. Society is moving towards future connected smart homes, in which, for example, all the appliances could be managed from the smartphones. In addition to the connectivity with appliances, lot of work is also being done to develop semi-autonomous guided cooking systems, which allow the consumer make correct decisions based on the degree of cooking they want and what they want to cook.

Due to these applications, the development of numerical models for simulating food cooking represents a great advantage. Computational analysis of cooking processes saves time and money when collecting the necessary data to characterize the cooking of food against experimental tests. Cooking meat is one of the simplest processes to start with, since is relatively easy to add variability such as the type of meat, its size and the way it is cooked.

The data obtained by numerical simulation can be implemented in smart kitchens. These results can be used to predict the behavior of food when it is cooked in a certain way and based on some initial parameters. In this way, the user could be guided throughout the cooking depending on the degree of cooking that is desired. With the help of sensors, such as balances or temperature ones, a feedback system could be created that would allow access to every variable involved in cooking at any point in the piece and at any moment in time. With the help of these sensors and the information from the models, the kitchen might also be able to recalculate the power supplied based on how the cooking was taking place up to that moment, to guarantee the highest quality.

To take into account this quality, it is necessary to introduce in the models indicators such as color and shrinkage. Shrinkage is the change of dimensions of the product during the process of heating. The consumer may conclude that a certain shrinkage of the meat may be a low quality indicator, as a result of excessive water content or the effect of hormonal treatments in the animal. The user can get an idea of the degree of cooking that the meat is acquiring based on how much the piece has shrunk.

The content of water in the meat and the shrinkage are related. Both have to do with the process of denaturation suffered by proteins when they are heated (Fig. 1.4).

From a culinary perspective, the proteins actin and myosin have the greatest interest. When actin is denatured, the meat looks drier. That is why most people prefer those cooking degrees in which the myosin has already been denatured but not yet the actin, that is, the less done cooked degrees.

Other qualities that indicate the quality of meat cooking are its texture and its color. Texture is not appreciated by the user until the moment of consumption, but the color that it acquires during cooking it is. Through color the consumer judges whether the degree of cooking of the meat is acceptable for consumption. There is also differences in the preferences of each person: studies such as the one by López Osornio et al. (2008) shows the differences between individuals from different countries and age range. The *American Meat Science Association* has a *Beef Steak Color Guide* where it classified the color from a very rare degree of doneness (very rare) to a well-well done degree, as we can see in Fig. 1.9.
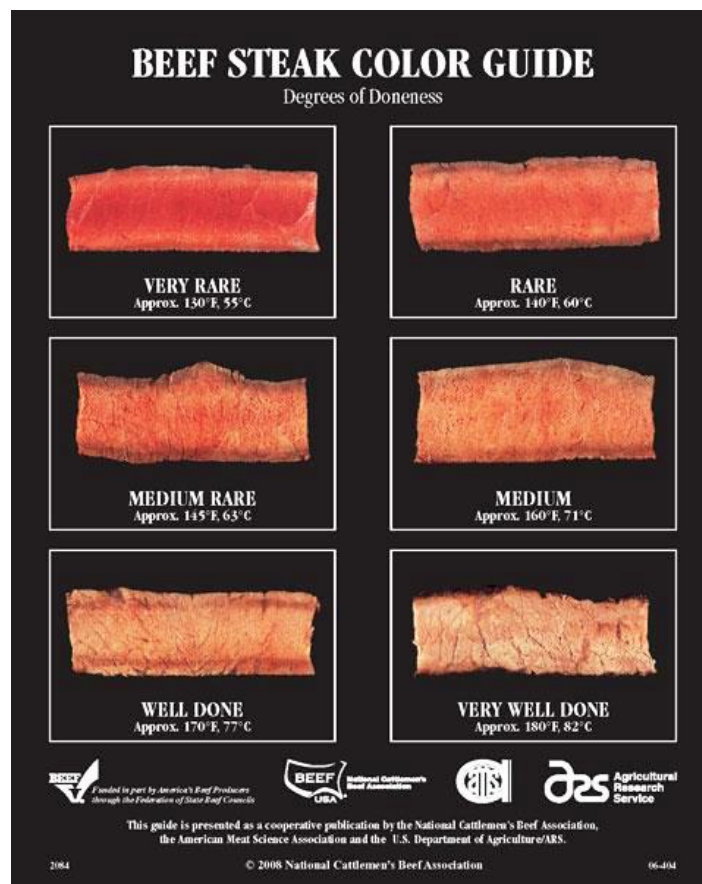


Figura 1.9: Beef color for different degrees of cooking according to the Beef Steak Color Guide described by the American Meat Science Association, AMSA (1995).

Regarding industrial treatment of food and as mentioned in section 1.3, PEF is a high interest technology in the field of preservation and processing of food at industrial level and it could be an excellent alternative to conventional heating treatments.

However, as has been observed in other studies such as that of Ariza-Gracia et al. (2020), the heating produced with this methodology to a thechnical Agar sample in a parallel electrode chamber caused a temperature gradient between the coldest and the hottest point (around 10 °C), causing a non-uniformity degree of microbial inactivation. As this fact is not desirable, it would be interesting to explore different ways to avoid it, either by analyzing the parameters involved as well as with new camera designs. In this study, the one used for experimental and numerical analysis is a parallel electrode chamber composed of two stainless steel cylinders of 20 mm in diameter with a gap between them of 20 mm where the sample of technical agar was placed, based on the design of Saldaña et al. (2010). The representation and a picture of this chamber are shown in Fig. 1.10. With this design, hot oil is recycled inside the electrodes which are empty inside, allowing in this way to thermostat the electrodes achieving a preheating of them, which favors higher temperatures at the points of the Agar surface in contact with them, reducing the temperature difference.
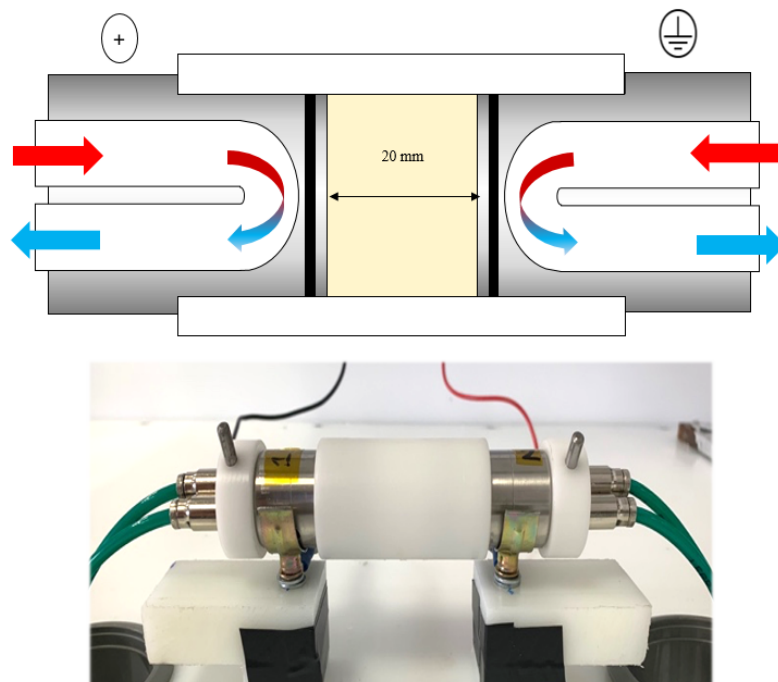


Figura 1.10: Parallel electrode PEF chamber.

## 1.5.   Objectives

Based on the motivation previously explained, the main objective of this Thesis is to design a numerical methodology that allows addressing the main physical phenomena that occur in food as a result of heat treatments both during domestic and industrial

cooking.

Regarding industrial processing, the goal would be to analyze the development of new PEFs techniques, which, as an industrial application, optimise the process parameters such as electric field, frequency or thermostating parameters, in order to achieve adequate levels of solid food safety.

As to domestic meat cooking, a coupled multiphysics problem of heat transfer, transfer mass and solid mechanics must be solved. Regarding the PEF process, a coupled multiphysics problem of heat transfer and electric field has to be solved. The commercial software *COMSOL Multiphysics 5.2a* has been used to simulate both processes.

To reach the main goals above exposed, the following partial objectives have also been achieved throughout the development of this Thesis.

- To expand the physical understanding of the main physical phenomena that appear in food when a heat source is applied and study of the different mathematical models proposed in the literature, both for meat cooking and for PEF systems.

- Implementation in the software *COMSOL* of the different equations, such as heat transfer, mass transfer, deformable solid mechanics, the heat source and the contact heating interface, either due to the heating of meat, or through the application of high frequency pulses.

- Development of numerical models which can help the user to establish the desired cooking degrees through the color and weight loss of the food.

- Development of numerical models which can help to explore new ways to improve PEF methodology to achieve the death of microorganisms in solid food without altering the properties of the product.

- Analysis of the numerical results obtained and their validation by comparison with experimental results. In case of meat pan cooking, by comparing the temperature in the central point of the meat and its weight loss, and in case of PEF, by comparing the temperature at different points in the Agar sample.

- To obtain solutions oriented to semi-guided or semi-directed cooking that, based on a greater knowledge of the transformation of food, on information obtained from the system itself, as well as from external information sources (sensors, systems with artificial intelligence), allow to ensure the properties of the cooked

food and to improve efficiency and safety. For example some criteria have been obtained about the moment of turning over the meat based on its water loss or based on achieving a symmetrical color profile throughout the thickness of the meat.

- To increase the user experience during cooking, through the interactivity between the appliance and the user (connectivity, artificial intelligence).

- To optimize the parameters of the PEF treatment to improve the homogenization of microbial inactivation, specifically bacteria Salmonella Typhimitium 878, and reduce experimental workload.

The summary of the objectives regarding meat pan cooking can be seen in Fig 1.11 and for the PEF application in Fig. 1.12.

To carry out the experimental part of this Thesis, we have collaborated very closely with two group of the University of Zaragoza, the group T07-24R of Plant-based Food, led by Marisa Salvador in case of meat cooking, and with the group A03-17R of New Food Processing Technologies led by Ignacio Álvarez in case of PEF treatments of solid food.

## 1.6.   State of the art in the simulation of the cooking of the meat

The physical processes which occur in the structure of the meat when it is subjected to any kind of cooking, are based on the transport of energy and moisture in a deformable medium (Datta, 2007b). The development of mathematical and numerical models of these cooking processes allows obtaining information on how the food behaves during heating, which would allow optimizing these processes in order to achieve some guidelines for a guided cooking, according to the desired quality of food.

Most of the current food cooking models refers to curves based on empirical data (Ikediala et al., 1996, Fowler and Bejan, 1991), or in improved versions assuming purely conductive heat transfer for energy and purely diffusive transport for moisture, solving only one equation for conduction and another one for diffusion during the transient, making use of conductivity parameters and experimental effective diffusivity (Goñi and Salvadori, 2011, Kondjoyan, 2006). Only some physical models began to consider the pressure exerted by the retraction of the protein network (Datta, 2007a, Feyissa et al., 2013, van der Sman, 2013), and although these models take into account the
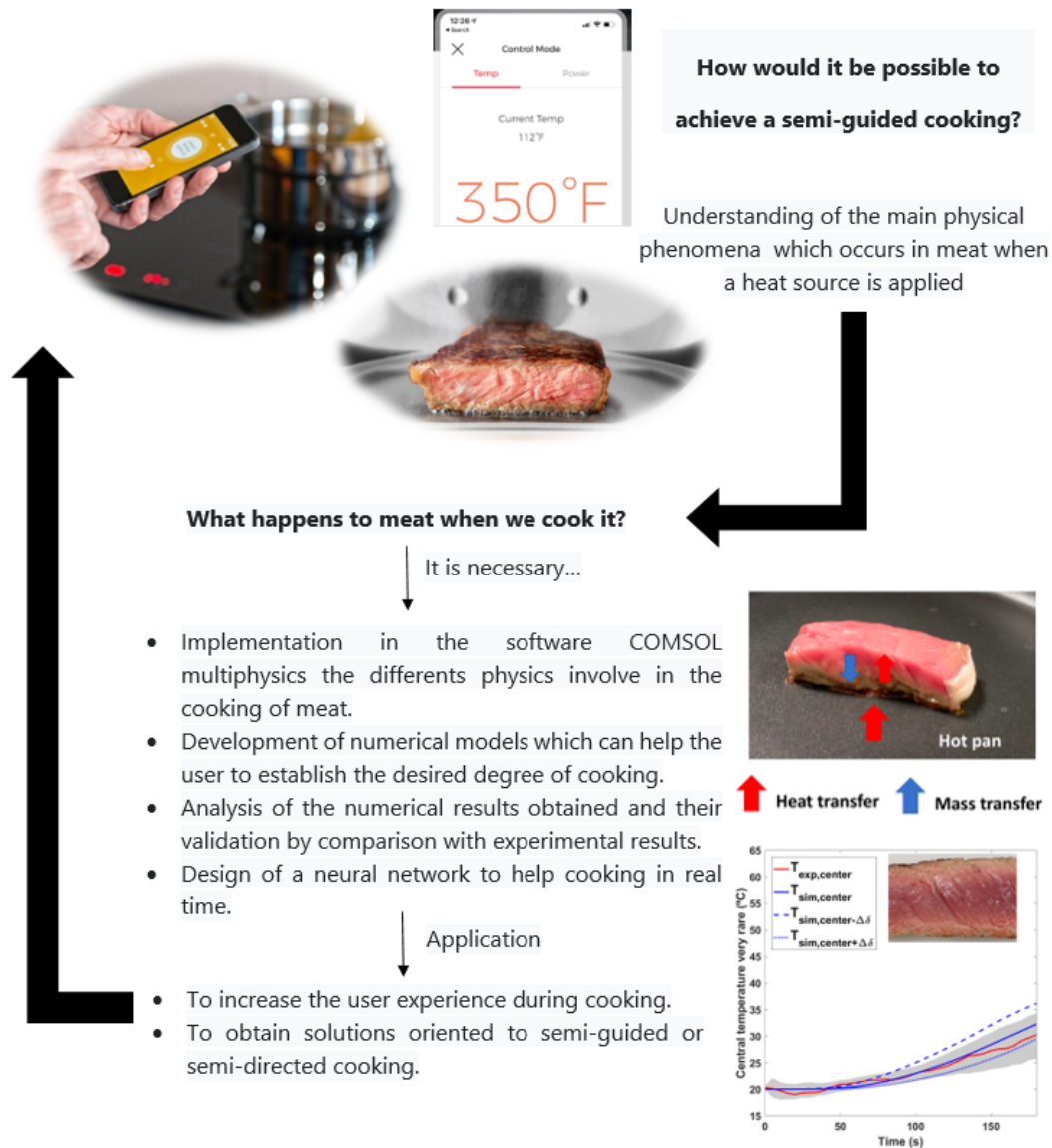
Figura 1.11: Outline of the Thesis objectives regarding meat pan cooking.

permeability and the Young's modulus according to the type of meat, they do not carry out the coupling with the solid mechanic problem.

In this context of solid mechanic and the shrinkage that the meat suffers during cooking, there is still little research and there are two fundamental currents. There are models in which the experimental shrinkage data fit depending on the values of the moisture content or the additive volumes of the various components. This information is used to predict deformation from moisture loss (Mayor and Sereno, 2004, Katekawa and Silva, 2006). On the other hand, there are models which model transport in deformable food as a solid mechanics problem and solve the equations of equilibrium of moments for the solid matrix. This approach has been applied in Gulati and Datta (2015) for rice grain puffing, Zhang et al. (2005) for baking bread in the oven and Dhall and Datta
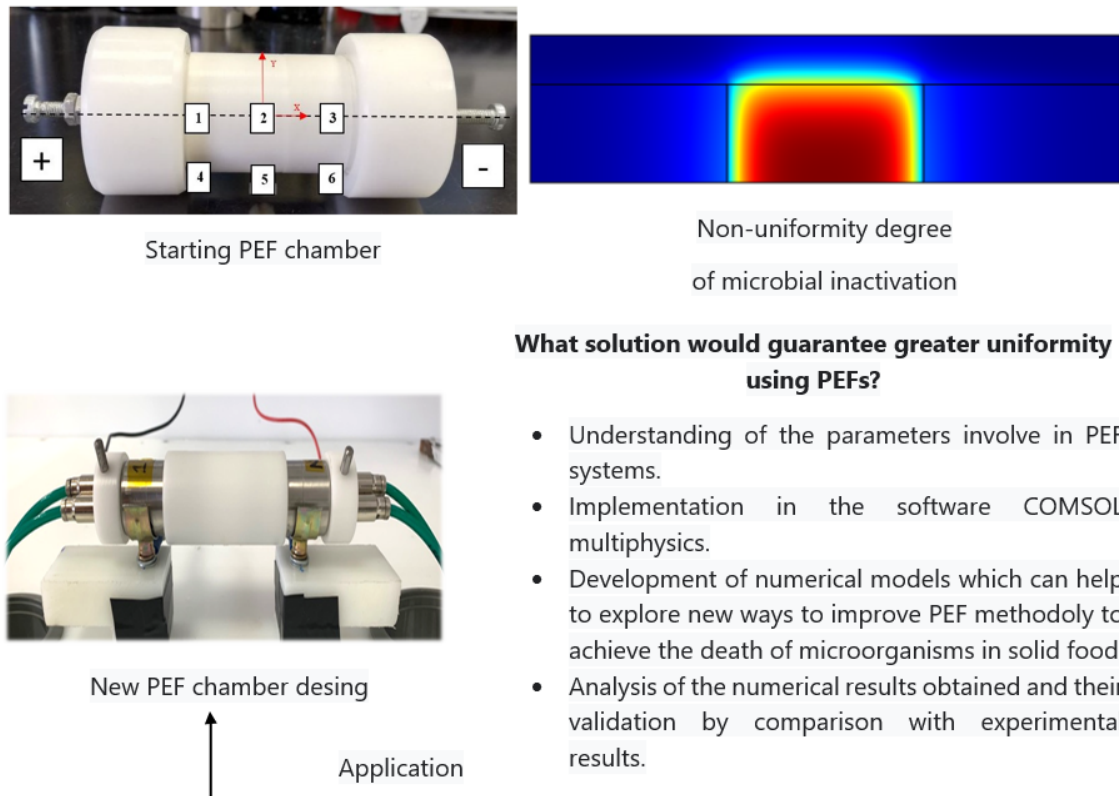
Figura 1.12: Outline of the Thesis objectives regarding the analysis of PEF systems.

(2011) for hamburger and drying potato snack.

Is in this last tendency where this thesis is framed, in the attempt to develop a model based in a poromechanical framework for the physics of moisture transport, transfer of heat and mechanics of the solid in the meat pan cooking, including the phenomenon of turning over the meat.

Regarding color evolution, the kinetics of color change by the heating of beef meat has not been clearly studied. There are some works such as that of Goñi and Salvadori (2011) in which the variation of the CIELab coordinate $a^*$ (related to the change of red hue) is described, but this does not include changes in lightness; or that of Kondjoyan et al. (2014) which only shows results for temperatures above 65 °C.

Thus, this Thesis also deal with the incorporation of color kinetic equations to the poromechanical model of meat coupled with all its mentioned physics by FEM.

## 1.7.  State of the art in the microbial inactivation through PEF

In the last years, there is a growing demand for long-life products that maintain their organoleptic and nutritional characteristics. Since the increase in temperature can cause a change in these properties, researches have been focused on non-thermal processing technologies that achieve the inactivation of microorganisms with only a minimal increase of its temperature, thereby preserving heat-sensitive food compounds (Smith, 2011). PEF system would be one of these processes.

This technology has been used for the pasteurization of liquid food, and for improving the extraction of intracellular compounds such as betalanin from red beets, polyphenols from grape skins or carotenoids from microalgae (Buckow et al., 2013, Álvarez and Raso, 2017, Wang et al., 2018). As this type of heating is volumetric and it occurs from the inside to the outside of the product (Sastry and Li, 1996), heating is supposed to be more homogeneously and quick, as in case of microwaves and radiowaves, but with greater penetration capacity (Sastry, 2005, Ramaswamy et al., 2014). This could be and advantage because many times, the outer medium is overheated with other traditional heating methods in order to achieve the same temperature inside of the food (Yildiz-Turp et al., 2013).

In the study of Ariza-Gracia et al. (2020) application of PEF at higher electric field strengths (> 1 kV/cm) in order to quadratically increase the heating rate (Equation 1.1) is proposed. In this work square pulses of 3 $\mu$s of 3.75 kV/cm at frequencies over 50 Hz were applied to an Agar cylinder. In 20 seconds, the sample reached 70 °C, demonstrating than PEF is an interesting alternative for achieving high temperatures in brief time intervals, also in solid food. As it was mentioned before, in this study a non-homogeneous distribution of temperature was observed, determining cold points in the contact zones between the treated product and the electrodes. This fact was similarly observed in others works as Choi et al. (2020) or Marra (2014).

This Thesis addresses the evaluation of strategies that reduce the occurrence of cold zones in the treated product by PEF, since it would be of interest in order to improve the heating uniformity in the solid product for guaranteeing the microbial inactivation. To achieve this objective, the optimization of the main operating parameters of the treatment has been carried out.

## 1.8.   Thesis outline

This Thesis is organized in 5 chapters. In the beginning of each of them, a brief summary is included so that the reader could be correctly situated. Each chapter corresponds to a publication, so it consists of a short introduction, the main body and a last section where the main conclusions were highlighted and properly discussed. More specifically, the work is structured as follows:

- **Chapter 1** exposes the main idea of the Thesis and the principles of meat pan cooking and the treatment of food using field electric pulses with a purpose of quality and safety in order to eliminate bacteria in solid foods. A review of the state of art was also included in both lines of research. It is completed with a general description of the techniques used throughout this Thesis and finally, the motivation, objectives and outline following in this work are itemized.

- **Chapter 2** develops a finite element model capable of reproducing the application of pulsed electric field in solid food through a PEF chamber system. The chapter includes both, experimental validation and the exploration of new techniques (thermostating the electrodes) to achieve a more uniform temperature throughout the food sample. A study of the main operating parameters has been carried out as well as a study on the inactivation of the bacteria Salmonella Typhimitium 878, which depends on the temperature reached and its homogeneity into the sample. The contents of this Chapter was published in a research paper published in the journal Frontiers in Food Science and Technology, in section Food Safety and Quality Control (Moya et al., 2022).

- **Chapter 3** presents an initial approach to the meat pan cooking problem and the development of a 3D finite element model capable of reproducing this process. The chapter also includes its experimental validation and and the verification that the model is valid for different thicknesses of meat and different degrees of cooking too. The novelty of the model is the incorporation of the moment of turning over the meat according to a criteria of water loss.The chapter was completed with the main conclusions and the discussion. The contents of this Chapter was published in a research paper published in the Journal of food Engineering (Moya et al., 2021b).

- **Chapter 4** focuses on the evolution of the color or the meat when it is cooked, based on the model of the previous chapter. This chapter includes the evolution of color in meat using CIELab coordinates and its experimental validation. It also

includes a study of the optimal time to turn over the meat if a color profile, and therefore a cooking degree, is desired on both sides of the meat. The contents of this Chapter was published in a research paper published in the European Food Research and Technology journal (Moya et al., 2021a).

- **Chapter 5** summarizes the main conclusions of this Thesis and proposes some possible future lines to complete the research initiated in these studies.

Additionally to the chapters, two annexes were added in the final part. Annex A includes a summary of the Thesis redacted in Spanish, and annex B remarks the original contributions of this study in form of publications.

# Chapter 2

# A numerical approach to analyze the performance of a PEF system in microbial inactivation of solid food

In this Chapter, different ways to avoid temperature differences between internal and surface points of solid food after using ohmic heating treatment have been explored. To do that, the parameters of these treatments have been analyzed, as well as the design of the chambers where the PEFs are carried out. For this analysis, a Finite Element Model capable of reproducing this phenomenon has been validated. Once it has been validated, through a sensitive analysis of the parameters, the optimal operating conditions of the treatment have been sought. This Chapter is about two publications:

- Moya, J., Astráin-Redín, L., Grasa, J., Cebrián, G., Calvo, B. and Álvarez, I. (2022). A numerical approach to analyze the performance of a PEF system in microbial inactivation of solid food. Frontiers in Food Science and Technology. 10.3389/frfst.2022.880688.

- Astráin-Redín, L., Moya, J., Alejandrez, M., Beitia, E., Raso, J., Calvo, B., Cebrián, G., and Álvarez, I. (2021). Improving the microbial inactivation uniformity of pulsed electric field ohmic heating treatments of solid products. LWT. 10.1016/j.lwt.2021.112709.

## 2.1.   Introduction

In recent years, the interest in novel thermal processing technologies as alternatives for the application of traditional thermal treatments in food has increased. Traditional convection and conduction treatments are very slow and can affect the nutritional and

sensory quality of food, especially in solid products, where the surface of the food is over-treated to ensure that the center receives the appropriate heat treatment to guarantee food safety. Novel thermal processing technologies include ohmic heating, dielectric heating (microwave and radio frequency) and inductive heating. All these technologies have the advantage that the heat is generated from the inside to the outside of the food, reducing the over-heat of the product surface (Ramaswamy et al., 2014, Alkanan et al., 2021). However, only ohmic heating allows the treatment of larger food as it has a higher penetration capacity and achieves more uniform heating (Sastry et al., 2014). Ohmic heating is based on the Joule Effect described by the Eq. 2.1, and it consists of the application of electrical currents up to 0.1 kV/cm in food, which works as an electrical resistance by heating itself internally (De Alwis and Fryer, 1990).

$$W = \int_0^W \chi \varXi^2 dT \qquad (2.1)$$

where $\chi$ is the electrical conductivity of the treated medium or product (S/m), $\varXi$ is the electric field strength (V/m); and dt is the time (s) during which the field strength is applied (Sastry and Li, 1996). From this equation it can be observed that the electric field strength is an important parameter, since slight modifications in it square the transferred energy to the treated product. Using stronger field strengths would make that the cellular permeability increases, favoring the release of intracellular material (ionic compounds). The result is the increase of the electrical conductivity of the food during the heating process. This phenomenon would allow the application of more rapid and uniform heating (Sastry, 2005), since the heating rate would be quadratically increased as shown by Joule's equation. Considering these advantages of the application of higher electric fields, Moderate Electric Fields (MEF) were developed, which consist of the application of electric pulses at intensities up to 1 kV/cm (Yoon et al., 2002). This technology has been studied for the blanching of vegetables, as a pre-treatment to promote sugar beet extraction or as a treatment prior to food drying (Wang and Sastry, 2002). Recently, and based on the same principle, Pulsed Electric Fields (PEF) have been evaluated as a new ohmic heating system for solid food treating the product over 1 kV/cm (Ariza-Gracia et al., 2020). Initially, the interest of PEF in the food industry was focused on the phenomenon of electroporation of cell membranes and its multiple applications, without hardly modifying the temperature of the food. As a consequence of this phenomenon, PEF enables the pasteurization of liquid foods with minimal increase in temperature (Álvarez and Raso, 2017) or the extraction of intracellular compounds of interest such as polyphenols from grapes and red potatoes or colorants from red beets, among others (Toepfl et al., 2006). However,

Ariza-Gracia et al. (2020) showed that PEF applied over 1 kV/cm could be a new way of applying ohmic heating in solid food, heating technical agar. In this study a cylinder of this material is heated up to 70 °C in 20 s by applying pulses at 3.75 kV/cm and 50 Hz. Nevertheless, despite this type of heating is considered as a uniform and volumetric process, cold points can be detected in the contact zone of the electrodes with the product (Marra, 2014). This is considered as a limitation when applying heat treatments to guarantee the safety of food, since cold points do not reach enough temperature to achieve a certain level of microbial inactivation, compromising in this manner the food safety. However and conversely, if cold areas are treated to achieve this inactivation, other areas would be over-treated affecting the quality of the food too. Thus, any evaluation or strategy that reduces the difference between cold and hot areas would be of interest to improve the heating uniformity.

Therefore, different solutions has been evaluated. On the one hand ones based on the modification of PEF parameters involved in the treatment (field strength or frequency), and on the other hand others based on the modification of the initial temperature of the electrodes of the treatment chamber, in order to reduce the temperature difference between the central areas of the product and the areas in contact with the electrodes.

Numerical simulation is a useful tool and it can be used as a complementary method to solve physical problems and to evaluate complex situations impossible to carry out in a real scenario. Numerical simulation can be very helpful to predict the temperature reached and its evolution in the whole product, determining the existence of coldest point, and to evaluate the influence of different process parameters in order to limit the overheating of the food sample center. Due to that, finite element simulations have been used, not only to obtain a detailed knowledge of the temporal and spatial distribution of the product's temperature as other studies as Gerlach et al. (2008), Schroeder et al. (2009), Pataro et al. (2011) and McLaren et al. (2019), but also to estimate the degree of microbial inactivation in an inhomogeneous or homogeneous PEF process, aspect that has hardly been investigated.

## 2.2. Theoretical model of PEF systems

### 2.2.1. PEF generator

With the objective of evaluating the effect of PEF based on numerical simulations, these PEF simulated treatments were based on the experimental conditions that can be applied with a ScandiNova 6 MW PEF equipment (Modulator PG, ScandiNova,

Uppsala, Sweden). This device generates monopolar square wave pulses of 3 µs width. The frequency applied vary from 0.5 to 300 Hz. The maximum output voltage and current of the equipment is of 30 kV and 200 A, respectively. The equipment has a direct current power supply which converts the 3-phase line voltage to a regulated DC voltage. It has six IGBT switching modules (high-power solid-state switches) with a primary voltage around 1000 V. The discharge of a primary pulsed signal of 1000 V is controlled by an external trigger pulse, which gates all the modules. Finally, the primary 1000 V pulse is converted by a pulse transformer to a 3 µs-high voltage pulse of desired high voltage. The electric current delivered in the treatment chamber by the device is limited to a range of 80 to 150 A for a safe manipulation of the PEF chamber and to obtain rectangular 3 µs-pulses. Using numerical simulation, solutions for PEF treatments of electric field strength between 2.5 and 3.75 kV/cm and frequency between 50 to 200 Hz have been obtained, applying 3-µs pulses. First of all, an experimental validation for a 2.5 kV/cm and 50 Hz case have been carried out.

## 2.2.2. PEF treatment chamber

A parallel electrode treatment chamber was used for the simulations and for the experimental tests. The treatment chamber was based on the one described by Saldaña et al. (2010) (Fig. 2.1). It was a parallel electrode chamber composed of two stainless steel cylinders of 20 mm in diameter with a space between them of 20 mm (gap) where the sample of Agar was placed. The sample and the electrodes were introduced in a hollow cylinder made of polytetrafluoroethylene (Teflon, insulating material) of internal and external diameters of 20 and 30 mm, respectively, and 60 mm long.
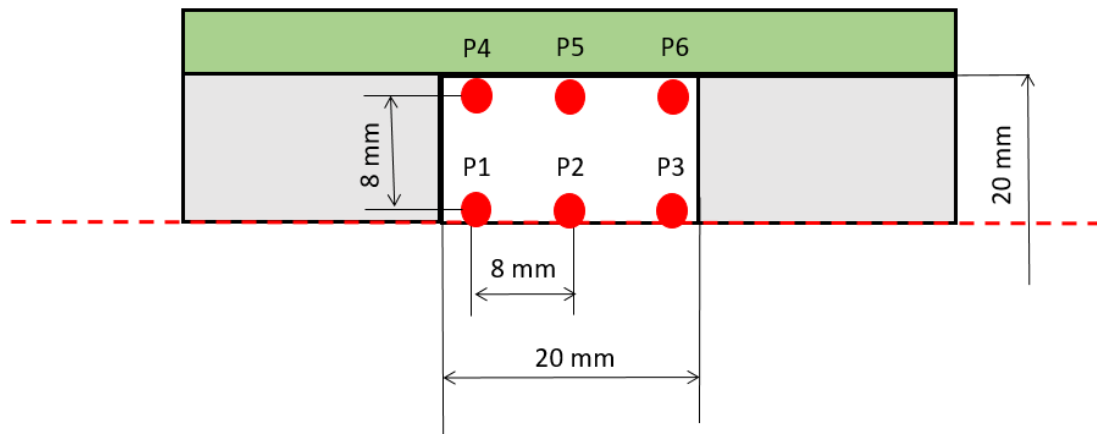
Figura 2.1: PEF treatment chamber and the position of the evaluated points on the agar cylinder based on Ariza-Gracia et al. (2020). Location coordinates (Z and R) in mm of each simulated point: Point 1 (-8, 0); point 2 (0, 0); point 3 (8, 0); point 4 (-8, 8); point 5 (0, 8); point 6 (8, 8).

With this chamber, the electrodes could be thermostat making dielectric hot oil (electrical conductivity of 1.4 µS/cm) to be recycled inside them. This way of applying pulses in the PEF chamber is a novelty in this field. In practice, a thermostatic water bath was used to heat the oil which was then pumped to the electrodes with a peristaltic pump. The electrodes were preheated to a defined temperature before the application of the PEF, by recirculating the hot oil the necessary time to ensure that the temperature was stable ("tempering time"). This time is an important parameter to be analysed in order to assure the established initial temperature in all the solid sample before starting the experiments. This time depends on the necessary temperature to be achieved in electrodes and sample before PEF treatments. The uniformity of the PEF-ohmic heating depends largely on this time, so it is a key parameter. Due to that, tempering times of 5 and 10 minutes and initial temperatures of 45 and 55 °C on the electrodes haven been simulated using the software Comsol Multiphysics 5.2.a, based on the Finite Element Method (FEM).

## 2.2.3.  Evaluation of heating uniformity of the PEF treated samples

In this research, 20 mm x 20 mm technical agar cylinders (Oxoid Basingstoke Hants, United Kingdom) with 0.24 % NaCl (VWR International LTD, Radnor, USA) were used as described in Ariza-Gracia et al. (2020). In order to validate the developed model, 6 points were selected to make a comparison of the heating rate and the uniformity

of this heating in the whole agar cylinder. These points were distributed all over the cylinder, as we can observe in Fig. 2.1. Point 2 was considered as reference for the rest of points, since it was the geometric center. It was located 10 mm from the electrodes and from the insulating material of the chamber. Points 1 and 3 were at 8 mm from this reference point moving in the X-axis. Points 4, 5, and 6, were at the same positions in X-axis than points 1, 2, and 3, but displaced 8 mm in the Y-axis to the extreme of the cylinder, and 2 mm from the chamber Teflon coating. Based on this temperature mapping, a longitudinal and radial temperature difference between pairs of points were evaluated in the FE model when applying PEF. Longitudinal temperature difference evaluated the heating from the inside to the outside of the cylinder caused by the PEF treatment, and the radial one, the temperature difference due to the proximity of the cylinder surface points to the coating. These two temperature differences must be reduced with the objective of achieving a better uniformity.

## 2.3.    Finite Element model

Assuming that the treatment chamber (Fig. 2.1 presents a perfect symmetry of revolution, a computational axisymmetric model was developed in the commercial software COMSOL Multiphysics 5.2a in order to reproduce the ohmic heating in the sample of agar when applying PEF treatments. The scheme of this model can be seen in Fig. 2.2. Imitating the experimental treatment chamber, the model consists of two electrodes with radius of 10 mm and thickness of 20 mm, the Teflon coating around them, and the technical agar with 20 mm diameter and 20 mm length. This geometry simplification was experimentally validated and it reduced the computational time.
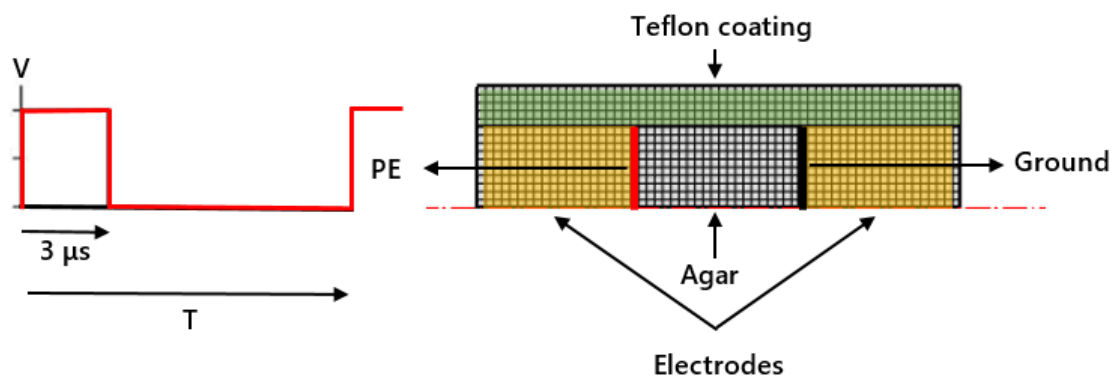


Figura 2.2: Scheme of the finite element model and boundary conditions.

In order to confirm the accuracy of the predictions done with this model and

its simplifications, heat rates curves in different points of the agar cylinder were experimentally obtained. This evaluation will be described later on and using the PEF chamber developed by Ariza-Gracia et al. (2020), with no tempered electrodes. After this first step, a sensitivity analysis of the main parameters which govern the problem of ohmic heating (electric field strength, frequency of the pulses, temperature of the electrodes, and tempering time of the electrodes) was addressed. Once the model has been validated and based on those sensitive analysis conditions, the uniformity of the PEF heating in the agar was evaluated using FEM. Temperature difference was evaluated in the two axis, longitudinal and radial. Longitudinal one will give information about the heating from inside to the outside of the cylinder caused by the PEF treatment, and the radial one about the temperature differences due to the proximity of the cylinder surface points to the coating. Finally, for the best and worst functioning condition, the theoretical inactivation of Salmonella Typhimurium 878 in the agar cylinder was numerically simulated and evaluated.

The model was meshed with quadrilateral elements using a quadratic approximation. Mesh sensitivity analysis was realized to set the mesh size. The total number of degrees of freedom and elements was 6050 and 720, respectively (120 elements for the Teflon, 200 for each electrode and 200 elements for the agar).

## 2.3.1.  Initial and boundary conditions

Ohmic heating is a coupled thermo-electrical problem. The electric field intensity is solved by Lapace equations, and the internal energy generated by this electric field is determined by the Joule's equation (Ariza-Gracia et al., 2020). The heat generated Q (J) during ohmic heating is governed by the Joule's equation. This heat is proportional to the square of the electrical current which flow's through the agar, the resistance of the sample, and the time on which this current is applied. The heat transfer process is described in Eq. 2.2:

$$Q = \rho C_p(T)\frac{\partial T}{\partial t} - \nabla \cdot (k(T)\nabla T) \tag{2.2}$$

$C_p$ (T) is the specific heat and $k(T)$ is the thermal conductivity. $Q$ is at the same time the electrical energy caused by the Joule's heating (Eq. 2.3):

$$Q = \chi(T) \cdot \varXi^2 \tag{2.3}$$

where $\chi$ (T) represents the electrical conductivity, and $\varXi$ is the electric field strength. This electric field strength depends on the electrical potential, V (Eq. 2.4), and based on charge conservation, the electrical potential can be defined as in Eq. 2.5, being $J$ the current density.

$$\varXi = \nabla V \tag{2.4}$$

$$\nabla \cdot J = \nabla J \cdot [\chi(T)\nabla V] \tag{2.5}$$

In the simulation, time was stopped at the moment when any of the point of the agar cylinder arrived at 80 °C. The simulation time was composed of different temporal studies in order to fit the moments in which the applied voltage to the electrodes is in a high or low level. Due to all that, two different types of boundary conditions are needed in the model, electrical and thermal. A squared electric pulse of 3 µs, a load amplitude of 2.5 kV/cm and 50 Hz of frequency was used for defined the electric potential between the electrodes as a first approach. On one electrode was set the high voltage electrode (red line Fig. 2.2) and on the other the ground (black line Fig. 2.2). In order to reproduce the natural convection and its corresponding heat transfer between the treatment chamber and the surrounding media, the condition defined by Eq. 2.6 was defined in the boundary of the Teflon:

$$\overline{n} \cdot (k_{\text{Teflon}}\nabla T) = h \cdot (T_{amb} - T) \tag{2.6}$$

where $k_{\text{Teflon}}$ is thermal conductivity of the Teflon; $T_{amb}$ is the initial room temperature (20 °C), and h is the convection coefficient.

Depending the scenario, different initial conditions have been considered. For the cases on which no thermostating was applied, the initial room temperature condition was 24 °C on both, the agar sample and the electrodes, in order to reproduce the experimental test. Meanwhile, on cases on which a previous thermostating was carried out, the initial temperature of agar and Teflon when start the pulsing phase was set as the temperature distribution caused by the contact with the warm electrodes which were stabilized at the dielectric oil temperature.

## 2.3.2.   Material properties

Based on the described treatment chamber, three materials were considered on the finite element model: the cylinder of technical agar, the electrodes of stainless steel, and the Teflon as insulating material. For technical agar, a 0.24 % of NaCl was used to improve the transmission of the electric current through them. The properties of this material were experimentally determined in the study of Ariza-Gracia et al. (2020), and are shown in Eq. 2.7 (electrical conductivity, $\chi(T)$ in mS/cm), Eq. 2.8 (thermal conductivity, $k(T)$, in W/mK) and in Eq. 2.9 (specific heat, $C_p$ in J/kgK).

$$\chi(T) = 0.433 - 0.0096 \cdot T + 3.192 \cdot 10^{-5} \cdot T^2 \tag{2.7}$$

$$k(T) = -0.732 + 0.007 \cdot T - 9.492 \cdot 10^{-6} \cdot T^2 \tag{2.8}$$

$$C_p(T) = 3.991 \cdot 10^{-4} - 423.184 \cdot T + 1.880 \cdot T^2 - 0.004 \cdot T^3 + 2.762 \cdot 10^{-6} \cdot T^4 \tag{2.9}$$

Table 2.1 shows the material properties for the stainless steel of the electrodes and for the Teflon.

|                        | Stainless steel     | Teflon       |
| ---------------------- | ------------------- | ------------ |
| k [W/(mK)]             | 12                  | 0.25         |
| $\chi$ [S/m]           | $1.45 \cdot 10^6$   | $10^{-24}$   |
| $C_p$ [J/(kgK)]        | 502                 | 1450         |
| $\rho$ [kg/m$^3$]      | 7850                | 970          |

Table 2.1: Thermal conductivity, electrical conductivity, specific heat and density of stainless steel and Teflon.

## 2.3.3.   Finite element model validation

The experimental validation of the FEM model using the simplified geometry of the PEF treatment chamber, was carried out by determining the heating rate ($^oC/s$) at the different points of the agar cylinder, mentioned in section 2.2.3 using the treatment chamber described. For this objective, the experimental 20 mm x 20 mm technical agar cylinders with 0.24 % NaCl were prepared. PEF treatments of 2.5 kV/cm, 50 Hz and 3µ-pulse width, were applied using the equipment of section 2.2.1. To record

the temperature over time in the different points of the cylinder (points 1 to 6), fibre optic probes (Fiberoptic Components, USA) were used. With the recorded results, heat penetration graphs were obtained, and according to the linear heating kinetics, the heating rate was associated to the slope of these heat penetration curves. For comparing the experimental and simulated heating reates, the coefficient of determination (R2) and the root mean square error (RMSE) were obtained (Baranyi et al., 1999). For that, GraphPad PRISM software was used. With this software the statistical analyses (one-way ANOVA with Tukey post-test and Student's t-test) ($p = 0.05$) was carried out in order to compare the results of the different tested points of the sample cylinder.

## 2.3.4.    Sensitivity analysis

Once validated the simplified model, a FEM sensitivity analysis of the main parameters governing the described problem was carried out, in order to study the influence of four parameters: the frequency of the applied pulses (100 and 200 Hz), the electric field strength of these pulses (2.5 and 3.75 kV/cm), the thermostating temperature of the chamber through the thermostat with oil (45 and 55 °C) and the time of this thermostating process (5 and 10 min). Fist of simulating the application of PEF, it has been necessary to simulate the heating of the agar and the electrodes when pumping the oil at 45 and 55 °C during 5 or 10 minutes. In this manner, the obtained temperature distributions in these cases were used as the initial temperature distribution in the sample of agar and electrode once PEF treatment started. Then, the different conditions of field strength and frequency were simulated. For determining the radial and longitudinal temperature difference, the final temperatures reached in the different points of the agar when any of these points achieved 80 °C (Fig. 2.1) were used. The longitudinal temperature difference was calculated with point 4 and 5 and the radial difference between point 1 and 4. These temperature differences are the maximum in each direction.

Using a $2^k$ full factorial design (Montgomery, 2017) the influence of these four parameters was analyzed. This design considers $k$ different variables at two different levels (low and high). Longitudinal and radial temperature differences were selected as output variables of this design. As the full factorial analysis consists of four parameters (frequency, $fr$; field strength, $\Xi$; preheating temperature, $T$; and preheating time, $t$) at two different levels, the resulting simulations were 16. From the data set obtained from these 16 combinations, the maximum temperature differences in both directions allowed to analyzed the main effect and interactions of each parameter by multiple

regression.

Once the results of this four variable design were obtained and with the purpose of simplifying and clarifying it, a three variable at two different levels design was carried out. Now, the parameters of the study were the frequency of the pulses (100 and 200 Hz), the electric field strength (2.5 and 3.75 kV/cm) and the thermostating temperature of the electrodes through the thermostat with oil at 45 and 55 °C. This design resulted in 8 simulations. Again, results were analyzed by multiple regression. The results of each simulations were obtained using Comsol Multiphysics 5.2.a. and the sensitive analysis (fit analysis, regression coefficient estimations, model significance evaluations) was done with the software Minitab 19 (Minitab Inc).

### 2.3.5.   Simulating microbial inactivation

The inactivation of Salmonella Typhimurium 878 in all over the agar cylinder when applying PEF heat treatments has been estimated. As described in Ariza-Gracia et al. (2020), the thermal resistance values ($D_{60°C}$ = 0.39 ± 0.04 min and z value = 5.0 ± 0.1 °C) was obtained in isothermal conditions in McIlvaine buffer of pH 6.8. $D_t$ value is the time to inactivate 90 % of the microbes, and the z value is the temperature increase needed to reduce the $D_t$ value by 90 %. Following Eq. 2.10, the lethal effect of the treatment on all over the agar was calculated, measuring this variable in $Log_10$ cycles of inactivation of the microbial population.

$$L = \int_0^{t'} \frac{t}{D_{Tref} \cdot 10^{\frac{T_{ref}-T}{z}}} \cdot dt \tag{2.10}$$

t is the PEF heating time, $D_{Tref}$ is the $D_t$ value at a reference temperature (60 °C ), obtained under isothermal conditions, and $T$ is the temperature of the agar at a determine point. As the simulation time was divided into different temporal studies, the inactivation equation could be implemented in the finite element model. Each of these temporal studies last 1 s, so the model use this increment time to integrate the inactivation integral based on the acquired temperature. With the aim of accumulate the lethal effect ($L$) over time, a stationary study was set after each temporal study. Thus, the lethal effect was calculated each second and it has been added to the cumulative lethal effect every second throughout the simulation time.

## 2.4.    Results and discussion

### 2.4.1.    FE model validation

In order to validate the numerical results obtained from the finite element model, the heating rate of the different points of the experimental agar cylinders was measured, in case of PEF treatments at 2.5 kV/cm and 50 Hz and without tempering the electrodes. In Fig. 2.3 we can see the experimental and the numerical heating rates obtained in the different points of the agar (a), and the comparison between both values (b). These results show a R2 = 0.916 and a RMSE = 0.060, indicating the goodness of the fits.



(a)                                (b)
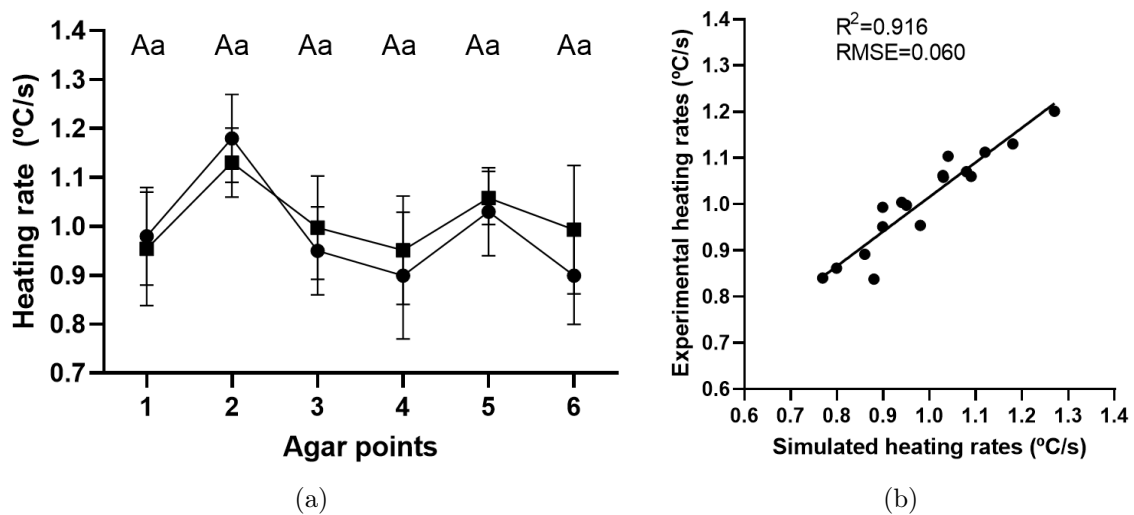
Figura 2.3: a) Heating rates obtained experimentally (square) and by numerical (circle) simulation at the different points of the agar for a PEF treatment of 2.5 kV/cm and 50 Hz, without tempering the electrodes (room temperature). b) Comparison of the experimental and simulated heating rates in all tested points of the agar cylinder.

Experimental values are slightly higher than numerical, with exception of point 1 and 2, but these differences between numerical and experimental values are, in the worst case scenario around 0.05 °C/s, and since the application of PEF takes place for a few seconds, the temperature difference will be hardly significant. This fact allowed us to affirm that the FE model optimally reproduced the experimental results, so that this numerical methodology could be used in future studies. when comparing heating rates (experimental or simulated), points 2 and 5 are the ones that showed highest heating rates. These points corresponded to the central points of the cylinder of agar. Meanwhile, points 1 and 3 (points in the edge of the cylinder of agar and in contact with the electrodes), and points 4 and 6 (points in the surface of the cylinder of agar and in contact with the electrodes), were the ones with the lowest heating rates. This

phenomenon was previously described in other studies such as Icier and Ilicali (2005) and in Ariza-Gracia et al. (2020). These studies show how some cold points appear in the zones of the product in contact with the electrodes, while the hottest points are located at the center of the sample of food. In practice, this means that when PEF treatments are applied, differences between point 2 and 6 could be of around 10 °C, which could mean that in point 2 the final temperature would be lethal for microorganisms (for example 67 °C , but at point 6 (57 °C) this lethality would be limited. This effect indicated the need of finding the optimal operating parameters affecting the heating of the food (thermostating time and temperature of the electrodes and agar, electric field strength and frequency of the pulses).

## 2.4.2.   Sensitive analysis of PEF-ohmic heating

Once the FE model was validated, the next step was identifying and statistically analyzing the influence of the main parameters of PEF treatments in the heating uniformity of the agar cylinder by using this model.

### 2.4.2.1.   Sensitive analysis of 4 variables

First of all, a full factorial analysis of 4 variables was achieved, resulting in a total of 16 FEM models. Table 2.2 shows the different tested combinations for the FEM simulations. Table 2.3 shows the resulted temperature differences (longitudinal and radial direction) in terms of the 4 evaluated processing conditions (field strength, frequency of the pulses, thermostating time, and thermostating oil temperature).

| Case | Thermostating time (min) | Thermostating temperature (°C) | Electric field strength (kV/cm) | Frequency (Hz) |
|------|--------------------------|-------------------------------|--------------------------------|----------------|
| 1    | 10 | 45 | 3.75 | 200 |
| 2    | 10 | 45 | 3.75 | 100 |
| 3    | 10 | 55 | 3.75 | 200 |
| 4    | 10 | 55 | 2.5  | 200 |
| 5    | 10 | 55 | 2.5  | 100 |
| 6    | 10 | 55 | 3.75 | 100 |
| 7    | 10 | 45 | 2.5  | 200 |
| 8    | 5  | 45 | 2.5  | 200 |
| 9    | 5  | 45 | 3.75 | 100 |
| 10   | 5  | 45 | 3.75 | 200 |
| 11   | 5  | 55 | 2.5  | 100 |
| 12   | 5  | 55 | 2.5  | 200 |
| 13   | 10 | 45 | 2.5  | 200 |
| 14   | 5  | 45 | 2.5  | 200 |
| 15   | 5  | 55 | 3.75 | 200 |
| 16   | 5  | 55 | 3.75 | 100 |

Table 2.2: List of experiments carried out for the 4 variable-sensitive factorial analysis.

| Case | Longitudinal temperature difference (°C) | Radial temperature difference (°C) |
|------|------------------------------------------|-------------------------------------|
| 1 | 3.994 | 5.323 |
| 2 | 5.767 | 5.371 |
| 3 | 2.833 | 6.230 |
| 4 | 4.588 | 6.837 |
| 5 | 6.402 | 5.323 |
| 6 | 4.179 | 6.476 |
| 7 | 6.255 | 5.155 |
| 8 | 7.081 | 7.496 |
| 9 | 6.442 | 7.776 |
| 10 | 4.429 | 7.908 |
| 11 | 6.690 | 10.253 |
| 12 | 5.357 | 10.382 |
| 13 | 8.031 | 3.724 |
| 14 | 9.240 | 5.552 |
| 15 | 2.842 | 11.925 |
| 16 | 4.266 | 12.042 |

Table 2.3: Longitudinal and radial temperature differences of each case for the 4 variable-sensitive factorial analysis.

Based on these results and by multiple regression, the equations which describe the temperature variation in the agar in both axis (longitudinal, $\nabla T_{Longitudinal}$, and radial, $\nabla T_{Radial}$) are obtained for the 4 variable-sensitive analysis:

$$\nabla T_{Longitudinal} = 27.52 - 0.672 \cdot t - 0.337 \cdot T - 0.1269 \cdot \Xi - 0.4029 \cdot fr +$$
$$0.1021 \cdot t \cdot T + 0.000262 \cdot t \cdot \Xi + 7.91 \cdot 10^5 \cdot T \cdot \Xi + 0.000463 \cdot T \cdot fr \tag{2.11}$$

$$\nabla T_{Radial} = -28.86 + 2.113 \cdot T + 0.771 \cdot t + 0.1171 \cdot \Xi + 0.4515 \cdot fr -$$
$$0.05514 \cdot T \cdot t - 0.000451 \cdot T \cdot \Xi - 0.000657 \cdot t \cdot fr - 3.46 \cdot 10^5 \cdot \Xi \cdot fr \tag{2.12}$$

where $\Xi$ is the field strength; $fr$ the frequency of the pulses; $t$ the thermostating time and $T$ the oil temperature. The $R^2$ for the longitudinal temperature difference was 0.997 and for the radial one was 0.994.

Based on these equations, the influence of the 4 parameters in both directions of the agar cylinder has been obtained (Fig. 2.4).
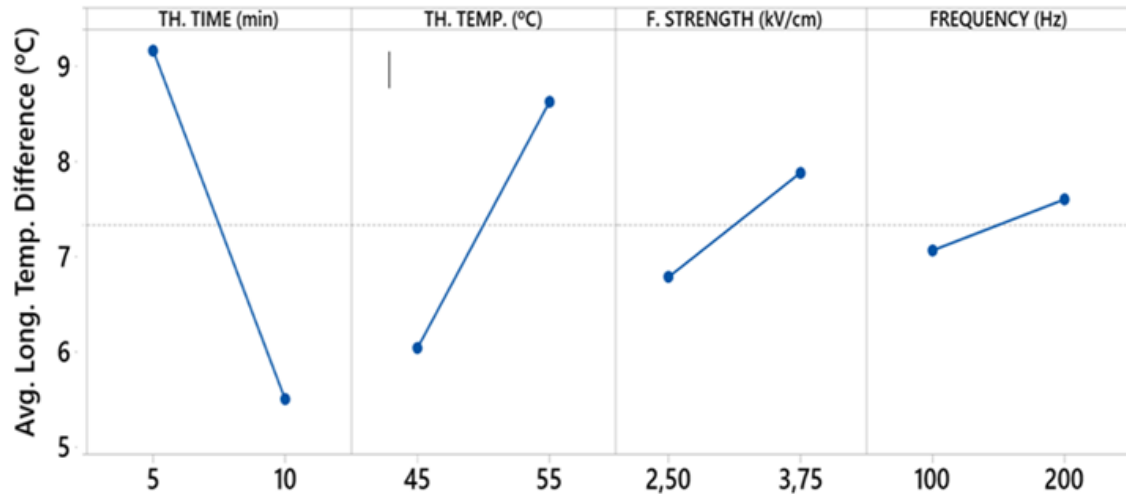
(a)
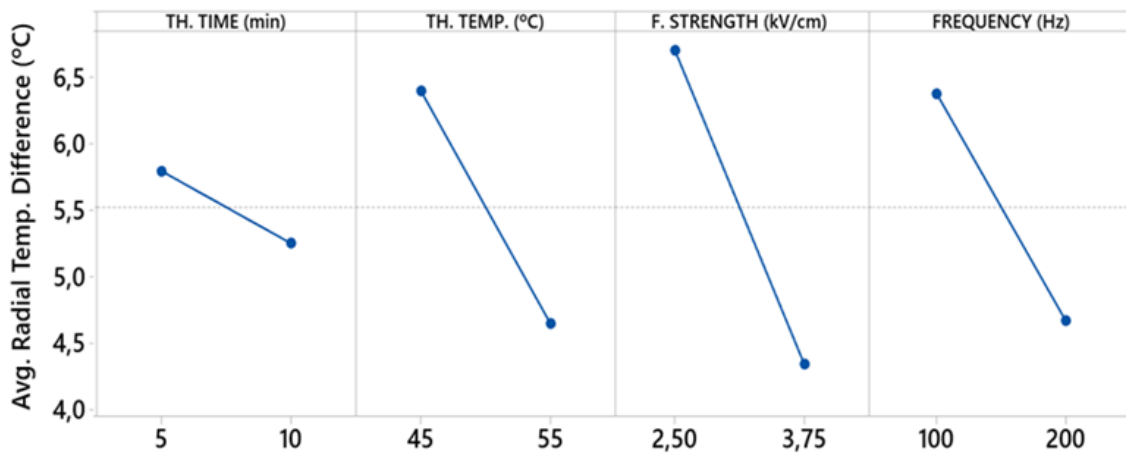


(b)

Figura 2.4: Main effects for a) longitudinal and b) radial temperature difference for the sensitive factorial analysis of 4 variables when applying PEF treatments.

The only parameter that coincided in trend for both temperature differences was the thermostating time of the electrodes, although it is more important in the longitudinal one. In this direction, an increase from 5 minutes to 10 minutes made possible to reduce the temperature difference from 9 to 5 °C, while in the radial direction, the variation is only around 0.5 °C. Regarding the thermostating temperature, it showed an opposite trend in both directions. The longitudinal difference raised 3 °C when the oil temperature was increase from 45 °C to 55 °C, while the radial one decreased 2 °C. The other three parameters, had more importance in terms of radial temperature difference than in terms of longitudinal one. If the field strength was increased from 2.5 to 3.75 kV/cm the radial temperature difference was reduce in more than 2 °C (while in longitudinal direction it increased only 1 °C). If the frequency was increased from 100

Hz to 200 Hz, the radial difference was reduced in around 2 °C (while in longitudinal direction it increased only 1 °C too).

This opposite trend may be due to the way the heating takes place. In the thermostating phase, the heat transfer occurs by contact of the tempered electrode with the agar sample. Therefore, the areas of the product which would be heated in a first place would be those in contact with the electrodes (heating from the outside to the inside). In this manner, a more temperature homogenization could be explain in the longitudinal direction in case of longer thermostating time, due to the approached to thermal equilibrium by conduction. The heating occurs from the inside to the outside in the pulsing phase. The contact between the electrodes and the sample of agar would provoke an abrupt discontinuity of the electrical conductivity in the longitudinal direction due to the different characteristics of the materials (steel and agar). The ohmic heating is proportional to the electrical conductivity of the product, as Joule's effect dictates. The higher the temperature difference is in the longitudinal direction, the higher the heat transfer is. This difference is less pronounced in the radial axis since the electric field varies in the axial direction but not so much in the radial direction. In addition, the agar is in contact with the Teflon on the outside, and this one has an insulation function, its electrical and thermal properties prevent heat transfer. For this reason, when factors which favor the amount of energy involved in the process are increased, such as electric field and frequency, an increase on longitudinal temperature difference is more notable.

With this factorial analysis it can be concluded that the unique parameter which has a clear trend is the thermostating time. This analysis also indicates that a better temperature uniformity in the agar before and once pulsing is obtained when the thermostating time is longer. With this results, an experimental test proved that a 30 minutes would be required to assure that every point of the product sample would achieve the desired temperature with a variation of less than 1 °C. This effect can be seen in Fig. 2.5, where the oil used to temper the electrodes was recirculated at 45 °C for 30 minutes. In this figure we can see that a mean temperature of 38.6 ± 0.9 °C would be obtained in every point of the agar before the pulsing stage. In the same way, when the oil temperature is 55 °C, instead of 45 °C, the initial agar temperature resulted in 50 ± 0.5 °C (data not shown).

(a)                                          (b)
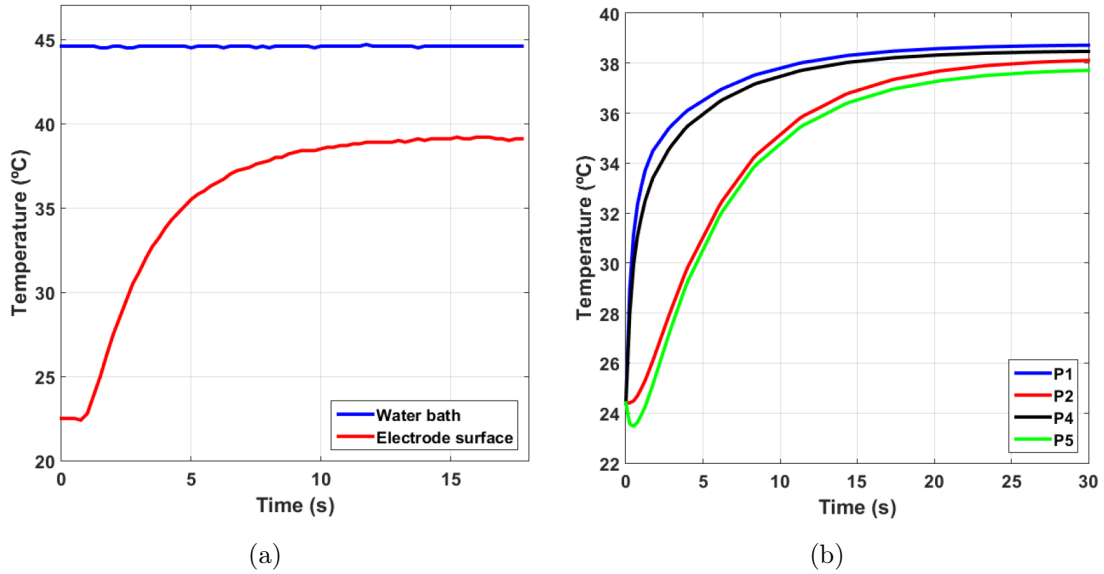
Figura 2.5: a) Temperature evolution (°C) of the electrode surface during thermostating with dielectric oil at 45 °C. b) Temperature evolution in different points of the agar cylinder (°C) when thermostating the electrodes with dielectric oil at 45 °C.

However, the analysis for the other factors does not achieve clear conclusions. Therefore and in order to simplify the study of the influence of these three parameters, a 3-factor design study was then done. For this new study, the thermostating time of the electrodes was fixed in 30 minutes, and the initial temperature of the sample of agar and the electrodes was considered the same that the reached in the simulated case.

### 2.4.2.2.   Sensitive analysis of 3 variables

As in the $2^4$ analysis, the resulted heating differences in both directions of the new tested combinations in terms of the 3 mentioned parameters (field strength and frequency of the pulses, and thermostating oil temperature) was carried out (Table 2.4 and Table 2.5).

| Case | Thermostating temperature (°C) | Electric field strength (kV/cm) | Frequency (Hz) |
|------|-------------------------------|--------------------------------|----------------|
| 1 | 3.75 | 200 | 55 |
| 2 | 3.75 | 100 | 45 |
| 3 | 2.5 | 200 | 45 |
| 4 | 3.75 | 200 | 45 |
| 5 | 2.5 | 100 | 45 |
| 6 | 2.5 | 200 | 55 |
| 7 | 2.5 | 100 | 55 |
| 8 | 3.75 | 100 | 55 |

Table 2.4: List of experiments carried out for the 3 variable-sensitive factorial analysis.

| Case | Longitudinal temperature difference (°C) | Radial temperature difference (°C) |
|------|------------------------------------------|-------------------------------------|
| 1 | 1.630 | 2.111 |
| 2 | 2.696 | 6.125 |
| 3 | 2.738 | 7.740 |
| 4 | 2.650 | 3.950 |
| 5 | 1.690 | 11.720 |
| 6 | 2.010 | 4.380 |
| 7 | 1.550 | 6.820 |
| 8 | 2.010 | 3.790 |

Table 2.5: Longitudinal and radial temperature differences of each case for the 3 variable-sensitive factorial analysis.

The following equations define the temperature variation in the OX and OY axis when PEF treatments are applied at different functioning conditions, field strength (2.5-3.75 kV/cm), frequency of the pulses (100-200 Hz) and temperature of the oil (45-55 °C):

$$\nabla T_{Longitudinal} = 91.96 - 9.456 \cdot \Xi - 0.2392 \cdot fr - 1.366 \cdot T + 0.02601 \cdot \Xi \cdot fr +$$
$$0.1444 \cdot \Xi \cdot T + 0.003628 \cdot fr \cdot T - 0.000418 \cdot \Xi \cdot fr \cdot T \tag{2.13}$$

$$\nabla T_{Radial} = -12.77 + 2.280 \cdot \Xi + 0.08168 \cdot fr + 0.2048 \cdot T - 0.008948 \cdot \Xi \cdot fr$$
$$-0.03200 \cdot \Xi \cdot T - 0.001096 \cdot fr \cdot T + 0.000102 \cdot \Xi \cdot fr \cdot T \tag{2.14}$$

This equations were obtained by multiple regression and based on the results of Table 2.4, and the $R^2$ for the longitudinal temperature difference was 0.99 and for the radial one was 0.99 too. $\Xi$ is the field strength; fr the frequency of the pulses;

and T, the temperature of the oil, as in the 4-variable analysis. The main effects for this analysis have been obtained (Fig. 2.6). As we can see, electric field strength and frequency have different trends for each temperature difference: if strength and frequency are increased, radial temperature difference decreases around 3 °C or 4 °C, while in case of longitudinal temperature difference increases around 0.25 °C. These trends remains the as for the results obtained from the 4-variable factor analysis, but in case of thermostating temperature, we can see that its trend are the same for both directions. If thermostating temperature is increased from 45 to 55 °C, the radial temperature difference decreases 3 °C, and the longitudinal one decreases 0.7 °C. As explained in the previous section, we can see now that a considerably increasing in the thermostating time supposes a reduction of the influence of factors on the longitudinal temperature difference. Doubling the frequency or the electric field slightly increased the temperature difference in the longitudinal axis. On the other hand, it is remarkable that the change of trend for the thermostating temperature influence, is quite related to the new duration of the thermostating treatment.

Due to the high conduction heating during the phase of thermostating, the initial temperature differences achieved for the next stage when the PEF treatment starts, would be much smaller. That is, the effect of the oil temperature during the previous step would be now the determining factor. Fig. 2.7 shows the Pareto charts for radial and longitudinal temperature differences obtained from Eq. 2.13 and Eq. 2.14. With these charts we can define the parameter or combination of them with the most influence on the evaluated temperature difference. In case of radial difference, the most important parameter was the field strength, followed by the thermostating temperature. On the other hand, the most decisive parameter in case of longitudinal difference was the thermostating temperature. With the results of this analysis, it could be concluded that if we want to achieve objectives of temperature uniformity after applying PEF treatments, thermostating the electrodes in a first place would be fundamental. So, a higher thermostating temperature would lead to lower temperature differences. Bearing in mind that an increase in the electric field strength would also suppose smaller temperature differences in case of radial direction, without compromising the longitudinal one. However, it should not be forgotten that the joint effect of frequency and electric field strength is not negligible.
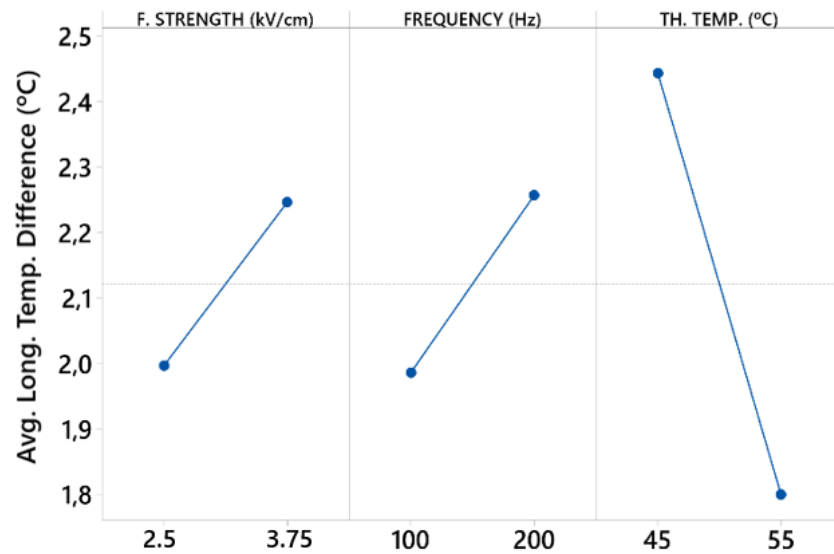
(a)
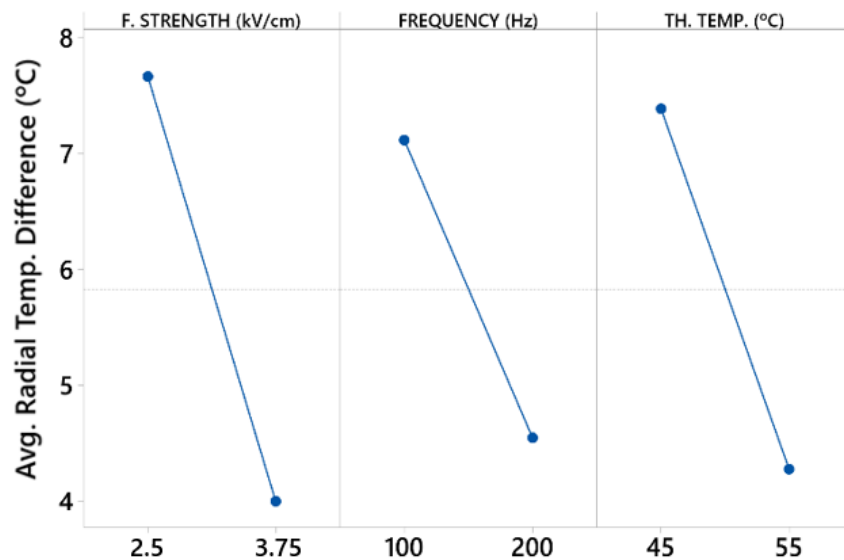


(b)

Figura 2.6: Main effects for a) longitudinal and b) radial temperature difference for the sensitive factorial analysis of 3 variables when applying PEF treatments.

Once this sensitivity analysis has been performed and according to the obtained results, it was possible to select the combination of parameters that lead to an optimum degree of temperature homogenization. First of all, a thermostating time of 30 minutes would be fixed, as it has been seen from the first 4-variable analysis. Regarding the thermostating temperature, the higher it is, the smaller temperature differences it will offer in both directions, so the highest possible was chosen: 55 °C for the temper oil which corresponded to an initial agar temperature of 50 °C. To end with and in order to guarantee a reduction in the longitudinal temperature difference without notably

increasing the radial one, a compromise between the electric field and frequency was
sought: 3.75 kV/cm and 200 Hz.
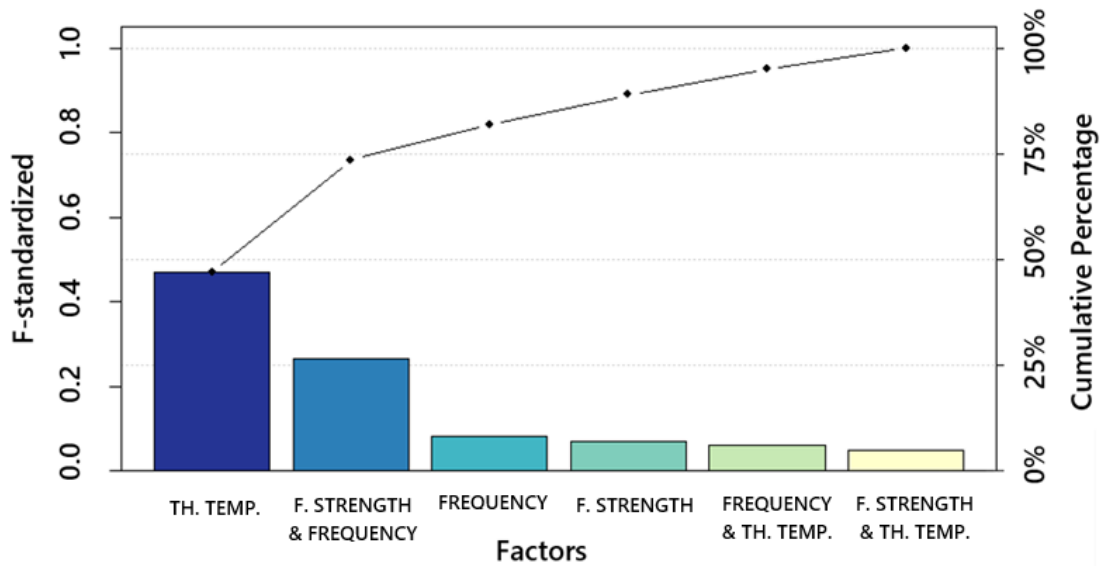


(a)
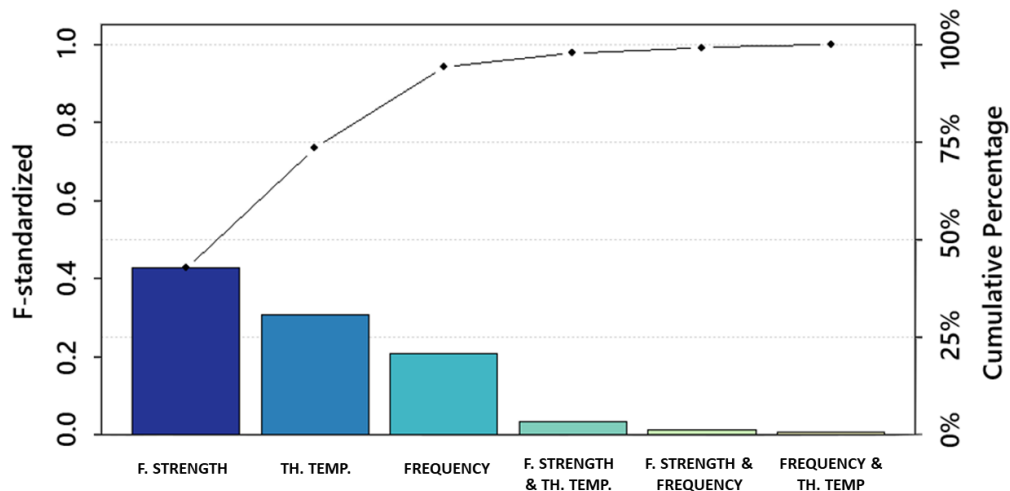


(b)

Figura 2.7: Pareto charts for a) longitudinal and b) radial temperature difference
obtained from the 3-factor design when applying PEF treatments.

### 2.4.3.    Microbial inactivation simulation

Time and temperature are the most important factors when it comes to microbial
inactivation. Thus, depending on the received treatment in the different parts of agar, it
is possible that the same inactivation may not be achieved in all points of the sample.

For this study, a certain microorganism, Salmonella Typhimurium 878, was chosen, and it was evaluated to determine the influence of the investigated parameters on its inactivation in all parts of the sample of agar. Also, the demonstration of how the lack of temperature uniformity can affect in the lethality of this microorganism has been shown. The simulation of microbial inactivation by PEF-ohmic heating in a solid product considering the investigated parameters is a novelty in this field of study.

The temperature distribution and the $Log_{10}$ cycles of inactivation (L) of Salmonella Typhimurium 878 when applying different PEF treatment conditions are shown in Fig. 2.8. Based on the sensitivity study, one of the chosen conditions were this estimated as the one which offered the best temperature uniformity (3.75 kV/cm, 200 Hz, and initial agar temperature of 50 °C by tempering with oil at 55 °C). This figure also includes the same case as above but with an initial temperature of the agar of 39 °C (tempering with oil at 45 °C), in order to analyze the effect of that thermostating temperature on the microbial lethality. Finally, it has also been added the case with the conditions described by Ariza-Gracia et al. (2020), 2.5 kV/cm, 50 Hz and without thermostating the electrodes, in order to observed the effect of no optimized PEF-ohmic conditions. At the bottom of Fig. 2.8 a more detailed image of the lethality at the corner of the agar-electrode-Teflon area has been shown (point 6 is indicated with a red circle). Simulations have been stopped when any point of the sample of agar achieved 80 °C. For the case of initial temperature of the agar 50 °C this time was 2 seconds, for an initial temperature of 39 °C it was of 2.7 seconds and finally, in case of no thermostating the electrodes, this time was of 45 seconds. As it can be observed, a more uniform temperature distribution was achieved when the initial temperature of the agar was higher. A fact to remark is that a noticeably temperature variation, of more than 30 °C, was appreciated when the electrodes not were tempered. This leads to a great variation in microbial lethality (L) compared to the best combination of functioning parameters. However, also the best scenario do not exceed the 5-Log10 cycles of inactivation in the coldest point, where the final temperature would be around 66 °C.

In the bottom of Fig. 2.8 inactivation levels at the area around point 6 have been pointed out in order to make a more clear comparison. In that point it is highlighted that only in case 1 (thermostating at 55 °C, agar at 50 °C) the inactivation exceeds the 20 $Log_{10}$ cycles. In case 2 and 3 this level was of 15 and 2.5 $Log_{10}$ cycles respectively. However, the most dramatic situation was observed in the contact zone between the Teflon, the electrode and the agar. To go deeper in the analysis of this area, Fig. 2.9 shows the temperature and the $Log_{10}$ cycles in that contact line for the three previous cases.
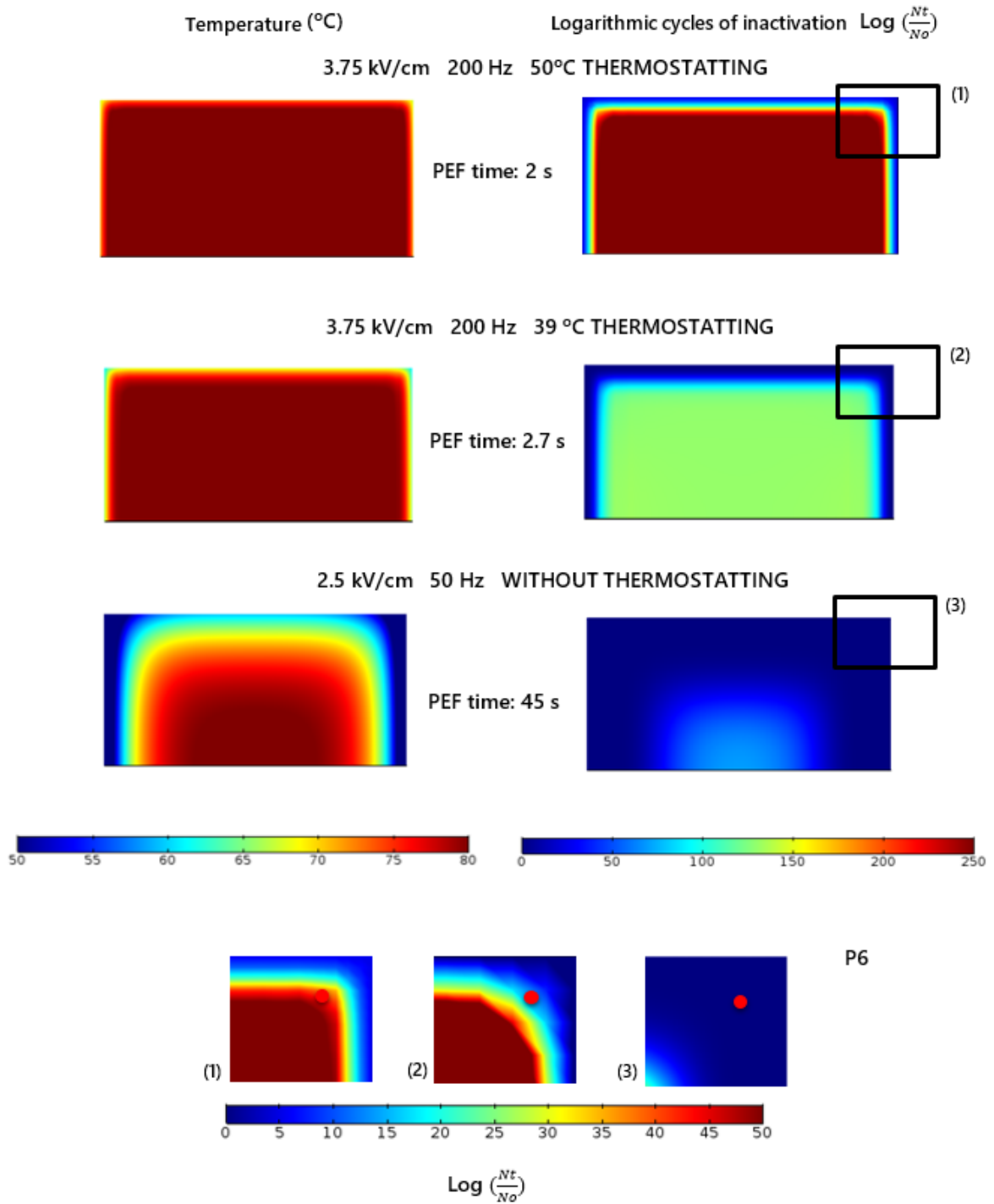
Figura 2.8: Temperature (left images) and Log10 cycles of inactivation of Salmonella Typhimurium 878 (right images) distribution achieved with different operating parameters: 1) 3.75 kV/cm, 200 Hz and 50 °C; 2) 3.75 kV/cm, 200 Hz and 39 °C; 3) 2.5 kV/cm, 50 Hz and no thermostating. In the bottom of the Figure, the red circles correspond to point 6 and corners are enlarged.
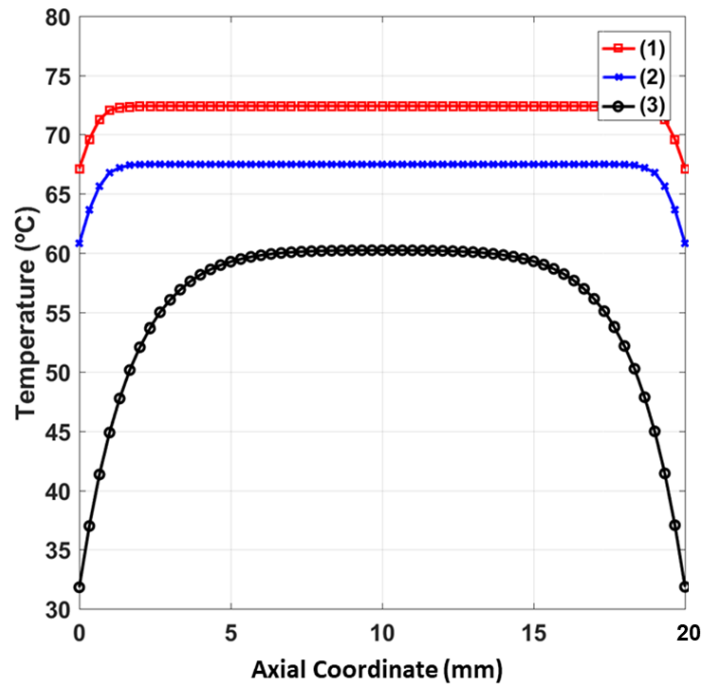
(a)
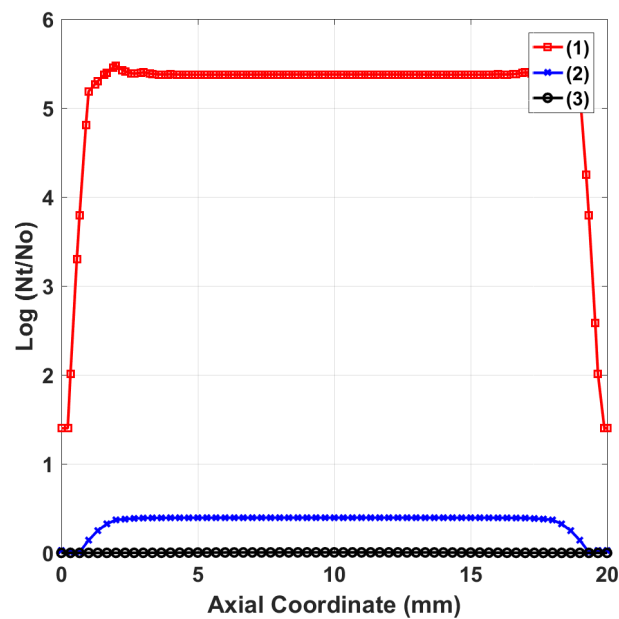


(b)

Figura 2.9: a)Temperature and b) Log10 cycles of inactivation of Salmonella Typhimurium 878 in the contact zone between the Teflon and the agar along coordinate z for each operating condition: 1) 3.75 kV/cm, 200 Hz and 50 °C; 2) 3.75 kV/cm, 200 Hz and 39 °C; 3) 2.5 kV/cm, 50 Hz and no thermostating.

Only in cases 2 and 3 the inactivation level was below a food safety target of 5 $Log_{10}$ reductions (Peng et al., 2017). Nevertheless, not in all the contact line of case 1 this level was below 5 $Log_{10}$ reductions. In the central area, it is just above this level (71.9

°C and 5.35 $\text{Log}_{10}$ cycles of inactivation), but in the corner areas this inactivation level
would not reach the desirable value of L=5 $\text{Log}_{10}$ reductions of target microorganism.
To reach the desired inactivation goal even in the corner areas, a time study of how long
has to be the treatment under these conditions (200 Hz and 50 °C agar temperature)
must be in order to achieve that L target. In Fig. 2.10 the temperature and the $\text{Log}_{10}$
cycles of inactivation in the most unfavorable point (the one corresponding to the corner
between agar, Teflon and electrode) was represented. At 2.3 seconds of treatment this
point reach a temperature of 72.5 °C and L= 5 $\text{Log}_{10}$ reductions. This indicated that
the other points of the agar sample would achieve at least this level. In the other
cases of study, a longer treatment time would have been necessary to achieve a greater
variation in the temperature (data not shown).



(a)                                               (b)
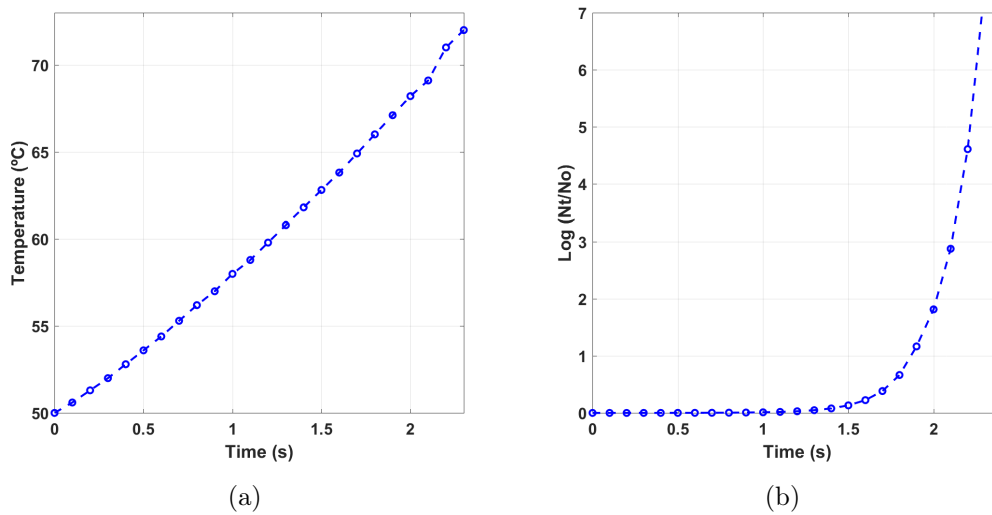
Figura 2.10: Evolution of a) temperature and b) lethality expressed in °C and $\text{Log}_{10}$
cycles of inactivation of Salmonella Typhimitium 878, respectively, in the corner of
the agar cylinder in contact with the electrode and Teflon when applying PEF-ohmic
treatment at 3.75 kV/cm, 200 Hz and thermostating the agar at 50 °C.

Although at the mos problematic point 5 $\text{Log}_{10}$ reductions would be achieved (Fig.
2.10), temperatures around 90 °C would be reach after 2.3 seconds in the center of the
agar at the simulated conditions. This could provoke a thermal impact in the quality
of the product. Thus, an alternative solution has been considered. The lethality just
after stopping the PEF treatment has been evaluated: the final temperatures even in
the coldest point after appyling the PEF-ohmic treatment were lethal (68 °C). So,
inactivation would be advancing only few seconds after the application of pulses. Fig.
2.11 shows the inactivation at the same corner point as previously studied in Fig. 2.10
but until 2 seconds of PEF treatment and including a resting time of 1 second after

this treatment. After this 3 seconds, temperature slightly increased due to the heating inertia and then it is maintained, so inactivation can exceed the 5 $Log_{10}$ reductions of Salmonella Typhimurium 878. With this technique the increment of temperature in the center of the agar would not reach the 80 °C but the target level of inactivation in every point of the agar would be reached, with a total processing time of 3 seconds.



(a)                              (b)
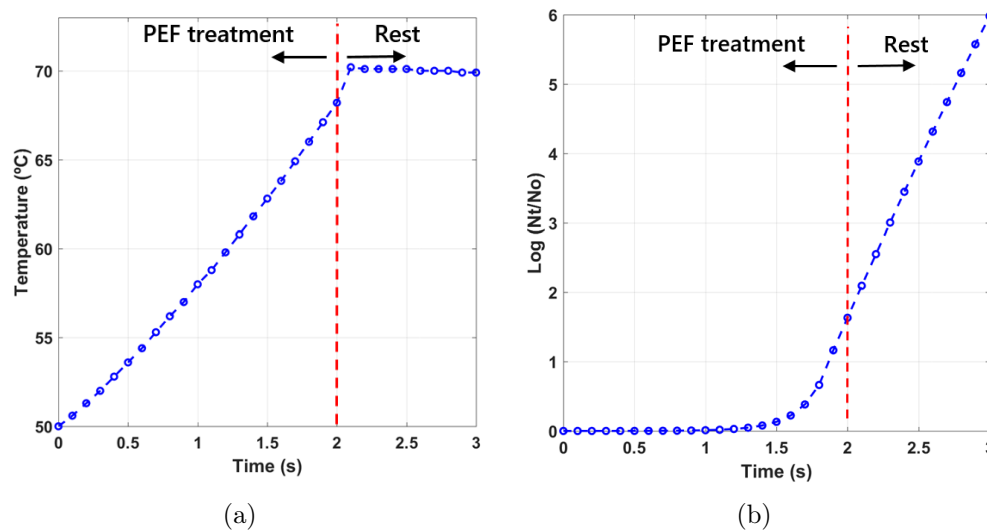
Figura 2.11: Evolution of a) temperature and b) lethality expressed in °C and $Log_{10}$ cycles of inactivation of Salmonella Typhimitium 878, respectively, in the corner of the agar cylinder in contact with the electrode and Teflon for a 2-second-PEF-ohmic treatment (3.75 kV/cm, 200 Hz and thermostating the agar at 50 °C), and 1 second after the PEF treatment ("Resting time").

## 2.5.    Conclusions

In this study, a numerical model which reproduced the treatment by PEF in solid food has been implemented in the finite element software COMSOL Multyphisics 5.2.a. This model included for the first time the simulation of the microbial inactivation due to the heat caused by this PEF treatment. PEF systems has been demonstrated to have a high potential to rapidly achieve microbial inactivation in a solid product when applying electric fields over 1 kV/cm. A sensitivity analysis for the crucial treatment parameters (electrode thermostating time and temperature, frequency and intensity of the electric field) has been carried out. Parameters that lead to a higher initial pulsing temperature will lead to a better homogenisation of the sample. Thus, the thermostating phase played an important role in the temperature uniformity in the whole solid product. Nevertheless, the influence of electric field strength and frequency should not be neglected, since it has been demonstrated that an increase in both parameters leads to

highest heating rates and heating uniformity. The results of the simulations indicated that a treatment with highest initial non-lethal agar temperature (50 °C for the agar achieved by pumping oil at 55 °C through the electrodes during 30 minutes in our case) would mean a better temperature uniformity. With a time of only 2-3 seconds an inactivation of 5 $Log_{10}$ for Salmonella Typhimurium 878 was achieved in the whole sample of agar. This study demonstrated the potential of PEF-ohmic as a quick heating system for solid products and that the previous stage of thermostating the electrodes is an efficient and simple way of considerably improving temperature uniformity in the peripheral zones of the sample. Nevertheless, more research is necessary in order to experimentally confirm the simulated obtained results.

# Chapter 3

# Computational model for steak double-sided pan cooking

In this Chapter, the development of a computational model for steak double-sided pan cooking is detailed. To do so, a bibliography study related to the design of models of all types of meat cooking has been carried out, in order to identify the main equations of the physics that govern the pan cooking of beef meat. This equations have been implemented in COMSOL Multiphysics 5.2.a, a finite element software, with the aim of modeling the problem depending on the main cooking parameters. Experimental tests have been carried out to obtain some properties of the meat, and also to validate the model with real results. This Chapter is about the publication: Moya, J., Lorente-Bailo, S., Salvador, María, Ferrer-Mairal, A., Martínez, M.A., Calvo, B. and Grasa, J. (2021). Development and validation of a computational model for steak double-sided pan cooking. Journal of Food Engineering. 298. 110498. 10.1016/j.jfoodeng.2021.110498.

## 3.1. Introduction

The growing interest in knowing how meat behaves when its cooking in order to use this information to control and optimize cooking processes, has made this field of quite interest in recent years and there are numerous studies about its behavior through experimental tests but also about the development of numerical models that simulate these processes. The physics involved in any meat cooking are the phenomenons of heat transfer, mass transfer and solid mechanics, since meat is treated as a deforming porous medium.

However, the state of the art of the models that reproduce different cooking processes vary both in complexity and in the degrees of approximation. Most models

reproduce the baking or frying of meat (Ahmad et al., 2015, Bansal et al., 2015, Bottani and Volpi, 2009, Feyissa et al., 2013, Isleroglu and Kaymak-Ertekin, 2016, Kondjoyan et al., 2013, Rabeler and Feyissa, 2018a, van der Sman, 2007, van Koerten et al., 2017), but there are hardly any studies on pan-meat cooking, despite being very common in domestic kitchens. This may be because it is necessary to study and quantify the effect of the contact of the meat with the heat source, in this case, the pan. This contact may not be perfect, and there may be gaps between the surfaces (Rocca-Poliméni et al., 2019). Another aspect that is not considered in other types of cooking is the fact that when cooking on a pan, the meat has to be turned over, something complex to deal with in the development of these numerical models. For this reason, the studies that exist of this type of cooking are limited only to simulating the cooking of one-side of the meat (Myhrvold, 2017).

As for the existing physical models, there are ones that only consider heat transfer by conduction and diffusive mass transfer. Others consider the convection heat transfer due to the flow of liquid water from the meat, describing the moisture transport by the Flory-Rehner theory (van der Sman, 2007, Feyissa et al., 2013, Ahmad et al., 2015, Nelson et al., 2020). However, there are few studies in which meat is treated as a porous medium which is deformed when its heating and due to the transport and loss of water, with some exceptions such as Dhall and Datta (2011) and Feyissa et al. (2013). During cooking, the meat proteins undergo a denaturation process causing structural changes in the meat such as the shrinkage of muscle fibers and connective tissue, and the formation of larger pores in parts closer to the surface, being smaller in parts closer to the center (Feyissa et al., 2013). Changes in porosity lead to changes in water permeability and therefore to changes in how water varies in space and time within the meat. Not considering the possible shrinkage derived from this fact could lead to errors in the measurement of meat weight loss (Datta, 2016). In addition, this changes also decrease the water holding capacity of the meat: moisture is expelled from the meat due to the mechanical force exerted by the contracting protein network on the interstitial fluid, denoted swelling pressure (Tornberg, 2005). This swelling pressure is much more important than surface evaporation in relation to the weight loss of the meat. Darcy's law is used to associate the hydraulic pressure with the moisture transport (Rabeler and Feyissa, 2018a).

In this work, these effects are taken into account, as a contribution of novelty to the state of the art. Therefore, the objectives to be addressed in this chapter are, not only to define and validate a computational model which describes the coupled transfer of heat and humidity during the domestic pan cooking of beef meat, if not also treat

the deformation of the meat as a solid mechanical problem while including the turn over process and the problem of the contact heating interface between the pan and the meat. In order to achieve this objectives, an experimental protocol which gather information during meat cooking was developed, to obtain some of the needed beef meat properties and to validate the model. The computational results were compared to theses experimental results, specifically the evolution of temperature and water loss over time. Also, once the model has been validated, the model was tested for different thicknesses of meat with the purpose of checking its adaptability for use it as assistance to cooking in a domestic environment. These results has been also experimentally verified in this chapter.

## 3.2.   Mathematical model

First of all, it is necessary to make some assumptions about the pan-cooking of meat which will lead the mathematical model. The phenomena that will be taken into account in this process will be implemented in the software COMSOL Multiphysics 5.2a. The following assumptions has been made: (1) meat was considered as a continuum biphasic (liquid-solid) porous material. For simplicity, the structure of the meat was assumed to be homogeneous, since in this case, the majority of the meat does not reach very high temperatures so that the existence of larger pores on the surface can be neglected. (2) Due to the rubbery nature of the meat, it was addressed as a hyper-elastic material in which the total volume change was equal to the volume of moisture loss and consequently the solid matrix remained saturated. (3) The temperature was assumed to be the same for the two phases. (4) The moisture flow due to the pressure gradient caused by the shrinking connective tissue on the aqueous solution in the extracellular void followed Darcy's law, (5) Water evaporates on the surface of the meat which is in contact with the pan (Moya et al., 2021b).

Since the distinction of different phases in the meat is made, it is convenient to introduce the volume fraction $\phi_\alpha$ for each phase:

$$\phi_\alpha = \lim_{V \to 0} \frac{V_\alpha}{V}, \qquad \alpha = s, f \tag{3.1}$$

where $V_\alpha$ is the volume occupied by the $\alpha$ phase (being $s$ the solid phase and $f$ the fluid one) and $V = V_s + V_f$ is the total volume. The volume fractions $\phi_\alpha$ in (3.1) satisfy the volume fraction condition $\phi_s + \phi_f = 1$. The density of the solid and fluid phase is related to its true density $\overline{\rho}_\alpha$:

$$\rho_\alpha = \overline{\rho}_\alpha \phi_\alpha, \qquad \alpha = s, f \tag{3.2}$$

$\boldsymbol{x} = \boldsymbol{\chi}(\boldsymbol{X}, t) : \Omega_0 \times \mathbb{R} \rightarrow \mathbb{R}^3$ denotes the motion mapping which describes the kinematics of the biphasic media, and with $\boldsymbol{F}$ the associated deformation gradient. For representig a measure of the deformation, $\boldsymbol{X}$ and $\boldsymbol{x}$ define the respective positions of a particle in the reference $\Omega_0$ and current $\Omega$ configurations such that $\boldsymbol{F} = \frac{d\boldsymbol{x}}{d\boldsymbol{X}}$. $J \equiv det\boldsymbol{F}$ is the the Jacobian of the motion that provides the ratio between the volume in the present configuration and the volume in the reference configuration. The following kinematic decomposition made in Flory (1961) is made, in order to define volumetric and deviatoric responses in the nonlinear range:

$$\boldsymbol{F} = J^{\frac{1}{3}} \bar{\boldsymbol{F}}, \qquad \bar{\boldsymbol{F}} = J^{-\frac{1}{3}} \boldsymbol{F} \tag{3.3}$$

$$\boldsymbol{C} = \boldsymbol{F}^T \boldsymbol{F}, \qquad \bar{\boldsymbol{C}} = J^{-\frac{2}{3}} \boldsymbol{C} = \bar{\boldsymbol{F}}^T \bar{\boldsymbol{F}} \tag{3.4}$$

where $J^{\frac{1}{3}}$ and $\bar{\boldsymbol{F}}$ represent the volumetric and distortional components, respectively. $\bar{\boldsymbol{F}}$ and $\bar{\boldsymbol{C}}$ are the modified deformation gradient and the modified right Cauchy-Green tensors.
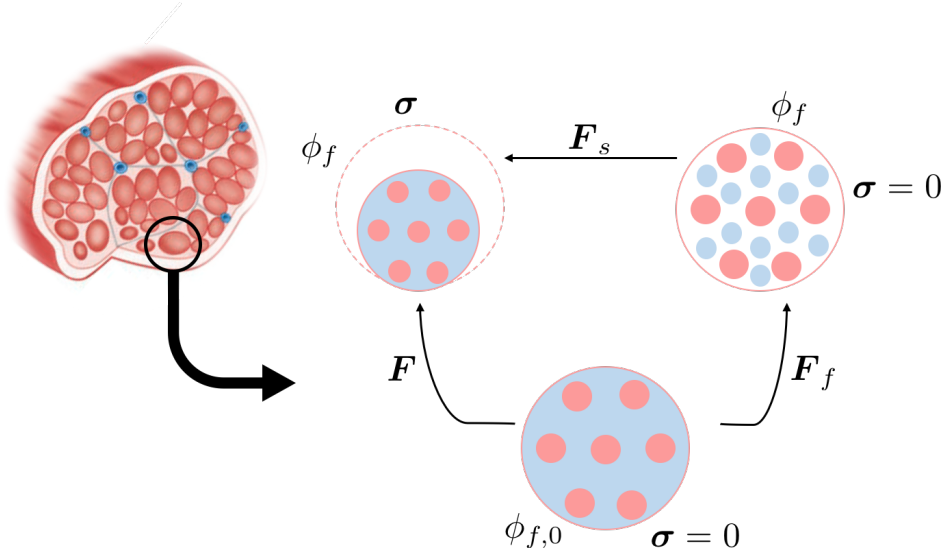


Figura 3.1: Modeling the moisture loss and deformation of the meat using a fictitious intermediate step. Quasi-static equilibrium was considered ($\nabla \boldsymbol{\sigma} = 0$ with $\boldsymbol{\sigma}$ being the Cauchy stress tensor) and the deformation gradient tensor $\boldsymbol{F}$ was decomposed multiplicatively in two parts associated with the water volume change, $\boldsymbol{F}_f$, and the elastic deformation of the solid phase $\boldsymbol{F}_s$ (Moya et al., 2021b).

As the deformation of the meat due to temperature effects is small, it can be neglected. In this manner, the moisture loss and the deformation of the meat can

be modelled as two fictitious processes (Vujosevic and Lubarda, 2002a, Dhall and Datta, 2011, Moya et al., 2021b), as is observed in Fig. 3.1, using a multiplicative decomposition of the deformation gradient tensor $\boldsymbol{F}$ with $\boldsymbol{F}_f$ the deformation associated with water volume changes and ($\boldsymbol{F}_s$) the elastic deformation of the solid phase:

$$\boldsymbol{F} = \boldsymbol{F}_f \boldsymbol{F}_s \tag{3.5}$$

The volumetric part of the elastic tensor could be written as a function of the deviatoric part taking the Jacobian as $\boldsymbol{F}_s = J_s^{1/3} \bar{\boldsymbol{F}}_s$, whereas the water loss implies only a pure volumetric process $\boldsymbol{F}_f = J_f^{1/3} \boldsymbol{I}$, being $\boldsymbol{I}$ the identity matrix (Moya et al., 2021b). Through Eq. (3.4), strain measures can be obtained for both solid and fluid phases. The modified right Cauchy-Green tensor for the solid phase $\bar{\boldsymbol{C}}_s = \bar{\boldsymbol{F}}_s^T \bar{\boldsymbol{F}}_s$ will be used later for constitutive modelling.

Due to the absence of body forces and accelerations, the assumption of quasi-static equilibrium equation $\nabla \boldsymbol{\sigma} = 0$, with $\boldsymbol{\sigma}$ being the total Cauchy stress, can be made, since the linear momentum for the bulk material is kept. The symmetry of this stress tensor is also a consequence of the angular momentum conservation. The Cauchy stress tensor can be expressed as the sum of partial solid stress and the partial fluid stress:

$$\boldsymbol{\sigma} = \hat{\boldsymbol{\sigma}}_s + \hat{\boldsymbol{\sigma}}_f \tag{3.6}$$

where

$$\hat{\boldsymbol{\sigma}}_s = \phi_s \boldsymbol{\sigma}_s \qquad \text{and} \qquad \hat{\boldsymbol{\sigma}}_f = \phi_f \boldsymbol{\sigma}_f = -\phi_f p_f \boldsymbol{I} \tag{3.7}$$

$p_f$ being the pore fluid pressure.

Because of the rubbery nature of meat, the behaviour of it during the cooking process has been approximated to a cuasi-incompressible isotropic hyperelastic model. The strain energy function is defined as a decoupled representation of the strain energy, it is based on kinematic assumption (3.4):

$$\Psi_s(\boldsymbol{C}_s) = \Psi_s^{vol}(J_s) + \bar{\Psi}_s(\bar{\boldsymbol{C}}_s) \tag{3.8}$$

where $\Psi_s^{vol}$ describe the volumetric elastic response and $\bar{\Psi}_s(\bar{\boldsymbol{C}}_s)$ the isochoric elastic response of material.

The beef meet has been modeled by a quasi-incompressible Neo-Hookean material model:

$$\Psi_s\left(\boldsymbol{C}_s\right) = \frac{K}{2}\left(J_s - 1\right)^2 + \frac{G'}{2}\left(\bar{I}_1 - 3\right) \tag{3.9}$$

where $K$ and $G'$ are the bulk and the shear elastic modulus and $\bar{I}_1 = \mathrm{tr}\bar{\boldsymbol{C}}_s$ is the first invariant of the modified (deviatoric) right Cauchy-Green tensor, $\bar{C}_s$.

The entropy inequality allows us to obtain the second Piola-Kirchhoff stress tensor as the derivative of the strain energy in a non-dissipative process. $\boldsymbol{S} - \boldsymbol{S}$ consists of a volumetric contribution, $\boldsymbol{S}_{s,vol}$, and a purely deviatoric contribution $\bar{\boldsymbol{S}}_s$:

$$\boldsymbol{S}_s = 2\frac{\partial \Psi(\boldsymbol{C}_s)}{\partial \boldsymbol{C}_s} = \boldsymbol{S}_{s,vol} + \bar{\boldsymbol{S}}_s = J_s p_s \boldsymbol{C}_{\boldsymbol{s}}^{-1} + J_s^{-\frac{2}{3}}(\mathbb{I} - \frac{1}{3}\boldsymbol{C}_s^{-1} \otimes \boldsymbol{C}_s) : \widetilde{\boldsymbol{S}}_s \tag{3.10}$$

where $p_s$ is the hydrostatic pressure and $\widetilde{\boldsymbol{S}}_s$ the modified second Piola-Kirchhoff stress tensor:

$$p_s = \frac{d\Psi_{s,vol}(J_s)}{dJ_s} \qquad\qquad \widetilde{\boldsymbol{S}}_s = 2\frac{\partial \bar{\Psi}_s(\bar{\boldsymbol{C}}_s)}{\partial \bar{\boldsymbol{C}}_s} \tag{3.11}$$

The explicit expression for the second Piola-Kirchhoff stress tensor, as a function of the defined invariant, $\bar{I}_1$, using the Neo-Hookean model is:

$$\boldsymbol{S}_s = J_s p_s \boldsymbol{C}_s^{-1} + 2\left[\frac{\partial \bar{\Psi}_s}{\partial \bar{I}_1}\boldsymbol{I} - \frac{1}{3}\left(\frac{\partial \bar{\Psi}_s}{\partial \bar{I}_1}\bar{I}_1\right)\boldsymbol{C}_s^{-1}\right] \tag{3.12}$$

The Cauchy stress tensor $\boldsymbol{\sigma}_s$ is $1/J_s$ times the push-forward of $\boldsymbol{S}_s$ ($\boldsymbol{\sigma}_s = J_s^{-1}\boldsymbol{\chi}_*(\boldsymbol{S}_s)$) so, from (3.10), we obtain:

$$\boldsymbol{\sigma}_s = p_s\boldsymbol{I} + \frac{2}{J_s}dev\left[\bar{\boldsymbol{F}}_s\frac{\partial \bar{\Psi}_s(\bar{\boldsymbol{C}}_s)}{\partial \bar{\boldsymbol{C}}_s}\bar{\boldsymbol{F}}_s^T\right] = p_s\boldsymbol{I} + \frac{2}{J_s}\left(\frac{\partial \bar{\Psi}_s}{\partial \bar{I}_1}\bar{\boldsymbol{b}}_s - \frac{1}{3}\frac{\partial \bar{\Psi}_s}{\partial \bar{I}_1}\bar{I}_1\boldsymbol{I}\right) \tag{3.13}$$

with $\boldsymbol{I}$ being the second-order identity tensor and $dev$ the deviator operator in the spatial description and $\bar{\boldsymbol{b}}_s = \bar{\boldsymbol{F}}_s^T\bar{\boldsymbol{F}}_s$ the modified left Cauchy-Green tensor.

In this way, the product density in the deformed configuration $\rho = \rho(t)$ is:

$$\rho = \phi_s\bar{\rho}_s + \phi_f\bar{\rho}_f = \rho_s + \rho_f \tag{3.14}$$

Once at this point, the mass balance for both phases can be defined as:

$$\frac{\partial(\phi_s\bar{\rho}_s)}{\partial t} + \nabla\left(\phi_s\bar{\rho}_s\boldsymbol{v}_s\right) = 0 \tag{3.15}$$

$$\frac{\partial(\phi_f\bar{\rho}_f)}{\partial t} + \nabla\left(\phi_f\bar{\rho}_f\boldsymbol{v}_s\right) + \nabla\boldsymbol{n}_f = 0 \tag{3.16}$$

where $\boldsymbol{v}_s$ corresponds to the absolute velocity of the solid phase and $\boldsymbol{n}_f$ is the water mass flux, described later. No evaporation effect is considered in Eq. (3.16) because water is assumed to evaporates only on the surface.

Considering these hypotheses, the meat only shrinks due to the moisture lost, because no external loads are applied. $V(t)$ is the total volume of the product and $\phi_{f,0}$ the initial volume fraction of the fluid, so, the following balance could be established:

$$V(t) - V_0 = \phi_f V(t) - \phi_{f,0}V_0 \tag{3.17}$$

The solid matrix is always saturated with water, therefore, the product porosity coincides with the volumetric fraction of the fluid $\phi_f$. The porosity value can be calculated at each instant of time considering the solid skeleton of the product incompressible or quasi-incompressible ($J_s \approx 1$):

$$\phi_f(t) = 1 - \frac{1 - \phi_{f,0}}{V(t)/V_0} = 1 - \frac{1 - \phi_{f,0}}{J(t)} \tag{3.18}$$

Thus, the Jacobian associated with the fluid $J(t)$ is a state function which depends on its own content within the meat.

If same temperature fot all phases is assumed, The heat transfer process inside the product can be modeled with a unique energy balance equation for the entire product:

$$(\rho C_p)\frac{\partial T}{\partial t} + (\boldsymbol{n}_f \cdot \nabla(C_{p,w}T)) = \nabla \cdot (k_p \nabla T) \tag{3.19}$$

where $C_p$ and $C_{p,w}$ are the specific heat of the product and the water, respectively, and $k_p$ is the thermal conductivity of the product.

For processing the water flows in a porous medium due to the pressure gradient inside the solid matrix an gravity, Darcy's law is used. The water mass flux is defined as:

$$\boldsymbol{n}_f = -\rho_f \frac{\kappa}{\mu}(\nabla p_f - \rho_f\mathbf{g}) \tag{3.20}$$

where $\kappa$ is the permeability of the medium and $\mu$ its dynamic viscosity. Since the effect of gravity is negligible and $p_f$ is the swelling pressure which is proportional to the difference between the actual $\rho_f$ and the equilibrium water concentration $\rho_{f,eq}(T)$ (Dhall and Datta, 2011), the swelling pressure can be expressed as:

$$p_f = \vartheta(\rho_f - \rho_{f,eq}(T)) \tag{3.21}$$

where $\vartheta$ is a constant of proportionality. Introducing this relation in (3.20):

$$\boldsymbol{n}_f = -(D_f\nabla\rho_f - D_{f,T}\nabla T) \tag{3.22}$$

where $D_f = \rho_f\frac{\kappa}{\mu}\vartheta$ is the diffusivity due to the water gradient concentration and $D_{f,T} = \rho_f\frac{\kappa}{\mu}\vartheta\frac{\partial\rho_{f,eq}}{\partial T}$ is the diffusivity due to the temperature gradient, both will be parameters determined through the model.

With the definition of the swelling pressure and taking into account that there is no internal steam generation, the mass conservation equations are reduced only to that of liquid water:

$$\frac{\partial\phi_f\bar{\rho}_f}{\partial t} + \nabla\left(\phi_f\bar{\rho}_f\boldsymbol{v}_s\right) = \nabla\cdot\left(D_f\nabla\left(\phi_f\bar{\rho}_f\right) + D_{f,T}\nabla T\right) \tag{3.23}$$

## 3.3.  Material and experimental methods

To determine the meat properties used as inputs in the finite element model and to be able to validate the numerical results, several experimental tests have been carried out, both for the determination of these properties and for meat pan-cooking itself. For all experimental tests, *longissimus dorsi* muscles from two Asturiana de los Valles heifers (1 year old) 7 days post mortem were obtained from a local butcher the same day on which these experimental tests were performed.

For the pan cooking tests, eighteen steaks of three different thicknesses ($19 \pm 2$ mm, $26 \pm 2$ mm and $34 \pm 2$ mm), were cut perpendicular to the longitudinal axis of the middle part of these loins. So, for each thickness of steak, three pieces of approximately $81 \pm 21$ mm long and $26 \pm 1$ mm wide were obtained. The steaks of 19 mm weighed $43.7 \pm 6.7$ g, steaks of 26 mm, $51.9 \pm 12.9$ g and, steaks of 34 mm $71.9 \pm 16.3$ g.

For obtaining the water holding capacity and the rheological measurements, the loin of the heifer was sliced in a piece of 4 mm thickness and it was cut into pieces of about 8 g.

## 3.3.1. Meat properties

Not all properties of the meat were experimentally obtained. The density, the heat capacity and the heat conductivity of the solid phase of the meat were calculated as a function of temperature and composition, as in Choi and Okos (1986b). The mass fractions of the protein and $x_{\text{prot}}$ and fat $x_{\text{fat}}$ were experimentally obtained for the case of our meat sample, introduced as their composition in the following equation (Nesvadba, 2014):

$$\overline{\rho}_s(T) = \left( \frac{x_{\text{prot}}}{\overline{\rho}_{\text{prot}}(T)} + \frac{x_{\text{fat}}}{\overline{\rho}_{\text{fat}}(T)} \right)^{-1} \tag{3.24}$$

For each component, protein and fat, specific heat was defined. Then, the specific heat of the meat $C_{p,s}(T)$ was calculated using a mass fractions average mixing rule:

$$C_{p,s}(T) = x_{\text{prot}} C_{p_{\text{prot}}}(T) + x_{\text{fat}} C_{p_{\text{fat}}}(T) \tag{3.25}$$

An isotropic thermal conductivity in the product is assumed, which is between two limit models: i) The perpendicular model considering all the constituents in layers perpendicular to the flow of heat $\frac{1}{k_\perp(T)} = \sum_i \frac{\phi_i}{k_i(T)}$ and ii) The parallel model, in which the constituents are arranged as parallel layers $k_\parallel(T) = \sum_i \phi_i k_i(T)$. In this manner, the thermal conductivity of the meat is calculated as:

$$k_p(T) = g k_\perp(T) + (1 - g) k_\parallel(T) \tag{3.26}$$

where $g$ is a number between zero and one (Nesvadba, 2014, van der Sman, 2013).

## 3.3.2. Water holding capacity

The water holding capacity (WHC) is the ability of the meat to resist the removal of liquid caused by protein denaturation during cooking. In this study, this property was measured following the procedure described by Goñi and Salvadori (2011).

Slices of meat packaged into plastic bags (Digiterm S–150, JP Selecta, Abrera, Spain) were immersed in a thermostatic bath at a given temperature (from 30 °C to 100 °C) and waiting for equilibrium (30 min until there was no more weight loss) in order to analysis this effect. In this experimental test ten replicas were used for each temperature and the results were expressed as kg water/kg dry material. The process of this test can be seen in Fig. 3.2.



Figura 3.2: Meat water holding capacity test process.

### 3.3.3.   Rheological measurement

A Physica MRC 301 rheometer (Anton Paar GmbH, Graz, Austria), equipped with serrated parallel plate geometry (50 mm, 4 mm gap) and a temperature controller ($\pm 0.5$ °C) was used to measure the rheological characteristics of circular beef samples with a thickness of $4 \pm 0.5$ mm and a diameter of $50 \pm 2$. Dynamic oscillating analyses were performed at a frequency of 2 Hz and a constant stress of 3 Pa. These values were chosen within the linear viscoelastic region that was determined by performing frequency sweeps (0.1–10 Hz) and stress sweeps (0.1–1000 Pa). Again, for temperature-dependent results, the tests were carried out increasing the sample temperature from 25 °C to 100 °C with steps of 5 °C, holding each temperature step for 3 min (enough to ensure no further changes in the measurement). The results for the storage modulus ($G'$) and phase angle, the ratio of loss modulus to storage modulus ($\phi$), with temperature were recorded by the rheometer software using five replicas.

### 3.3.4.  Cooking procedure

Each piece of meat cut for the cooking tests was at an initial temperature of 20 °C. The pieces were individually cooked on a multilayer 210 mm diameter, 5.5 cm deep round frying pan (WMF, WMF Group GmbH, Geislingen an der Steige, Germany). This pan consists of three layers: 0.6 mm of steel at the bottom, 3.5 mm of aluminium in the middle, and 0.8 mm of steel with a Teflon non stick coating at the top (Fig. 3.3.a). For the cooking, an induction hob (BOSCH Schott Ceran PXY675DW4E/01 model, BSH, Munich, Germany) was used with frying sensor at level 5. When the hob is turned on, the temperature on the surface of the pan increases progressively until it stabilizes. This transition period lasts approximately 110 s. When the thermographic images taken with an infrared thermal imager (875-2 model, Testo, Lenzkirch, Germany) indicated that a stable temperature of 215 ± 3 °C has been reached, the meat was added to the pan. When this happens, the temperature drops slightly and recovers quickly, so it can be considered that cooking occurs at a constant temperature at the pan of 215 °C. Three degrees of doneness were carried out: very rare, medium rare and done, corresponding to cooking times of 180 s, 300 s, and 420 s, respectively, for the pieces of 19 mm thickness. For the other thickness (26 mm and 34 mm), the cooking times were established by the model predictions once this thickness was adjusted to experimental tests. The samples of meat were turned over at two thirds of the total cooking time. For each degree of doneness and thickness, six pieces obtained from steaks located in the loin at different longitudinal positions were cooked.

For measuring meat weight, a balance placed under the induction hob (DS30K0.1L, Kern & Sohn, Balinger-Frommern, Germany) with a precision of 0.1 g was used. Data was recorded every 1s in a measurement range up to 30 kg. For measuring the core temperature, a penetration *T type*, 1.5 mm diameter thermocouple connected to a data logger (177-T4, Testo, Lenzkirch, Germany), as shown in Fig. 3.3 was used. The data were presented as the mean ± standard deviation.

## 3.4.  Finite element model

With the purpose of reproduce the cooking process described in the previous section, a 3D computational model was developed in the software COMSOL Multiphysics 5.2a. This model consists of two different parts: an aluminium pan with a diameter of 210 mm and 5 mm thickness and a beef steak (see Fig. 3.4). The beef sample was modeled according to the geometry of the experimental tests through a 3D rectangular

(a)                 (b)
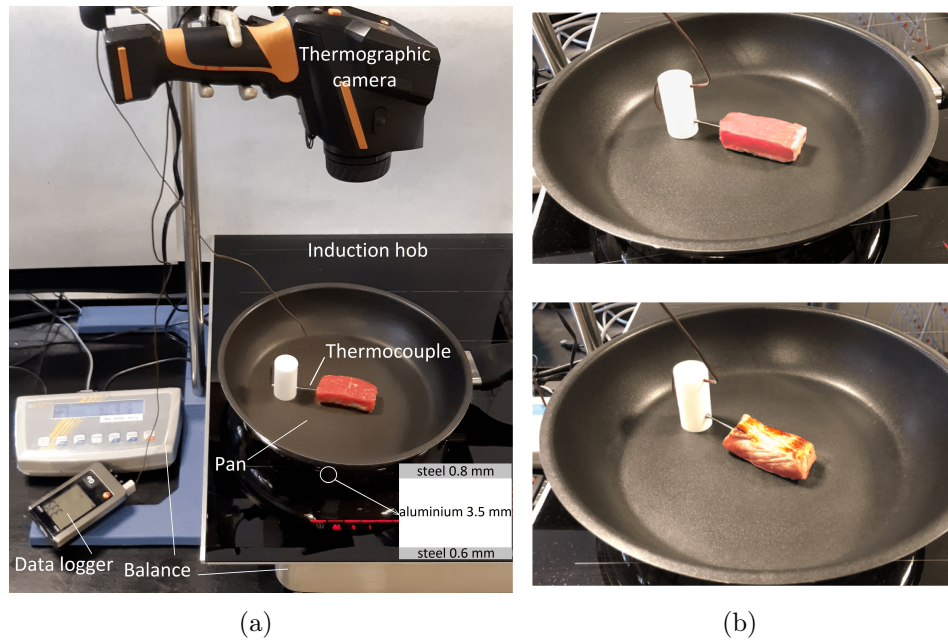
Figura 3.3: a) Experimental setup for temperature and weight loss measurement during the cooking process. b) Evolution of the geometry of the steak along the test comparing the beginning of the process (top) and the end (bottom) for a done doneness degree.

cuboid object. To reproduce the turning over of the steak, considering the insignificant relevance of gravity in this problem, two pans were considered. First, the bottom face of the steak is heated by a pan. Secondly, the top face of the same steak is heated by a second one. In order to simplify the process and to avoid problems when solving, it has been considered that the top and the bottom steak surfaces remain flat during the entire cooking time.

Due to the symmetry of the problem, a quarter of the geometry was recreated. This geometry was meshed with hexahedral elements using a quadratic approximation for mass transfer and temperature for the meat, and with tetrahedral elements for the pan. To optimize the number of elements, a mesh sensitivity analysis was carried out to establish the mesh size.

Many models as degrees of doneness were created varying the cooking times. The boundary conditions on the top and bottom surfaces were reversed after turning over by activating the contact of the upper surface of the meat with the pan and deactivating the contact of the lower surface.
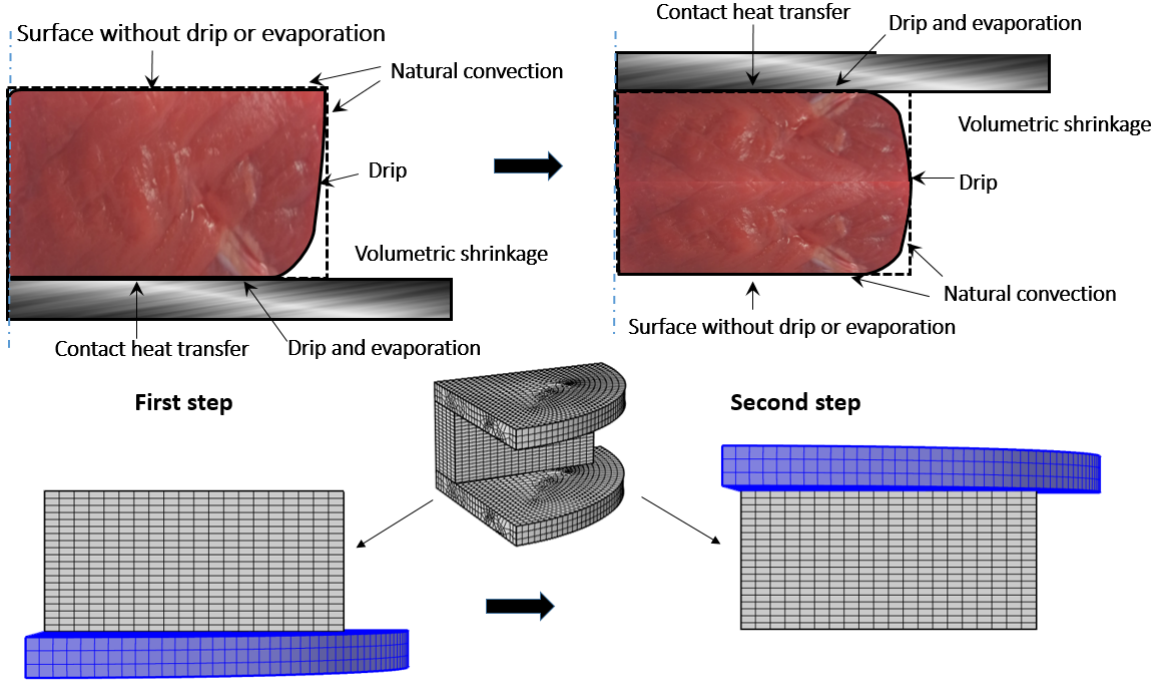
Figura 3.4: Finite element model and strategy defined for the turned over of the meat.

## 3.4.1.  Initial and boundary conditions

Since experimental temperature in the pan throughout the cooking time remains constant, an initial temperature condition of 215 °C is set on the surface of the model pan. Equally, a uniform initial temperature for the meat of 20 °C at the beginning of the simulation is established. The contact equation between the pan and the meat and the heat transfer general equation for the two faces are defined as:

$$-k_{pan} \left. \frac{\partial T}{\partial z} \right|_{z_{pan}=0} = -k_p \left. \frac{\partial T}{\partial z} \right|_{z_{meat}=0} = H_c \left( T_{pan} - T_{surf} \right) \tag{3.27}$$

$$q_{surf} = h(T_{amb} - T_{surf}) - \lambda n_{f,surf} - \mathbf{n}_f C_{p,w} T \cdot \mathbf{N}_{surf} \tag{3.28}$$

where $T_{pan}$, $T_{surf}$ are the temperature of the pan and the temperature of the meat on the surface where the boundary condition is being evaluated, $k_{pan}$ is the conductivity of the pan and $\mathbf{N}_{surf}$ is the surface normal. The parameter $H_c$ is the thermal conductance between both surfaces, which has been obtained computationally. This thermal conductance is the responsible of regulating the heat flow received by the meat through the contact heating surface. This parameter has a great importance for this cooking method, being therefore one of the most remarkable objects of the study. $h$ is the thermal convection coefficient. $T_{amb}$ is the temperature of the air surrounding the

meat, $\lambda$ is the vaporization latent heat and $n_{f,surf}$ the magnitude of the evaporation flux. The water holding capacity falls very quickly when temperature increases. It drops at a faster rate than water loss by evaporation, so, when meat is heated, the phenomenon of dripping appears (Hughes et al., 2014). On the surface of the meat in contact with the pan, where temperature is very high, phase change to steam and the dripping of liquid water were both included as boundary condition, while on the side walls only the dripping was considered. Neither of these two phenomena occur on the upper face. These conditions are reflected in the following equations. The steam flow in the evaporation process is given in Eq. (3.29) and the drip losses in Eq. (3.30):

$$n_{f,surf\ E} = h_m(\rho_{v,surf} - \rho_{v,amb}) \tag{3.29}$$

$$n_{f,surf\ D} = \mathbf{n}_f \cdot \mathbf{N}_{surf} - h_m(\rho_{v,surf} - \rho_{v,amb}) \tag{3.30}$$

where $h_m$ is the mass transfer coefficient by convection and $\rho_{v,surf}$ and $\rho_{v,amb}$ are the vapor density on the surface of the meat and the vapor density in the surrounding air, respectively, obtained by the ideal gas law.

## 3.4.2.   Mesh sensitivity
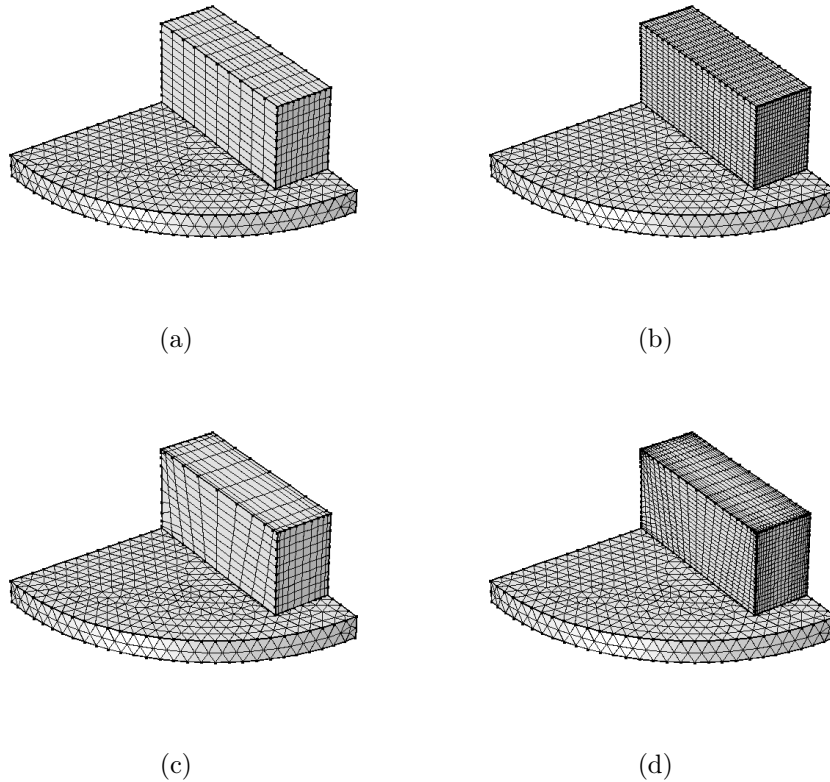


Figura 3.5: Sensitivity analysis mesh: a) regular mesh with less number of elements, b) regular mesh with more number of elements, c) mesh with smaller elements on the edges and less number of elements d) mesh with smaller elements on the edges and more number of elements

In order to know the most optimal type of mesh for the model, a mesh sensitivity analysis was performed before with two different mesh types and different element sizes. These type of meshes can be seen in Fig. 3.5 (only the bottom pan of the model is shown). Due to the meat water loss through the surface, a mesh with smaller elements on the edges of the meat has been considered. It could be possible that the mesh size in that region influences the loss weight of the meat during cooking. For a good validation of this influence, the study has been carried out in case of done degree of cooking, which has a longer cooking time. In every case the total number of degrees of freedom is 5 (the three displacements, the temperature and the water concentration). The number of elements and nodes for each mesh of Fig. 3.5 are shown in Table 3.1.

| Mesh | Number of elements | Number of nodes |
|------|--------------------|-----------------|
| (a)  | 5706               | 2631            |
| (b)  | 20231              | 12215           |
| (c)  | 7052               | 2788            |
| (d)  | 25003              | 12944           |

Table 3.1: Number of elements and nodes of each of the meshes considered in the sensitivity analysis.

### 3.4.3.  Parameters

The input parameters were obtained through experimental test measurements or from bibliography, while others were optimized through the model in order to fit the experimental results. These parameters are shown in Table 3.2.

| Name and description | Value | Source |
|----------------------|-------|--------|
| **Problem parameters** | | |
| $T_{amb}$ surrounding air temperature [°C] | 25 | Measured |
| $T_{pan}$ pan temperature [°C] | 215 | Measured |
| $P_{amb}$ environment pressure [kPa] | $1.013 \cdot 10^2$ | Measured |
| $H_c$ thermal conductance of pan-meat contact [W/(m² K)] | 120 | Computational |
| $g$ thermal conductivity parameter | 0.45 | Computational |
| | | |
| **Water properties** | | |
| $\overline{\rho}_f$ water density [kg/m³] | 997.2 | Choi and Okos (1986a) |
| $D_f$ water diffusivity [m²/s] | $1 \cdot 10^{-9}$ | Computational |
| $D_{f,T}$ water diffusivity due to temperature gradient [kg/(m s K)] | $D_f \cdot \frac{\partial \rho_{f,eq}}{\partial T}$ | Computational |
| $C_{p,f}$ water specific heat [KJ/(kg °C)] | $4.1289 - 9.0864 \cdot 10^{-5} \cdot T + 5.4731 \cdot 10^{-6} \cdot T^2$ | Choi and Okos (1986a) |
| $k_f$ water thermal conductivity [W/(m K)] | 0.57 | Choi and Okos (1986a) |
| $\lambda$ vaporization latent heat [J/kg] | $2.26 \cdot 10^6$ | Straub (1985) |
| $h_m$ mass transfer coefficient [m/s] | 0.008 | Computational |
| | | |
| **Meat properties** | | |
| $C_{p,s}$ meat specific heat [J/(kg K)] | $2.0082 + 1.2089 \cdot 10^{-3} \cdot T - 1.3129 \cdot 10^{-6} \cdot T^2$ | Choi and Okos (1986a) |
| $k_p$ product thermal conductivity [W/(m K)] | $1.7881 \cdot 10^{-1} + 1.1958 \cdot (10^{-3}) \cdot T - 2.7178 \cdot (10^{-6}) \cdot T^2$ | Choi and Okos (1986a) |
| WHC water holding capacity [kg water/kg dry material] | Fig. 3.6 | Measured |
| $G'$ storage modulus [kPa] | Fig. 3.7 | Measured |

Table 3.2: Model input parameters.

## 3.5.  Results and discussion

This section first shows the experimental results of the properties of the meat necessary for the development of the model. After that, the result of the sensitivity analysis of the mesh is indicated. Then, the results of the evolution of the temperature in the core of the meat and its weight loss are shown, both experimentally and numerically for its comparison and validation. Lastly, different thicknesses of meat are introduced in the model in order to set the cooking times regarding the degree of doneness desired.

## 3.5.1.   Meat properties as a function of temperature

### 3.5.1.1.   Water holding capacity

WHC as a function of temperature is shown in Fig.3.6. As said before, the WHC diminishes as the temperature increases since proteins suffer the thermal denaturation, provoking the reduction of the water retention capacity of the meat. The evolution of WHC with temperature follows a sigmoidal shape, as previously described by Goñi and Salvadori (2011) and van der Sman (2007). Using the Association of Official Analytical Chemists (AOAC) method no. 950.46 the experimental values of WHC were determined. These values have a great coincidence with those of other authors for beef, although the values can vary depending on the muscle (Kondjoyan et al., 2013). The sarcomere length is known to have a deep effect on WHC. The following function was fitted to the experimental data:

$$\text{WHC}(T) = c_i - \frac{a_1}{1 + a_2 exp\left(-a_3\left(T - T_4\right)\right)} \tag{3.31}$$

where $c_i = 2.986$, $a_1 = 1.69$, $a_2 = 0.56$, $a_3 = 0.08309$ and $T_4 = 66.76$ °C were estimated by a non-linear regression using the Levenberg-Marquardt method ($R^2 = 0.9853$). The equilibrium water concentration is related to the WHC through the equation $\rho_{f,eq}(T) = \text{WHC}(T)\rho_s$.
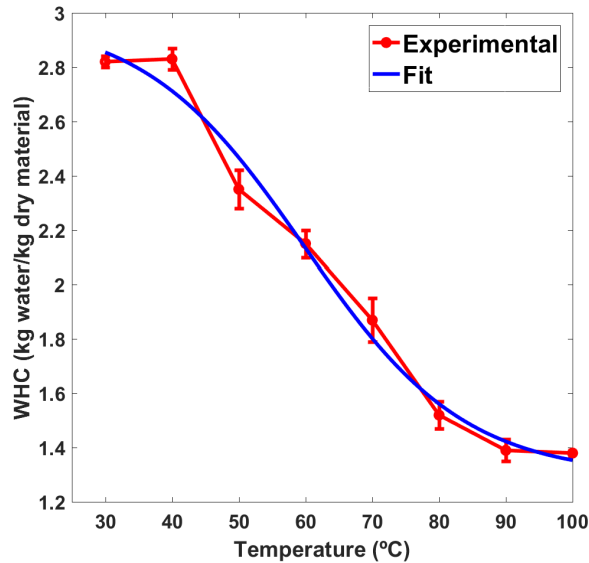


Figura 3.6: Water Holding Capacity as a function of temperature $T$ for beef meat.

### 3.5.1.2.   Rheological properties

The effect of temperature on the storage modulus $G'$ and the phase angle $\phi$ for the beef, is shown in Fig. 3.7. They were obtained from the experimental tests described in section 3.3.3. Firstly, the storage modulus decreases slightly until reaching a minimum value at 55 °C. Consecutively it increases markedly up to 40 kPa from 65 °C to 80 °C, and finally it decreases at temperatures above 80 °C. The increase in the storage modulus between 65 °C to 80 °C is due to the contraction of the connective tissue, resulting in an increase in the elasticity of the meat. The phase angle diminishes over the whole temperature range tested, it suffers a greater decrease from 50 °C to 60 °C. The values obtained by Tornberg (2005) and Rabeler and Feyissa (2018a) for chicken breast are similar between them, but they differ from those shown in Fig. 3.7 because they correspond to different muscles and species.
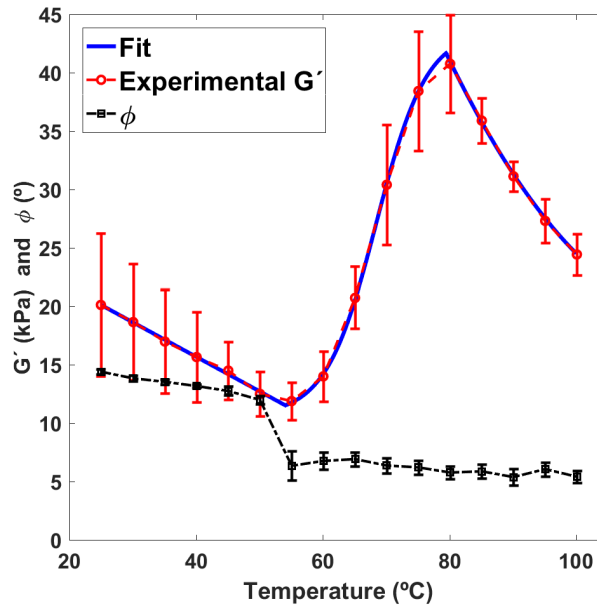


Figura 3.7: Storage modulus, $G'$ (kPa), and phase angle, $\phi$ (°), for beef *M. Longissimus dorsi* as a function of cooking temperature. Experimental values indicated by symbols and estimated values by the blue line.

For temperatures between 30 °C and 100 °C the storage modulus is defined by a piecewise Eq. (3.32) :

$$G'(T) = \begin{cases} G_a \cdot T + G_b & \text{if} \quad 30°C \leq T < 55°C \\[2ex] G_c + \frac{G_d}{(1+\exp{(-G_e(T-G_f))}} & \text{if} \quad 55°C \leq T < 80°C \\[2ex] G_g \cdot T^2 + G_h \cdot T + G_i & \text{if} \quad 80°C \leq T < 100°C \end{cases} \qquad (3.32)$$

where $G_a = -0.8816$ kPa °C$^{-1}$, $G_b$=82.06 kPa, $G_c$=36.40 kPa, $G_d$=85.32 kPa, $G_e$=0.3386, $G_f$=68.04, $G_g$=0.05647 kPa °C$^{-2}$, $G_h$=-12.74 kPa °C$^{-1}$ and $G_i$=781.8 kPa, values obtained by adjusting the experimental results obtaining a $R^2$ of 0.9998. Fig. 3.7 shows the experimental value of the storage modulus and its fitting.

### 3.5.1.3. Mesh sensitivity analysis

The mesh sensitivity analysis has been allowed us to select the mesh which will be used in the following simulations. As it has been mentioned, the more longer time of cooking has been chosen for the analysis and it has been considered that the output variable that can be affected the most is the weight loss of the meat. For this reason, we have taken this variable as a reference when choosing the mesh, although it has also been verified that changes in temperature are not significant. The results of the weight loss of the meat for the different types of mesh described in section 3.4.2 are shown in Fig. 3.8 a. The weight loss does not vary between the regular mesh with fewer elements and the regular mesh with more elements. These results are only 1 % lower than those obtained with the meshes with smaller elements on the edges. These other two meshes present the same results too. The mesh does not affect the variation in temperature (Figure 3.8. b), and in terms of the loss of volume of the meat, it behaves in the same way as with the loss of water. Since the computation time is very different between models (20 minutes for a regular mesh with fewer elements, 1 hour and 30 minutes for the mesh with fewer elements but refined on the edges and more than 8 hours for the case of the two meshes with more elements), the regular mesh with fewer elements has been chosen for the other simulations (see Fig.3.5.a). The total number of elements, in this model, is 5706, 1000 hexahedral elements for the beef sample and the rest for the two pans of the model.
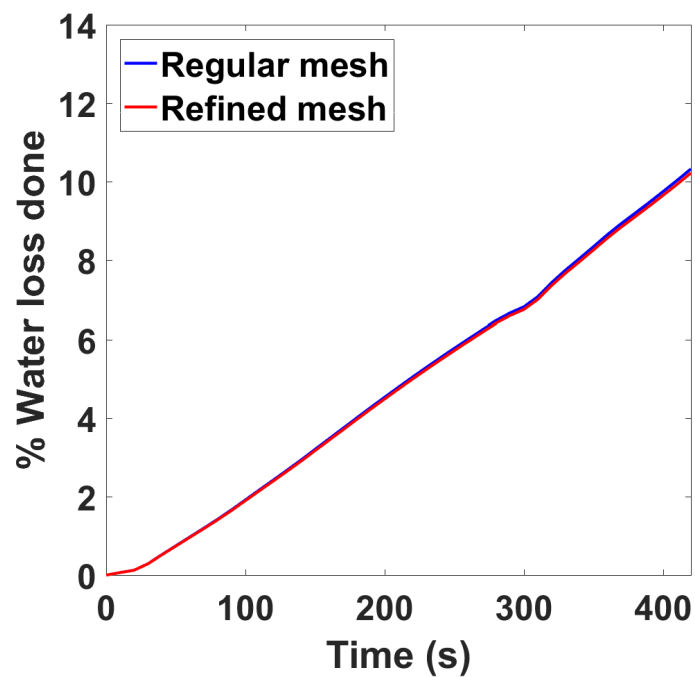
(a)
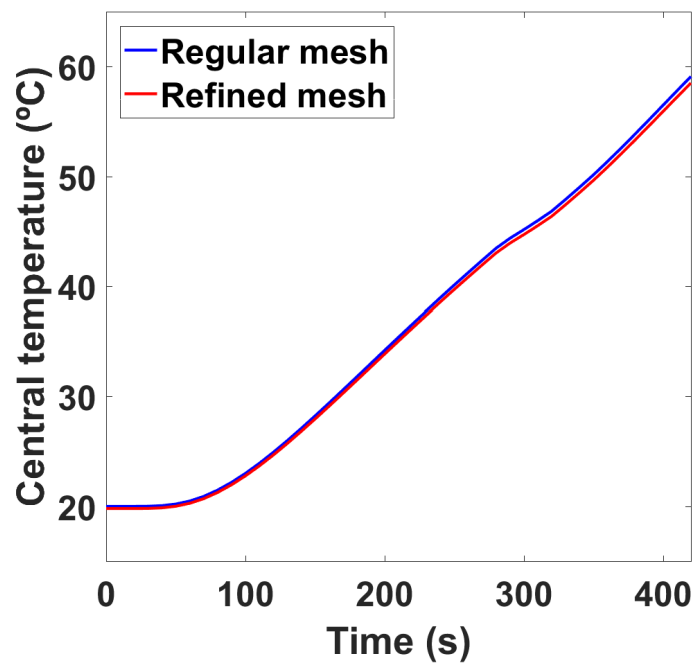


(b)

Figura 3.8: Comparison of the results of a) the weight loss of the meat and b) the central temperature of the meat for each type of mesh.

## 3.5.2.  Model fit: temperature and water loss for pieces of 19 mm

In order to validate the finite element model the temperature at the central point of the meat and the weigh loss obtained with the model are compared with the corresponding experimental results. In Fig. 3.9a. this comparison of the temperature at the central point for the three degrees of doneness is shown.



(a)



(b)



(c)
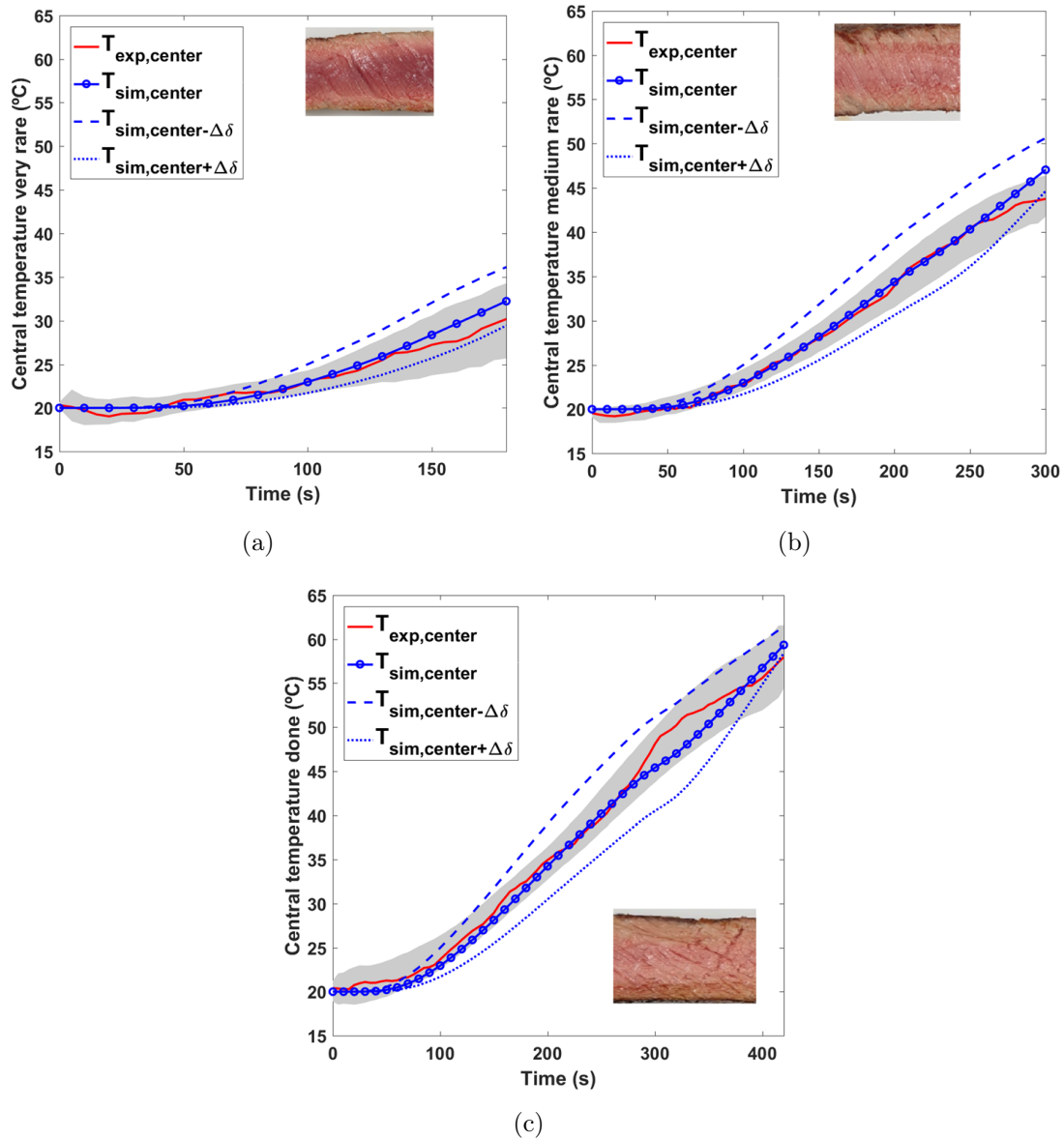
Figura 3.9: Central temperature evolution for a steak of 19 mm of thickness: a) very rare, b) medium rare, c) done cooking degree.

Since during the experimental tests the sensor may suffer deviations in its position, it is possible that differences in temperature measurements appear. These differences and others related to other influencing factors such as meat composition, are reflected

by the gray bands, which reflect the standard deviation of these measurements like in Figs. 3.9 to 3.15. Computational digressions were calculated considering a displacement of the thermocouple position of $\pm 1$ mm (see Fig. 3.10). For every degree of cooking, a linear behaviour after 80 s was observed. The maximum temperatures reached in the central point of the steak for the different times were 33 °C, 47 °C and 58 °C for 180 s (very rare), 300 s (medium rare) and 420 s (done), respectively. The Root Mean Squared Error, RMSE, obtained for these temperatures were: 2.16 °C (very rare), 3.56 °C (medium rare) and 4.57 °C (done). RMSE was calculated as square root of the sum of the squared differences between the predicted and experimental values divided by the number of data. Through the procedures described by the American Meat Science Association, AMSA (1995), the obtained temperatures of the different degrees of meat doneness, (55 °C-very rare, 60 °C-rare, 63 °C-medium rare, 71 °C-medium, 77 °C-done and 82 °C-well done) are very far from ours.
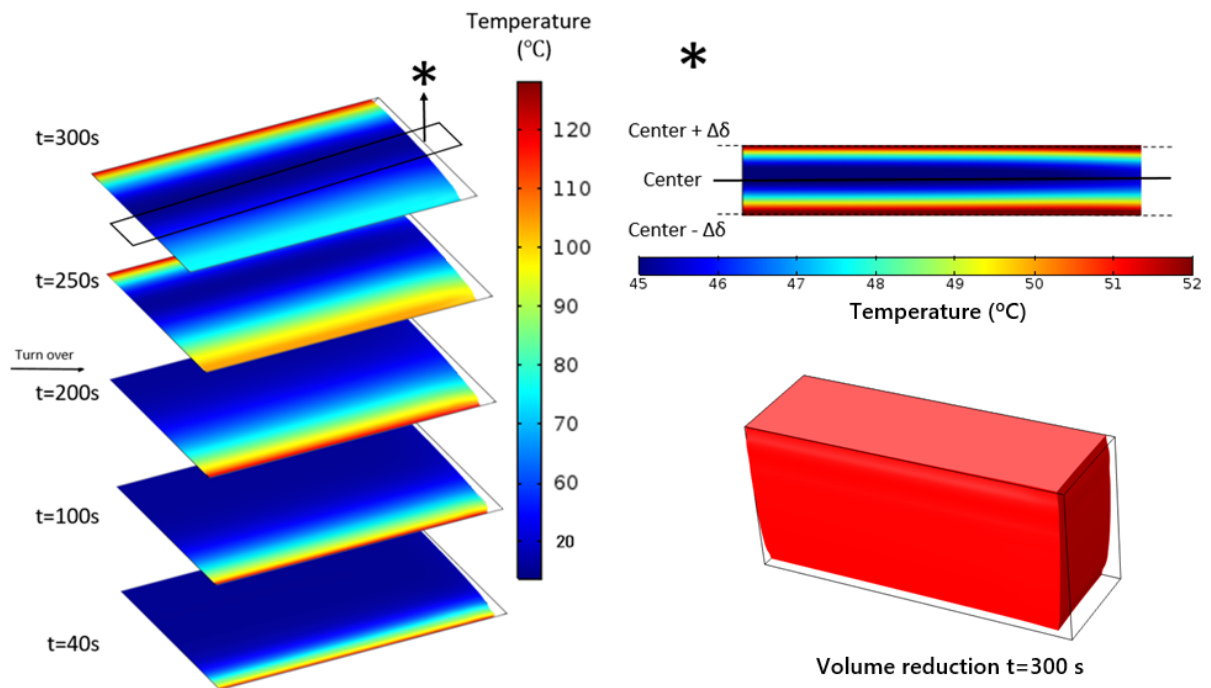


Figura 3.10: Temperature distribution in a cross section for different times in case of medium rare cooking degree and central section temperature gradient considering the sensor located at $\Delta \delta = \pm 1$ mm, and volume reduction.

Fig. 3.10 shows the temperature distribution in a cross section for different times of medium rare cooking degree. The temperature of the surface in contact with the pan is much higher (120 °C) than that of the meat core. This temperature is quickly reached and stabilizes only a few seconds after contact. When meat is turned over, this surface is no longer in contact with the pan and it starts to decrease. In this moment is the

other surface which suffers an increase in temperature, since it is now in contact with the heat source. When difference in temperature between the central point inside the steak and the central point of the surface in contact with the pan was similar to the difference of temperature at the moment of turning over the steak, the cooking process was stopped. It happens at 97 °C in case of very rare, at 93 °C for medium rare degree and at 87 °C in case of done degree. In this way, the time of turning over the steak coincides with two thirds of the total cooking time.

In Fig. 3.10 we can see the volume reduction of the steak and its change of shape for the medium rare degree of cooking too. At the beginning, small deformations are observed in the central part of the steak since it is the coldest area of the piece of meat, while the greatest deformations happen near the pan. As time progresses, this deformation extends to the central part until the moment of turning over the steak. In that moment, the maximum deformation occurs again in the face in contact with the pan. In case of medium rare degree, at 40 s of the beginning the volume reduction is around 1 % while at the end of the cooking (300 s) it is around 9 %. For done degree of cooking (420 s), meat suffers a final volume reduction of about 12 %. These volume reduction can be seen in Fig 3.12 too. The evolution of the shrinkage during cooking is due to the thermal denaturation of proteins, since it provokes an increasing rigidity of the myofibrillar structure. At temperatures from 40 °C to 60 °C transverse shrinkage occurs in the miofibrils attributed principally to myosin, and in the temperature range from 70 °C to 80 °C it is longitudinal and attributed fundamentally to actin (Hughes et al., 2014, Purslow et al., 2016). When this contraction takes place, the juice inside the meat is expelled.

The water loss evolution of the meat for the different cooking degrees is shown in Fig. 3.11. These cooking losses for the different cooking times were 4 %, 7 % and 10 % for 180 s (very rare), 300 s (medium rare) and 420 s (done), respectively. The RMSE for each degree of doneness is: 1.48 % (very rare), 2.08 % (medium rare) and 2.40 % (done). In case of the water loss, computational results fit optimally with the experimental ones, demonstrating a linear behavior with time in both cases. The research of Dhall and Datta (2011) mentions a water loss of 7 % for a cooking time of 300 s in patties, quite similar to our medium rare degree of cooking. Due to the minor role of collagen in the loss of water, it is not surprising that minced meat and whole meat have a similar behaviour regarding this loss (Hughes et al., 2014, Tornberg, 2005).

In Fig. 3.12 we can see the water concentration ($mol/m^3$) in the meat for the final moment of cooking in each degree of cooking. For every case, the meat mainly loses water through the surfaces that have been in contact with the pan. As the cooking time

increases, it is observed how the meat loses water concentration on these surfaces, due to a greater loss of it outward. In this Figure we can see the evolution of the shrinkage of the meat regarding the cooking degree. Changes in volume between cooking degrees are not very noticeable, varying by approximately 3 % from one to another. As mentioned, the meat loses volume not only due to the expelled juice due to the contraction of the meat fibers, but also for due to this contraction itself.



(a)

(b)

(c)
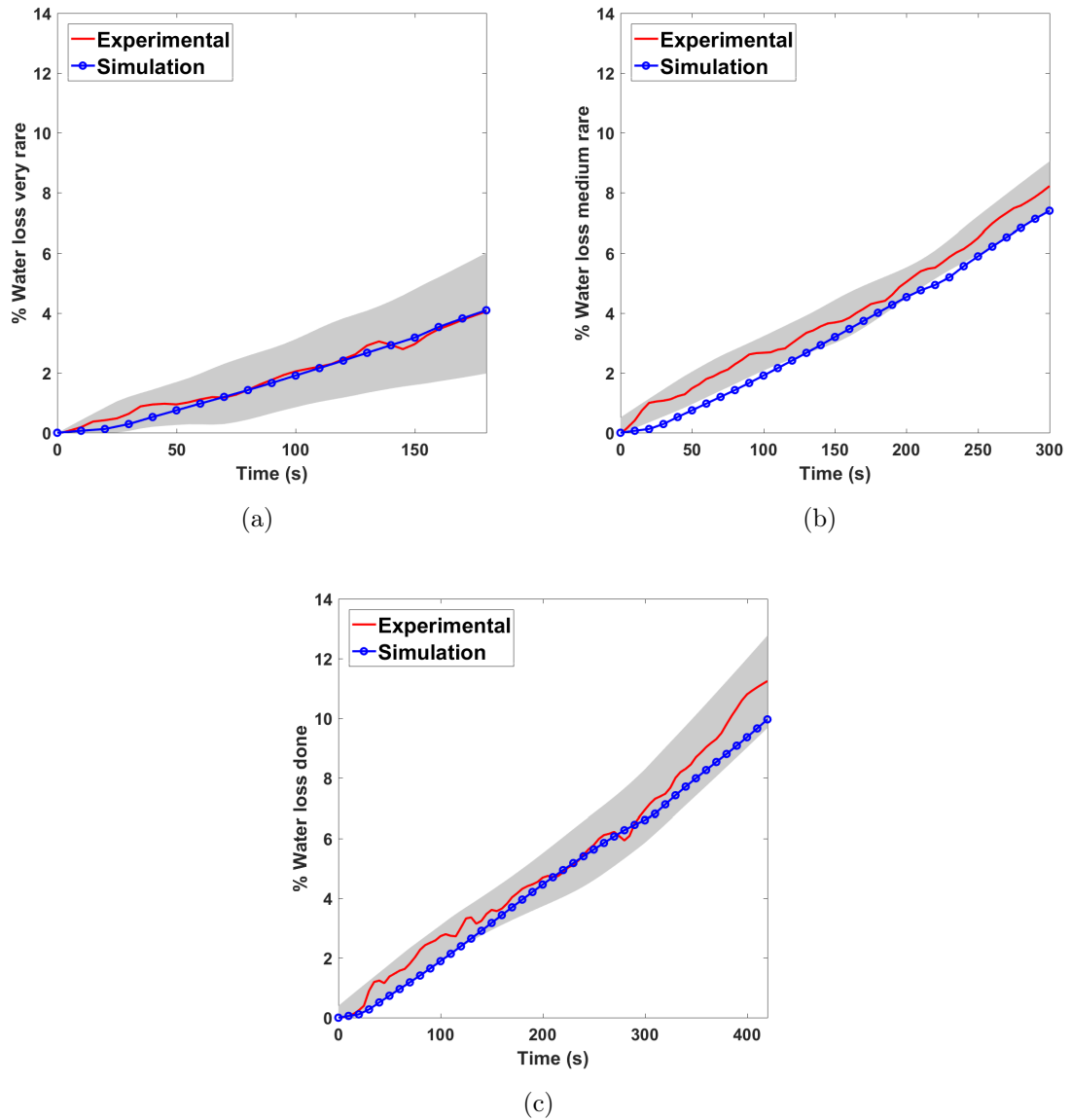
Figura 3.11: Water loss evolution for a steak of 19 mm of thickness: a) very rare, b) medium rare, c) done cooking degrees.

In Fig. 3.13 the final displacements of the meat in each direction for done cooking degree are shown. The maximum displacements occur on the y-axis. This direction coincides with the longitudinal direction of the miofibrils of the meat, where the main

shrinkage is taking place. In this direction the meat shrinks a maximum of 4 mm. This displacement is located at the short side corner of the steak. In x-axis the maximum shrinkage is located in the long side corner of the steak and it has a value of 2 mm. Finally, in z-axis displacements are hardly observed.
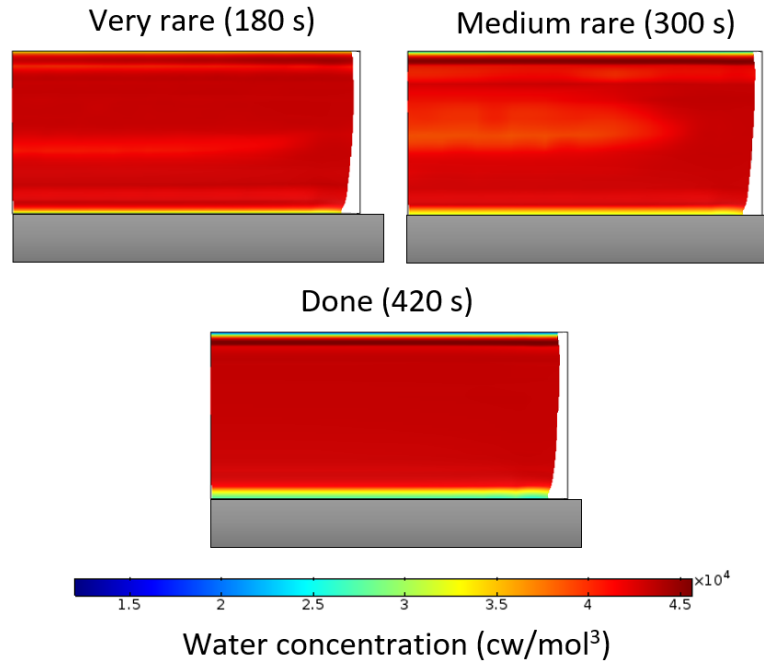


Figura 3.12: Water concentration $(\text{mol/m}^3)$ for each cooking degree at the end of the cooking process.

### 3.5.3.  Prediction of cooking times for different thicknesses of meat using water loss as indicator

One of the objectives of this study is to find an application for cooking systems, for example, providing assistance during cooking. Thus, it is very important to know the potential of the model to adapt to other cooking conditions. The thickness of the steak is a parameter that greatly affects to the final temperature acquired by the sample, being in addition one of the parameters that offers more variability during the user's cooking. According to the degree of cooking to be achieved, the cooking time for different thicknesses of meat has been calculated using the loss of water as a control variable. Experimental cooking tests were carried out with thicknesses of 26 mm and 34 mm in the same manner as with the 19 mm thickness. The time of turning over the steak and the final time of cooking were fixed at the moment when the meat reached the same water loss than as the 19 mm piece in each degree of cooking. This times for
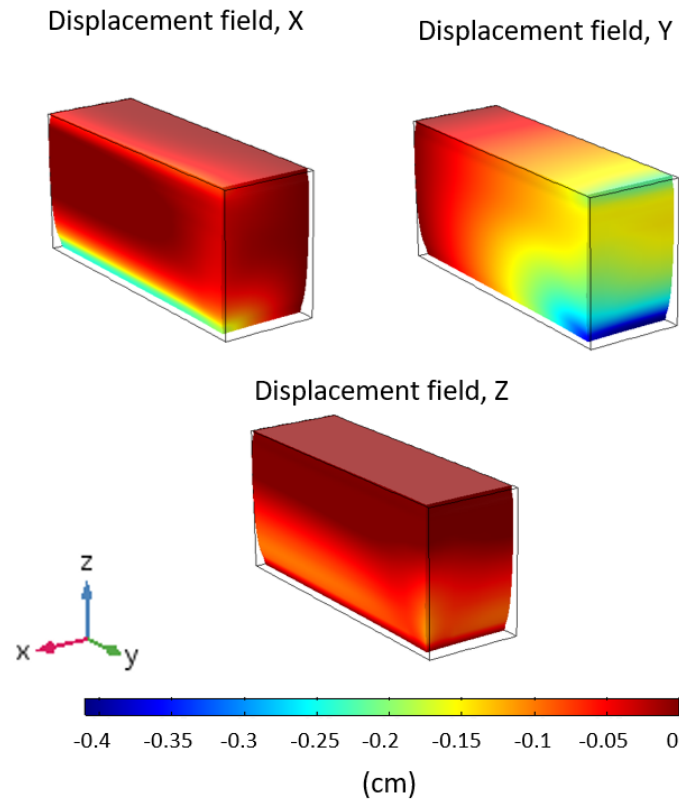
Figura 3.13: Final displacements (cm) in $x$, $y$ and $z$ directions for the done cooking degree.

the 26 mm thickness were 225 s (very rare), 450 s (medium rare) and 720 s (done). In case of the 34 mm thickness times were 265 s (very rare), 495 s (medium rare) and 770 s (done). The moment for turning over the steak were kept at two thirds of the total time, as in case of 19 mm thickness. Since the model was validated for thicknesses of 19 mm, it was subsequently checked whether it was capable of adjusting the core temperature and the water loss for these greater thicknesses. Results are shown in Fig. 3.14 and in Fig. 3.15. In this figures we can see that the model properly adjust the results in both cases. For the core temperature, a displacement deviation of 5 % in the location of the temperature probe was applied in each case as was done in case of 19 mm. Central temperatures hardly vary with respect to the first thickness, being the maximum temperatures reached for each thickness of: 26 mm (31 °C - very rare, 45 °C - medium rare, 58 °C - done) and 34 mm (32 °C - very rare, 46 °C - medium rare, 58 °C - done). Considering these results, an appropriate functioning of the model can be affirmed. Thus, this model may predict cooking times according to the weight loss of the meat during cooking.

(a)

(b)

(c)

(d)

(e)

(f)
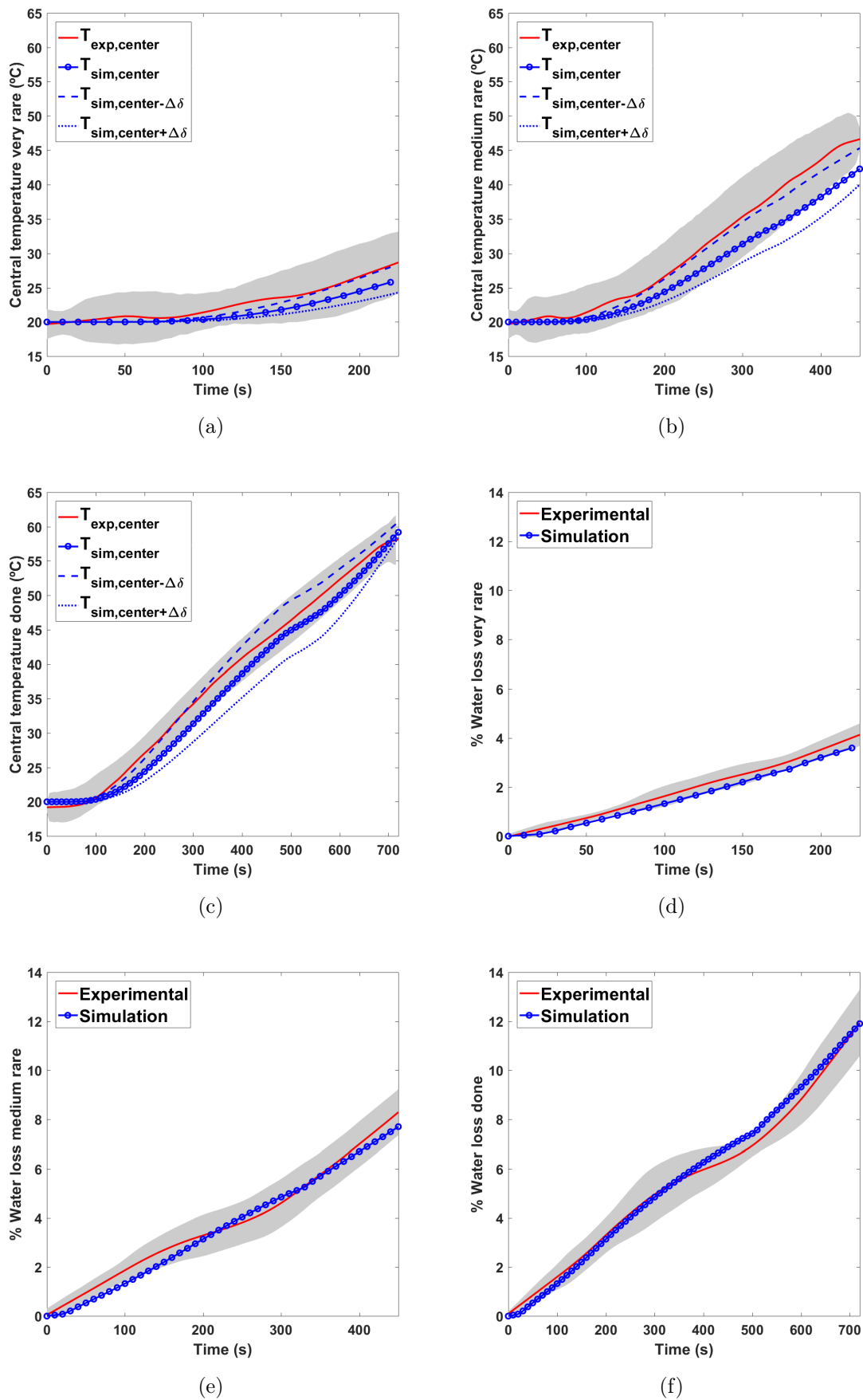
Figura 3.14: Central temperature evolution for a steak of 26 mm thickness: a) very rare, b) medium rare, c) done cooking degrees. Water loss evolution for d) very rare, e) medium rare, f) done.
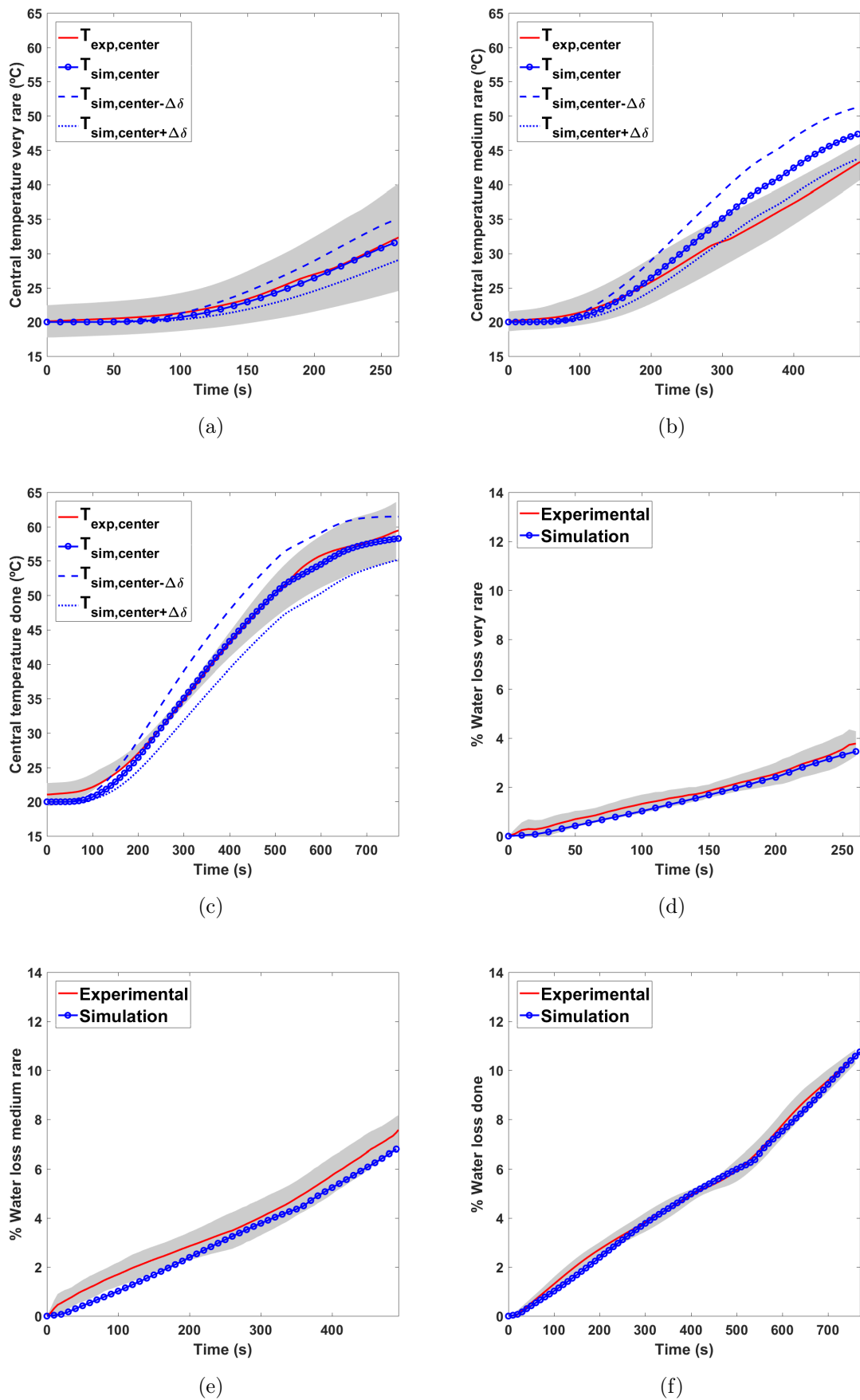
Figura 3.15: Central temperature evolution for a steak of 34 mm thickness: a) very rare, b) medium rare, c) done cooking degrees. Water loss evolution for d) very rare, e) medium rare, f) done.

### 3.5.4.  Analyzing the effect of the steak thickness

During the experimental tests, it was ensured that the thickness of the fillets hardly varied in the samples of the same thickness, but some uncertainties could be present in the measurement process. These small variations could cause changes in the expected temperature reached in the steak. A sensitivity analysis with the Monte Carlo method has been carried out in order to know this changes in temperature when the thickness varies. The analysis has been applied to the 3D model of the steak of 19 mm of thickness considering the three cooking degrees. Results for the done degree are shown in Fig. 3.16. A population of one hundred models was analyzed considering a uniform distributed thickness between $\pm 10\%$ the mean value. Since small differences in temperature and weight loss are observed if shrinkage is disabled in the model, the model was simplified disabling this shrinkage in order to reduce the computational cost. In Fig. 3.16.a the temperature at the central point is represented as a mean value and a standard deviation. With this simplification, its values were $35 \pm 2$ °C, $47 \pm 4$ °C and $63 \pm 5$ °C at 180 s (very rare), 300 s (medium rare) and 420 s (done), respectively. Regarding water loss, the same sensitivity analysis was carried out, obtaining results of $4 \pm 0.3\%$, $7 \pm 0.4\%$ and $10 \pm 0.5\%$ at 180 s (very rare), 300 s (medium rare) and 420 s (done), respectively. This analysis is show in Fig. 3.16.b in case of done degree. We can conclude that these dispersion values obtained with the Monte Carlo technique are very close to those obtained in the experimental tests.



(a)                                                (b)
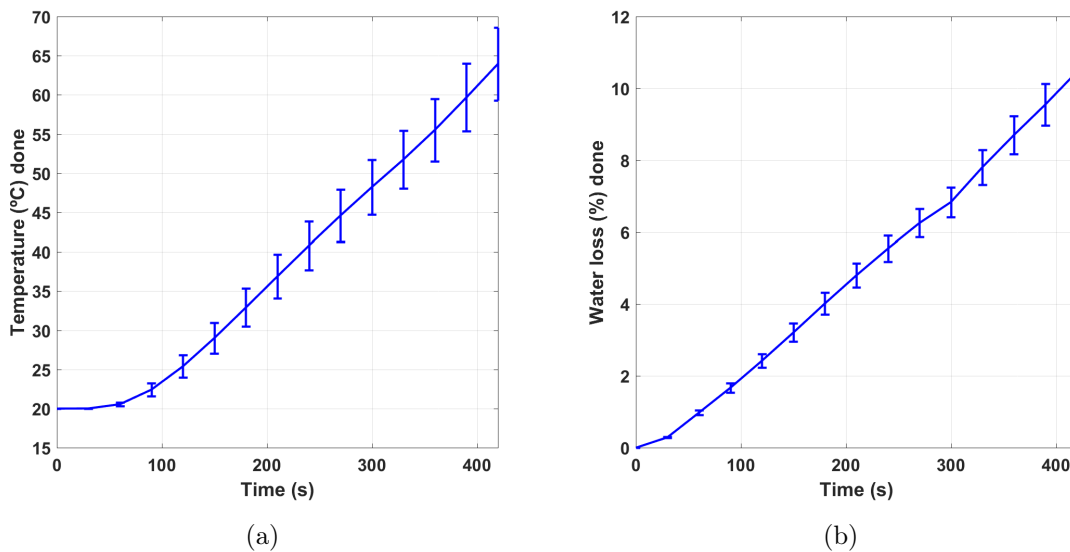
Figura 3.16: Sensitivity analysis of a) temperature in the central point of the steak and b) water loss regarding variations in thickness for the done degree.

## 3.6.    Conclusions

In this chapter, a 3D computational model of meat pan-cooking was developed. This model includes the phenomena of heat and moisture flow transfer and the deformation of meat during the heating. It has also been included the turn over of the steak. The equations which govern the problem were solved by the finite element method. The numerical results have been compared with experimental results. A good fit between these results indicates that the model reliably reproduces the described cooking process, including the variability in the thickness of the meat steaks. These results can be used to predict temperature and weight loss in meat based on cooking time, thus offering a broader understanding of this process. Therefore, this information could be used to guide the user of the induction hob to obtain the desired cooking degree, related to the reached temperature. An important observation obtained from this study is that the choice of weight loss as the reference parameter to estimate the cooking time of steaks of different thicknesses is a promising option for several reasons. Since it is difficult to measure the temperature exactly at the center of the steak, the measurement of the weight may be implemented in induction hobs in the future more easily. In addition, a small deviation in steak thickness involves a change in temperature prediction at the center of the same order of magnitude as that between doneness degrees. However, one of the limitations of the weight loss as a parameter of reference in cooking time is that it depends on the water holding capacity of the meat, which in turn it depends on the muscle and its quality. Regardless, it could be used as the main parameter and use the surface temperature of the meat as the complementary parameter for a greater reliability.

# Chapter 4

# Modeling color changes in beef meat during pan cooking

In this Chapter, a numerical approach of the color acquired by the meat during cooking has been carried out. Considering the 3D model of the previous chapter and using the temperature results, color kinetics has been modeled and validated with experimental tests. The CIELab color space was used to obtain the lightness (coordinate $L^*$) and the reddish tone (coordinate $a^*$) of the cooked meat. The applicability of this model for practical cooking purposes is also shown in this Chapter, by determining the optimum turn over time to achieve a similar color profile on both sides of the meat. This Chapter is about the publication: Moya, J., Lorente-Bailo, S., Ferrer-Mairal, A., Martínez, M.A., Calvo, B., Grasa, J. and Salvador, M. (2021). Color changes in beef meat during pan cooking: kinetics, modeling and application to predict turn over time. European Food Research and Technology. 247, 2751–2764. 10.1007/s00217-021-03821-y.

## 4.1.   Introduction

Knowing the evolution of the color inside the meat would be very interesting for practical domestic cooking purposes, since the consumer is guided more by sensory perceptions than by those of temperature. However, the reached temperature in the meat should not be forgotten, since microbiological safety depends on it. The United States Department of Agriculture, USDA, recommends a temperature of at least 62.8 °C for steaks and a rest time of three minutes before eating. However, preferences from the point of view of consumer sensory perception may not coincide with safe temperatures (López Osornio et al., 2008). Therefore, it would be necessary to study in depth the relationship of this temperature achieved in meat with the degrees of doneness, and to reach a compromise between safety and sensory preference.

Nevertheless, the relationship between cooking time, temperature and color of the meat depends on many factors such as the pH (Hughes et al., 2017, Trout, 1989), the source of the meat (Suman et al., 2014), the water holding capacity (Hughes et al., 2014), the packaging conditions (Stella et al., 2018) or the cooking method (Yancey et al., 2011). For example, high pH, modified atmosphere packaging, rapid thawing and low fat content can prolong the characteristic redness of raw meat, and, in contrast, brownish hues may appear prematurely in meat which has been frozen in bulk, thawed for a long time or packed in oxygen-rich packaging (King and Whyte, 2006, Stella et al., 2018). In addition, thermometers are usually employed when the meat is cooked, but not during the process of pan cooking, where meat is in continuous contact with a hot surface (Elshahat et al., 2019, McCurdy et al., 2005). In pan cooking, it is not easy to accurately measure the temperature in the center of the meat. A deviation of $\pm 1$ mm in the temperature sensor position can cause temperature changes of 3-5 °C (Kondjoyan et al., 2013, Moya et al., 2021b). All of this means that developing a model that includes the evolution of color as a function of temperature depending on so many factors is a great challenge. Despite the difficulties posed by these factors, color changes caused by heating can be quantified by chemical reaction kinetics in the same way as for other quality attributes Datta (2016), Ling et al. (2014) or meat properties such as water content Kondjoyan et al. (2013). In the study of the kinetics of color change by heating of beef meat, are only a few researches such as that of Goñi and Salvadori (2011) in which the variation of the CIELab coordinate $a^*$ is described, but this does not include changes in lightness; or that of Kondjoyan et al. (2014) in which no data below 65 °C are shown.

Implementing the kinetic equations in the computational model described in the previous Chapter, the evolution of meat color during cooking will be obtained, and with that, the application of the model to help with practical cooking will be achieved. As it was mentioned, this is a challenge since pan cooking modeling is complex mainly due to the difficulty of quantifying the heat transfer between the pan and the meat, and the need to turn the meat over. These key aspects are totally new to this field of study, since the evolution of the color has only been treated in oven cooking.

Due to that, in this Chapter the main objectives are: 1) to determine the kinetics of thermal color changes in beef meat, 2) to implement and validate the evolution of beef color during domestic pan cooking to the developed pan cooking model, which includes the turn over process, and 3) to predict the turning over time for the meat from model simulations to achieve a similar color profile throughout the thickness of the meat. In order to achieve a more reliable and useful study, since as it was mentioned

the color evolution depends on the initial conditions of the meat, the kinetic study was carried out with beef under three different conservation conditions (fresh, refrigerated and frozen). As in the previous Chapter, the model was experimentally verified for three degrees of doneness.

## 4.2. Material and methods

### 4.2.1. Material and properties

In the same manner as in the previous study, *Longissimus dorsi* muscles from 1-year-old Asturiana de los Valles heifers were acquired in a local market 7 days post mortem. In this case, three muscles were necessary for all the experimental test. From these muscles, nine 17 mm thick steaks perpendicular to the longitudinal axis were cut from the middle part of each loin for pan cooking. Thus, twenty seven steaks were obtained and were individually placed in zip lock bags and distributed in three homogeneous batches: frozen, refrigerated and fresh. The frozen batch was stored for 7 days at -20 °C, the refrigerated one was kept in a refrigerator at 4 °C for 7 days and the fresh batch was cooked on the day of acquisition. In case of frozen and refrigerated samples, a KGN36VW35 Combi Bosch household refrigerator (BSH, Munich, Germany) was used. In addition, for each conservation condition, samples were taken from the 17 mm thick steaks for moisture determination and pH measurement.

For the determination of color kinetics, eighty steaks with a thickness of 4 mm were cut from different longitudinal positions of the middle part of each loin. At the same time, these fillets were cut into pieces of approximately 8 g to ensure uniform and fast heating.

#### 4.2.1.1. Moisture content and pH

For the determination of the moisture content of the meat, the weight loss of 5 g samples was measured after drying in a convection oven at 105 °C for 16–24 h, using the Association of Official Analytical Chemists (AOAC) method 950.46. For each conservation condition, five samples were analyzed and the results were expressed as g of water per 100 g of sample.

In case of ph measurements, a Basic 20+ Crison pH-meter (Hach, Loveland, EE.UU.) equipped with a penetrating electrode was used, just before cooking, obtaining

in this way the pH of the meat in each one of five replicates for each conservation condition.

### 4.2.1.2. Color

For color kinetics determination, the pieces of meat were placed in plastic bags and immersed in a thermostatic water bath (Digiterm S-150, JP Selecta, Abrera, Spain). These pieces were kept for times from 10 s to 30 min at a given temperature from 30 to 130 °C before being cooled in iced water for 10 min. In the 100-130 °C range, sunflower oil was used instead of water as the heating fluid, in order to avoid the evaporation of the water, limitation that arises when exceeding 100 °C.

Once those 10 minutes are up, the color of the meat was determined by digital image analysis. The images were acquired with a Canon Scan Lide 210 (Canon, Tokyo, Japan) at 600 dpi resolution, and stored in JPEG format using the Canon MP Navigator EX 4.0 software. They were then processed with Matrox Inspector 8.0 software (Matrox Electronic Systems Ltd, Dorval, Canada). Calibration of the digital system was performed using the UNE 48-103-94 Spanish color norm. The correspondence between CIELab coordinates ($L^*$, $a^*$ and $b^*$) and RGB values were calculated using a quadratic model (León et al., 2006). Five replicates were analyzed for each time, temperature and storage condition.

## 4.2.2. Cooking procedure

Before cooking, frozen samples were thawed at 4 °C for 24 h inside the refrigerator and all the steaks were tempered to 20 °C. From these steaks, three pieces of approximately $43.7 \pm 6.7$ g, $81 \pm 21$ mm long, $26 \pm 1$ mm wide and $17 \pm 2$ mm high were obtained see Fig. 4.1.a.. Each piece was individually cooked in a forged aluminum pan with a Teflon platinum non-stick coating of 210 mm in diameter (WMF, WMF Group GmbH, Geislingen an der Steige, Germany) placed on an induction hob using the frying sensor at level 5 (BOSCH Schott Ceran PXY675DW4E/01 model, BSH, Munich, Germany). The meat was introduced in the pan when the images taken with an infrared thermal camera (875-2 model, Testo, Lenzkirch, Germany) indicated that the surface of the pan had reached a temperature of $215 \pm 3$ °C (Fig. 4.1.b.). Three degrees of doneness were cooked, as for the validation of the model developed in the previous chapter, with the purpose of incorporating the kinetics of the color in the model. These degree of doneness were very rare, medium rare and done, which corresponded to cooking times of 180 s, 300 s and 420 s respectively. Anew, the samples

were turned over at two thirds of the total cooking time. So, nine pieces were cooked for each degree of doneness and storage condition. Four of them were used to measure the evolution of the temperature in the center of the pieces by a penetration T type, 1.5 mm diameter thermocouple connected to a data logger (177-T4, Testo, Lenzkirch, Germany) and five to measure the meat weight loss during cooking using a balance (DS30K0.1L, Kern & Sohn, Balinger-Frommern, Germany) on which the induction hob was placed. In this way, the comparison between the numerical and experimental results was possible, showing again a good fit and ensuring the validity of the model. The pieces used to measure the weight loss were longitudinally cut two minutes after cooking, and then they were scanned following the same procedure as described in section 4.2.1. For the comparison with the numerical results, CIELab values were obtained at 21 different points along the thickness of the central region of the steaks.



(a)                                 (b)                                 (c)
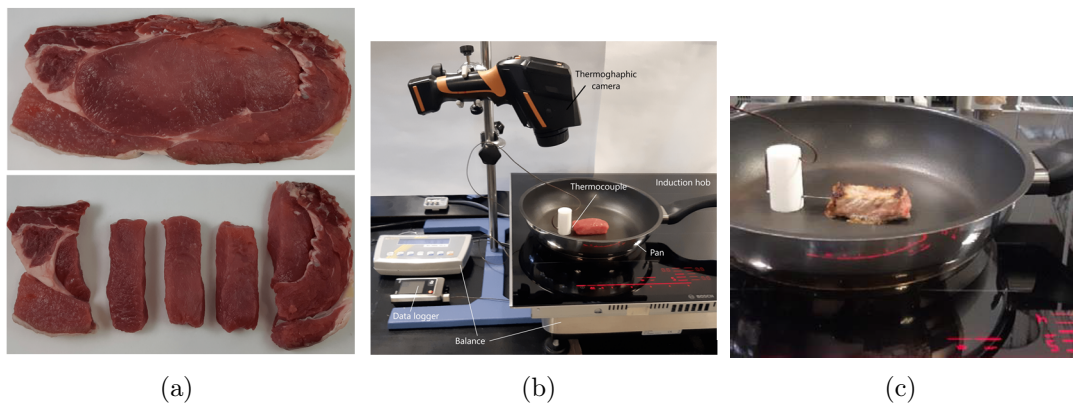
Figura 4.1: a) Samples of beef steak for the pan cooking procedure, b) experimental setup for temperature and weight loss measurement during the cooking process and c) final moment of cooking for a done degree of doneness.

## 4.2.3.   Numerical simulation using finite element methodology

The model developed with the software COMSOL Multiphysics 5.2a in 3 has been used to predict the color evolution in beef meat caused by pan cooking. The model described in that chapter is summarized below. It reproduces the experimental tests and only a quarter of the pan and the meat due to the symmetry was considered (Fig. 4.2). It is capable of reproducing the moment of turning over the steak by activating and deactivating the boundary conditions on the top and bottom surfaces related to the pan contact. The dimensions of the piece of meat and the pan were set as in the experimental tests, as well as the three cooking times for the different degrees of doneness.
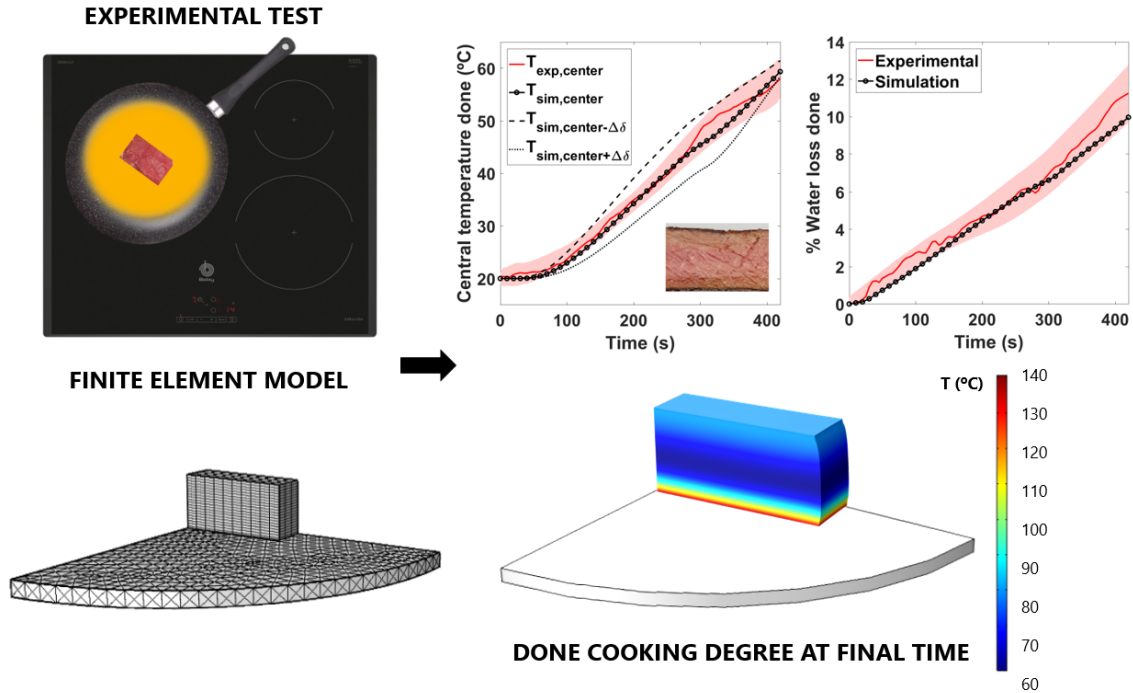
Figura 4.2: Finite element model and results obtained for temperature and water loss for a done degree of doneness using the model developed in Chapter 3.

## 4.3. Results and discussion

### 4.3.1. Experimental determination of color kinetics

The color of the beef changes from red to light brown passing through pink and grayish when it is heated, and these variations are reflected in the CIELab coordinates. The main coordinates on this scale that describe the evolution of meat are the lightness, $L^*$, that indicates the luminance of the color (the value 0 corresponds to white and 100 to black), $a^*$ which gives information on a scale from green (negative values) to red (positive values) and $b^*$ which correspond to a a scale from blue to yellow (a negative value indicates blue and positive color, yellow). Fig. 4.3 shows, for fresh samples, the evolution of these coordinates with the heating time at different temperatures expressed as normalized parameters relative to their initial values ($L_o^*$= 45.23 $\pm$ 0.99, $a_o^*$=13.55 $\pm$ 0.63 and $b_o^*$=12.92 $\pm$0.71). In Fig. 4.3 a. we can observe that the lightness, for temperatures below 60 °C, increases with time until it stabilizes. Instead, for higher temperatures, the lightness rises quickly to a maximum and subsequently decreases until it levels off at a value lower than this maximum. At temperatures above 100 °C, the lightness stabilizes at lower values, even lower than the initial one. Regarding the coordinate $a^*$, no changes were observed for temperatures below 45 °C. However,

at higher temperatures, the values of $a^*$ follow a trend similar to coordinate $L^*$; $a^*$ increases in the initial instants and then it has a decrease towards an equilibrium value (always lower than the initial one) due to the loss of the characteristic red hue of the raw meat. Above 100 °C, these coordinate decreases with time within reaching a maximum, until it reaches an equilibrium value that is lower as the temperature increases. The $b^*$ coordinate hardly changes over time during the warm-up with respect to its initial value and it shows a clear trend.

The heme proteins are responsible for the redness of the meat. Thus, when the denaturation of myoglobin and hemoglobin that occurs at 65-80 °C (Martens et al., 1982) takes place, raw meat suffers the loss of its characteristic redness. However, the change in the color of the meat during its heating can not be explained exclusively by this. Moreover, the lightness has greater relevance than redness in the absolute color change (Pakula and Stamminger, 2012), as can be seen from the data in Fig. 4.3, especially at temperatures below 60 °C. The increase in luminosity can be explained by the structural changes that meat undergoes during heating which modify the scattering of the light. The reflected light suffers an increase due to the gaps generated between the fibers due to the muscle and myofibril shrinkage caused by protein denaturation, reduction of the water holding capacity and disruption of the sarcolemma (Hughes et al., 2014). Our results on changes in lightness during heating are similar to the results found by (Kondjoyan et al., 2014) for beef meat at 66, 98 and 205 °C. However, the evolution of the redness differs from that obtained by (Goñi and Salvadori, 2011): the coordinate $a^*$ decreases over time for all temperatures until reaching a plateau at long cooking times. This could be described with a single fractional conversion first–order kinetics. However, in Goñi and Salvadori (2011) data are not available at times shorter than 2.5 min, being at those times when the increase in redness occurs.
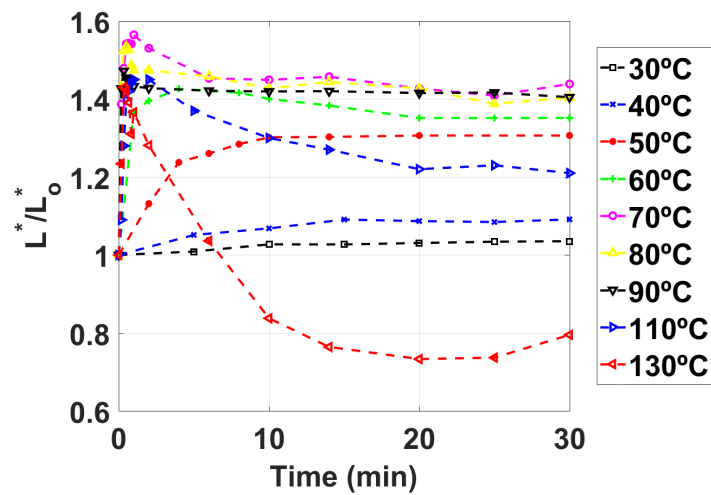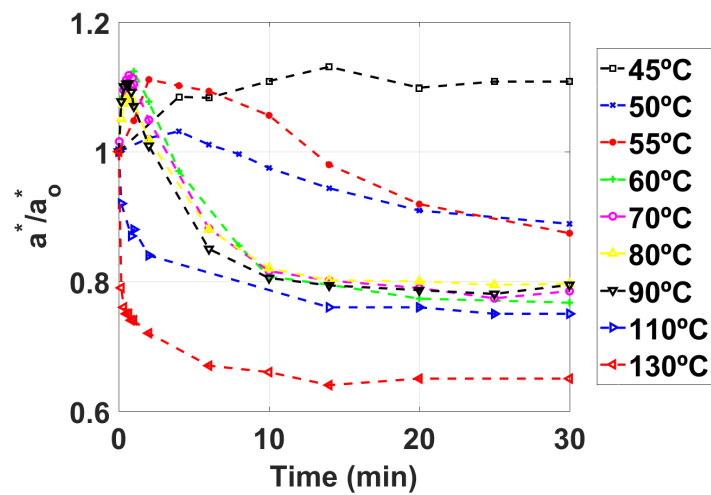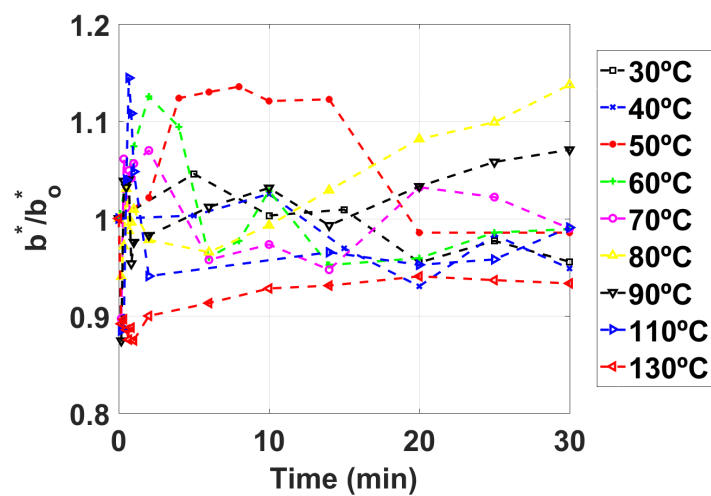
Figura 4.3: Experimental values for a) $L^*/L_o^*$, b) $a^*/a_o^*$ and c) $b^*/b_o^*$ over time and for different temperatures.

### 4.3.2. Influence of the domestic storage conditions on meat color

The moisture content of the raw samples was $74.61 \pm 0.58$ %, $74.10 \pm 0.65$ % and $72.29 \pm 0.77$ % for the fresh, refrigerated and frozen samples, respectively. Observing this results, we can affirm that during the defrosting process, the frozen meat lost 2.32 % of its water content compared to fresh meat, while the refrigeration hardly affected it. The CIELab coordinates values of the raw samples just before heat treatment ($L_0^*$, $a_0^*$, $b_0^*$) for fresh, refrigerated and frozen meat were, respectively: $45.23 \pm 0.99$, $46.43 \pm 0.50$ and $45.44 \pm 0.51$ for $L_0^*$, $13.55 \pm 0.63$, $13.27 \pm 0.30$ and $13.11 \pm 0.28$ for $a_0^*$ and $12.92 \pm 0.71$, $13.14 \pm 0.25$ and $13.87 \pm 0.42$ for $b_0^*$. The color of the raw meat was hardly affected by the storage condition, in the evaluated conditions. There were no significant differences in redness between the three conditions (p > 0.05), indicating that the rate of oxidation at which oxymyoglobin changed into metmyoglobin was slow during the storage time (Mancini and Hunt, 2005). On the other hand, the myoglobin denaturation in beef muscle is pH dependent, decreasing at high pH (Trout, 1989). Again, there were no significant differences ($p > 0.05$) in pH between the conditions before heat treatment: $5.64 \pm 0.05$, $5.62 \pm 0.07$, $5.63 \pm 0.05$ for the fresh, refrigerated and frozen samples, respectively.

Through the expression in eq. 4.1, the absolute color evolution, $\Delta E^*$, was calculated for fresh, refrigerated and frozen meat from the data of raw ($L_o^*$, $a_o^*$, $b_o^*$) and thermally treated samples ($L^*$, $a^*$, $b^*$):

$$\Delta E^* = \sqrt{(L_o^* - L^*)^2 + (a_o^* - a^*)^2 + (b_o^* - b^*)^2} \tag{4.1}$$

In Fig. 4.4, $\Delta E^*$ at different times and temperatures are shown. Since the absolute color follows the same trend as the lightness, it can be deduced that this is the CIELab coordinate that changes the most during heating. The absolute color evolution for the refrigerated or frozen samples was similar to that of fresh meat. That is, differences in absolute color between the three conditions are insignificant, $\Delta E^* < 1$ at practically all times and temperatures, so they were not visually detectable (Abril et al., 2001). Therefore, we could affirm that color kinetics obtained from fresh samples could be applied to predict color changes during cooking regardless of the domestic preservation method used, at least if the tested conditions are similar to those presented here.

(a)



(b)



(c)
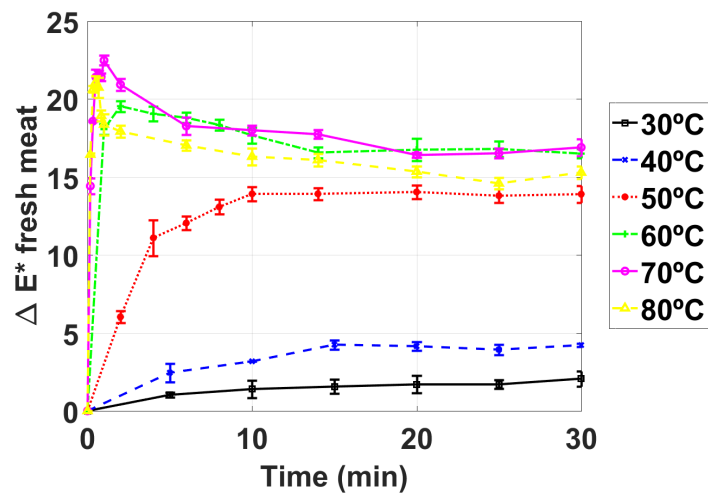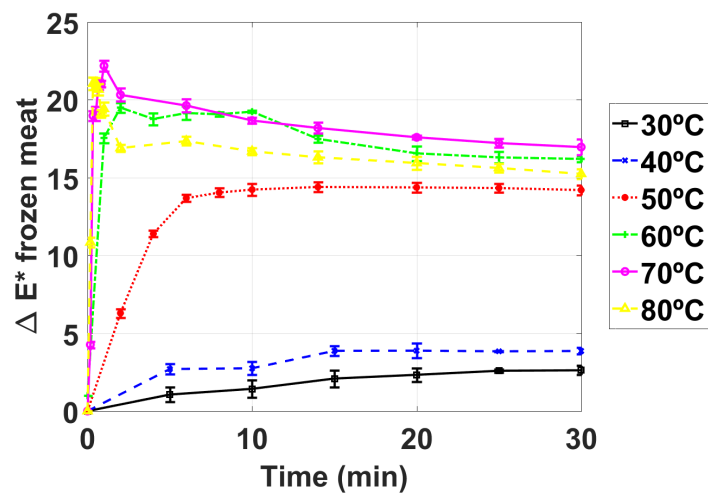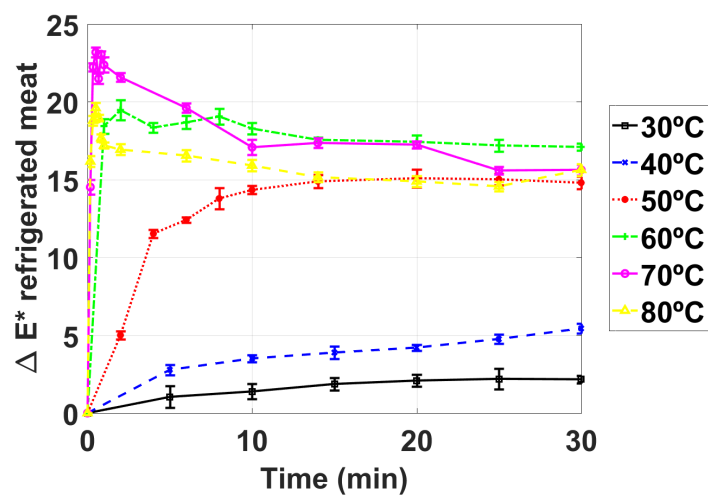
Figura 4.4: Absolute color, $\Delta E^*$, evolution with heating time and temperature for a) fresh, b) refrigerated and c) frozen beef.

### 4.3.3.  Kinetic modeling

The evolution of $L^*$ and $a^*$ with time and temperature could be described by two successive fractional conversion first-order reactions, as if it were a chemical reaction. The changes in food attributes by thermal treatments can be expressed by a kinetic model described in Rabeler and Feyissa (2018b), Eq. 4.2 and 4.3:

$$\frac{dQ}{dt} = -k(Q - Q_{-\infty})^n, \qquad Q_0 \geq Q \geq Q_{-\infty} \tag{4.2}$$

$$\frac{dQ}{dt} = k(Q_\infty - Q)^n, \qquad Q_0 \leq Q \leq Q_\infty \tag{4.3}$$

where $Q$ is the measured coordinate, $L^*$ and $a^*$ in this case, $t$ is the time, $n$ is the reaction order (mostly $n = 0$, 1 or 2), $Q_\infty$ is the final non zero equilibrium quality value and $k$ is the reaction rate constant, which is temperature dependent, usually expressed by the Arrhenius equation, Eq. 4.4:

$$k = k_0 \exp\left(\frac{-E_a}{RT}\right) \tag{4.4}$$

where $T$ (°C) is the absolute temperature, $k_0$ is the pre-exponential factor, $E_a$ is the activation energy (J/mol) and $R$ is the universal gas constant (8.31 J/molK).

However, the evolution with time of the $L^*$ and $a^*$ color coordinates during the thermal treatment of beef can not be described by a single reaction since these coordinates reach a maximum (Fig. 4.3). The changes in $L^*$ and $a^*$ during the cooking of beef were assumed to be those of the intermediate attribute, $Q$, involved in two successive reactions according to the following scheme:

$$R \xrightarrow{k_1} Q \xrightarrow{k_2} P$$

$$
\begin{array}{cccc}
t = 0 & R_0 & Q_0 & P_0 \\
t = \infty & R_\infty & Q_\infty & P_\infty
\end{array}
$$
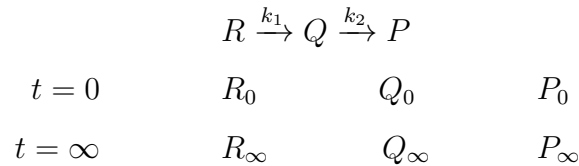
where $R_o$, $Q_o$ and $P_o$ are the initial values of the attributes $R, Q$ and $P$, and $R_\infty$, $Q_\infty$ and $P_\infty$ were the final non-zero equilibrium values after long heating times.

Therefore, the evolution of $L^*$ and $a^*$ with time and temperature was described by a kinetic model based on two successive fractional conversion first-order reactions, Eqs. 4.5 and 4.6.

$$\frac{L^*}{L_0^*} = 1 + (\frac{L_\infty^*}{L_0^*} - 1)(1 - e^{-k_2 t}) + \frac{k_1(R_0 - R_\infty)}{L_0^*(k_2 - k_1)}(e^{-k_1 t} - e^{-k_2 t}) \qquad (4.5)$$

$$\frac{a^*}{a_0^*} = 1 + (\frac{a_\infty^*}{a_0^*} - 1)(1 - e^{-k_2 t}) + \frac{k_1(R_0 - R_\infty)}{a_0^*(k_2 - k_1)}(e^{-k_1 t} - e^{-k_2 t}) \qquad (4.6)$$

Where, $L_\infty$ and $a_\infty$ and are the values of the coordinates at infinite time, $k_1$ and $k_2$ ($\text{min}^{-1}$) are the rate constants, t (min) is the time, and $R_o$-$R_\infty$ is the reactant consumed in the first reaction. In our study, the kinetic parameters were obtained by minimization of the sum of squared differences between calculated and experimental values using the Levenberg–Marquardt algorithm. Table 4.1 and 4.2 show the estimated kinetic parameters for both color CIELab coordinates. The color degradation rate constants increased with the temperature but this dependence could not be accurately described by the Arrhenius equation. In all cases, the coefficient of determination ($R^2$) was greater than 0.9469, indicating that the kinetic model proposed was suitable to describe the thermal degradation of the beef color.

| Temperature (°C) | $n = \frac{L_\infty^*}{L_0^*}$ | $m = \frac{R_0 - R_\infty}{L_0^*}$ | $k_1$ ($\text{min}^{-1}$) | $k_2$ ($\text{min}^{-1}$) | $R^2$ |
|---|---|---|---|---|---|
| 30 | 1 | 0.0383±0.0044 | 0.0014±0.0004 | 0 | 0.9469 |
| 40 | 1 | 0.0906±0.0032 | 0.0027±0.0004 | 0 | 0.9799 |
| 45 | 1 | 0.1642±0.0033 | 0.0031±0.0002 | 0 | 0.9944 |
| 50 | 1 | 0.3095±0.0057 | 0.0053±0.0.0004 | 0 | 0.9934 |
| 55 | 1 | 0.3339±0.0098 | 0.0123±0.0017 | 0 | 0.9731 |
| 60 | 1.2684±0.2263 | 0.4287±0.0112 | 0.0305±0.0051 | 0.0004±0.0009 | 0.9887 |
| 70 | 1.4320±0.0062 | 0.5541±0.0086 | 0.1100±0.0128 | 0.0036±0.0011 | 0.9656 |
| 80 | 1.4244±0.0068 | 0.5342±0.0179 | 0.1527±0.0417 | 0.0163±0.0082 | 0.9687 |
| 90 | 1.4172±0.0022 | 0.4462±0.0063 | 0.2009±0.0212 | 0.0163±0.0080 | 0.9977 |
| 110 | 1.2112±0.0236 | 4.9596±1.9946 | 0.1493±0.04933 | 2.2381±0.3711 | 0.9562 |
| 130 | 0.7366±0.0022 | 0.4739±0.0329 | 5.7775±1.4921 | 0.1795±0.0318 | 0.9764 |

Table 4.1: Kinetic parameters of thermal degradation of lightness $L^*$ for beef.

| Temperature (°C) | $n = \frac{a_\infty^*}{a_0^*}$ | $m = \frac{R_0 - R_\infty}{a_0^*}$ | $k_1$ ($\text{min}^{-1}$) | $k_2$ ($\text{min}^{-1}$) | $R^2$ |
|---|---|---|---|---|---|
| 45 | 1.0208±0.0270 | 0.1885±0.0740 | 0.0027±0.0031 | 0.0027±0.0006 | 0.98644 |
| 50 | 0.8810±0.0093 | 0.2467±0.0286 | 0.0029±0.0003 | 0.0029±0.0093 | 0.9949 |
| 55 | 0.8436±0.0411 | 1.1803±0.1220 | 0.0017±0.0010 | 0.0050±0.0026 | 0.9759 |
| 60 | 0.7669±0.0058 | 3.8473±0.6705 | 0.0037±0.0.0003 | 0.0328±0.0043 | 0.9970 |
| 70 | 0.7820±0.0024 | 4.3628±0.4253 | 0.0041±0.0002 | 0.0451±0.0035 | 0.9992 |
| 80 | 0.7945±0.0014 | 3.9168±0.2684 | 0.0042±0.0001 | 0.0484±0.0026 | 0.9996 |
| 90 | 0.7866±0.0025 | 5.4333±0.6253 | 0.0050±0.0002 | 0.0735±0.0066 | 0.9989 |
| 110 | 0.7520±0.0034 | 5.5574±1.5706 | 0.2686±0.0673 | 9.8448±3.4510 | 0.9952 |
| 130 | 0.6464±0.0025 | 6.6873±0.6940 | 0.2653±0.0242 | 14.5780±1.1707 | 0.9989 |

Table 4.2: Kinetic parameters of thermal degradation of redness $a^*$ for beef.

Fig. 4.5 shows the adjustment of this kinetic model with the experimental results described in section 4.3.1, for $a^*/a_o^*$ and $L^*/L_o^*$, and for different temperatures.

(a)



(b)
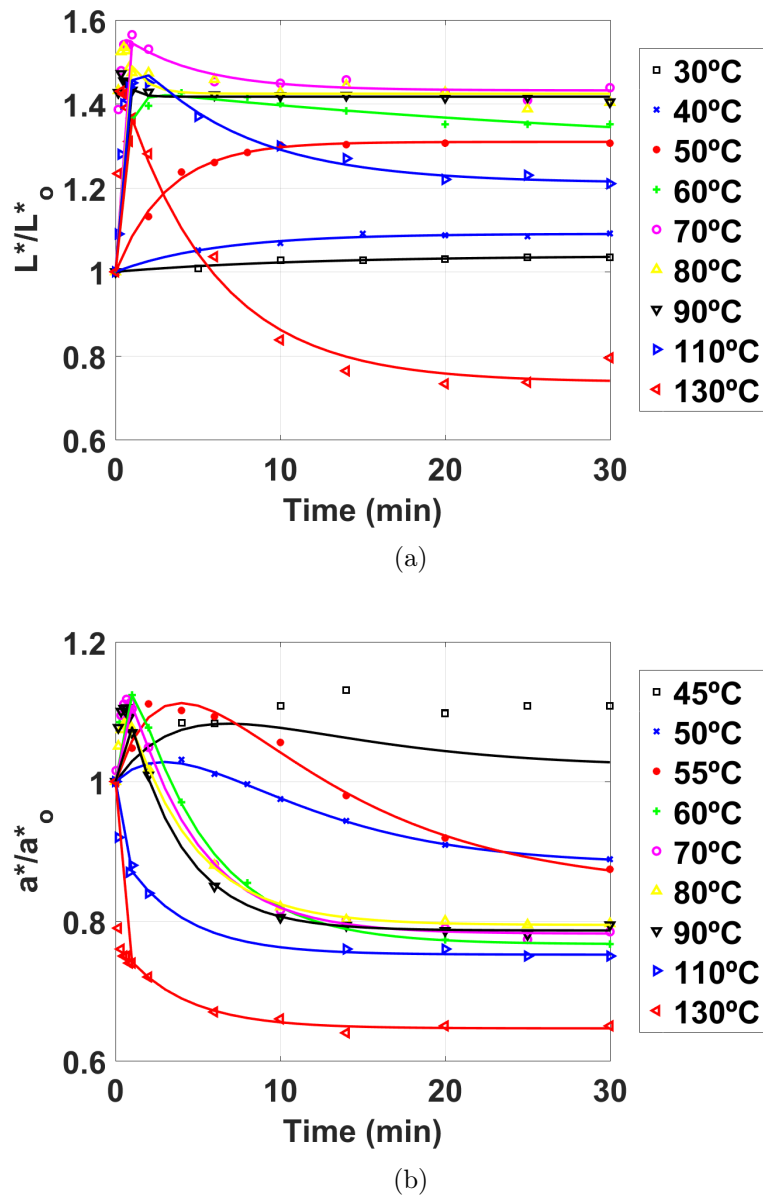
Figura 4.5: Adjustment of the kinetic model for a) $L^*/L_o^*$ and b) $a^*/a_o^*$ for different temperatures.

However, if we observed the kinetic parameters obtained in Tables 4.1 and 4.2 did not show a clear trend with temperature that would allow a continuous function to be obtained that could be easily implemented in the developed finite element model. Another alternative was proposed to describe the evolution of $L^*$ and $a^*$ using the experimental results, a response surface of each of the coordinates against time and temperature was fitted.

Fig. 4.6 shows these response surfaces. In order to obtain coordinates $L^*$ and $a^*$ as a function of the maximum temperature reached at each point of the meat and the time these points remain at that temperature, the Eqs. 4.7 and 4.8 have been used in

the finite element model.
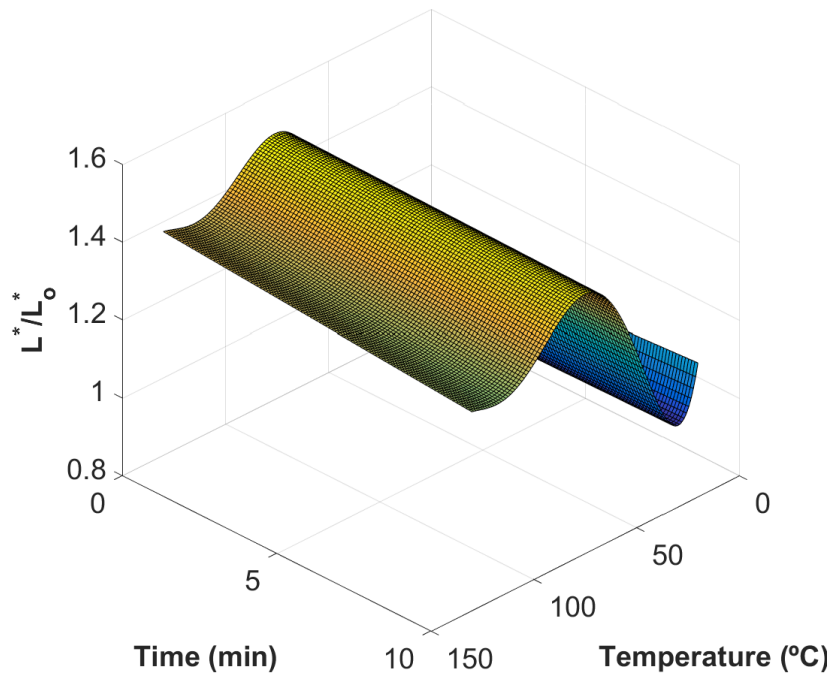


(a)
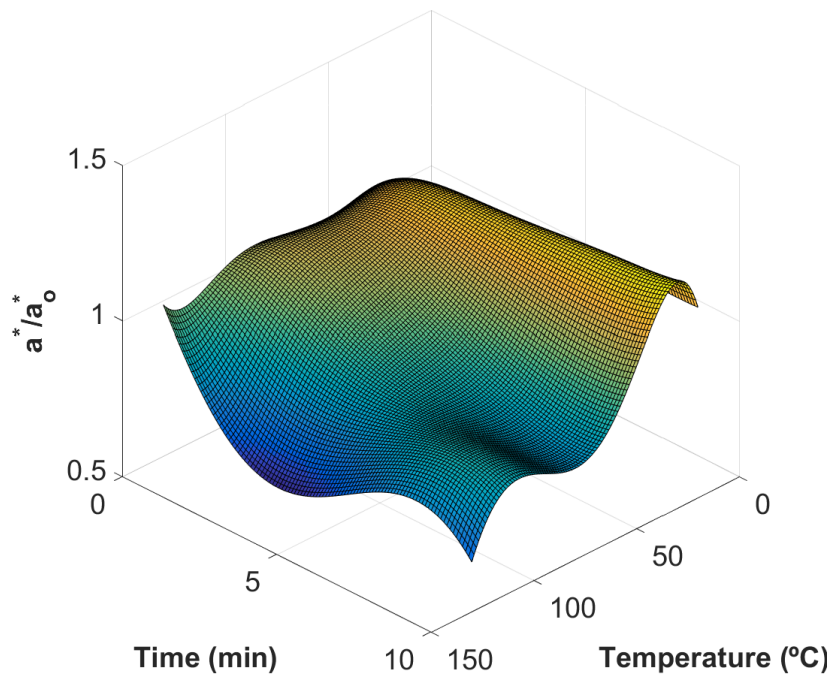


(b)

Figura 4.6: a) Response surface for $\frac{L^*}{L_o^*}$, b) Response surface for $\frac{a^*}{a_o^*}$.

The equation which represents the response surface of coordinate $L^*$ is a five-degree polynomial function for temperature $T$ (°C) and linear for time $t$ (min):

$$\frac{L^*}{L_o^*} = L_{00} + L_{10} \cdot T + L_{01} \cdot t + L_{20} \cdot T^2$$
$$+L_{11} \cdot T \cdot t + L_{30} \cdot T^3 + L_{21} \cdot T^2 \cdot t + L_{40} \cdot T^4 \quad (4.7)$$
$$+L_{31} \cdot T^3 \cdot t + L_{50} \cdot T^5 + L_{41} \cdot T^4 \cdot t$$

This adjustment has an $R^2$ of 0.9661. The coefficients of Eq. 4.7 are shown in Table 4.3:

| | | | | | |
|---------|-----------|----------|----------|----------|-----------|
| $L_{00}$ | 1.451    | $L_{10}$ | 0.06499  | $L_{01}$ | -0.01141 |
| $L_{20}$ | -0.315   | $L_{11}$ | -0.00843 | $L_{30}$ | 0.06247  |
| $L_{21}$ | -0.009398| $L_{40}$ | 0.08047  | $L_{31}$ | -0.006208|
| $L_{50}$ | -0.02618 | $L_{41}$ | 0.004121 | | |

Table 4.3: Coefficients for Eq. 4.7.

In the case of the surface for coordinate $a^*$, it is represented by a polynomial function of degree five for both temperature $T$ (°C) and time $t$ (min):

$$\frac{a^*}{a_o^*} = a_{00} + a_{10} \cdot T + a_{01} \cdot t + a_{20} \cdot T^2 + a_{11} \cdot T \cdot t + a_{02} \cdot t^2$$
$$+a_{30} \cdot T^3 + a_{21} \cdot T^2 \cdot t + a_{12} \cdot T \cdot t^2 + a_{03} \cdot t^3$$
$$+a_{40} \cdot T^4 + a_{31} \cdot T^3 \cdot t + a_{22} \cdot T^2 \cdot t^2 + a_{13} \cdot T \cdot t^3 \quad (4.8)$$
$$+a_{04} \cdot t^4 + a_{50} \cdot T^5 + a_{41} \cdot T^4 \cdot t + a_{32} \cdot T^3 \cdot t^2$$
$$+a_{23} \cdot T^2 \cdot t^3 + a_{14} \cdot T \cdot t^4 + a_{05} \cdot t^5$$

Regarding the goodness of the fit, a $R^2$ of 0.9184 was obtained. The coefficients of Eq. 4.8 are shown in Table 4.4:

| | | | | | |
|----------|----------|----------|-----------|----------|----------|
| $a_{00}$ | 0.9453   | $a_{10}$ | -0.1039   | $a_{01}$ | -0.1819  |
| $a_{20}$ | 0.06826  | $a_{11}$ | -0.001362 | $a_{02}$ | 0.03775  |
| $a_{30}$ | -0.05929 | $a_{21}$ | 0.1845    | $a_{12}$ | 0.07191  |
| $a_{03}$ | 0.03524  | $a_{40}$ | -0.03432  | $a_{31}$ | 0.01048  |
| $a_{22}$ | 0.03851  | $a_{13}$ | -0.04799  | $a_{04}$ | -0.05117 |
| $a_{50}$ | 0.01798  | $a_{41}$ | -0.03213  | $a_{32}$ | -0.00261 |
| $a_{23}$ | -0.04949 | $a_{14}$ | -0.005256 | $a_{05}$ | 0.02642  |

Table 4.4: Coefficients for eq. 4.8.

### 4.3.4. Validation of the computational model for color prediction

The kinetic model described in the previous section was coupled to the heat and mass transfer finite element model, in order to obtain the change of color during the process. The numerical results of coordinates $L^*$ and $a^*$ along the thickness of the meat was compared with the experimental values. These comparisons are shown in Fig. 4.7 and Fig. 4.8. A good agreement of the predictions with the experimental data is observed: the Root Mean Squared Errors, RMSE, for coordinate $L^*$ are 5.17 (very rare), 2.02 (medium rare) and 3.83 (done), and for coordinate $a^*$ are 1.44 (very rare), 1.26 (medium rare) and 0.89 (done). In this manner, this validation allowed the model to be verified and the assumptions made to be considered appropriate.
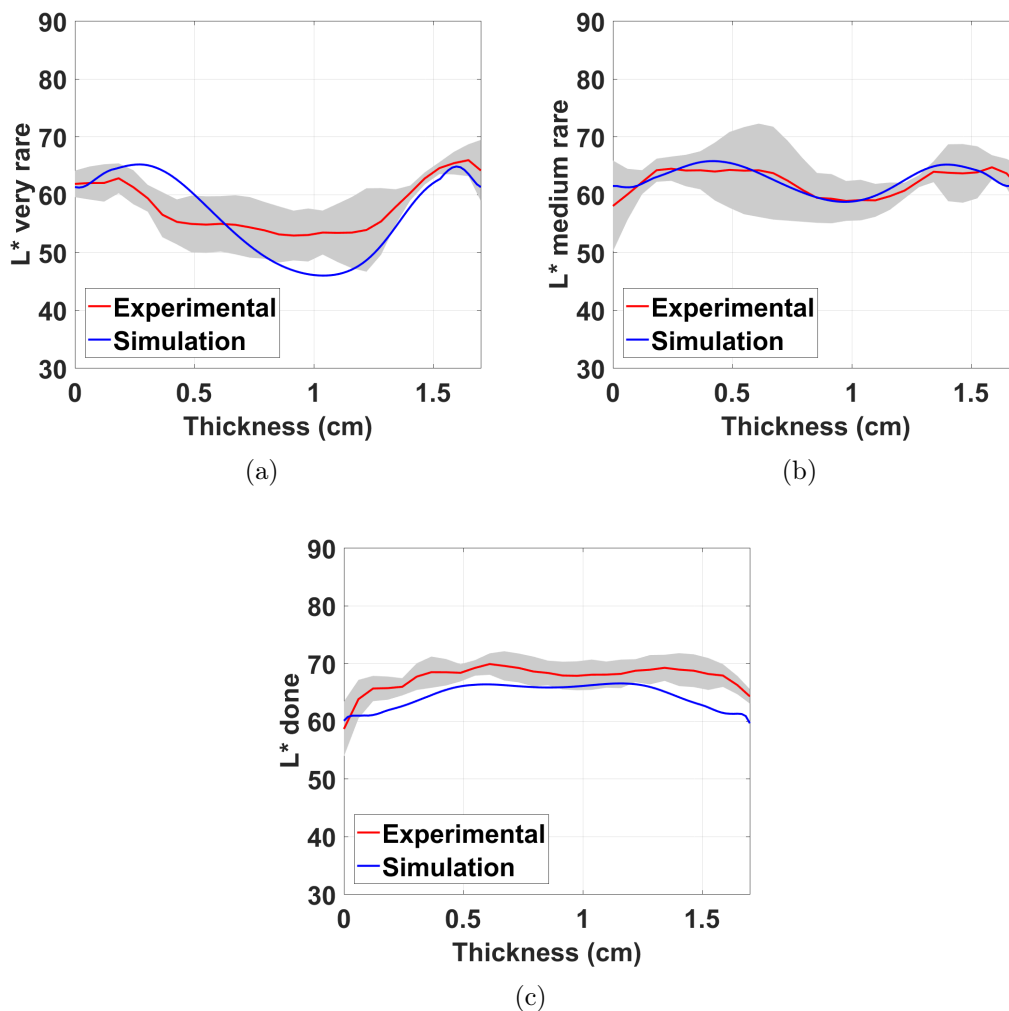


Figura 4.7: Experimental and numerical results for coordinate $L^*$ at a) very rare, b) medium rare and c) done degrees of cooking.
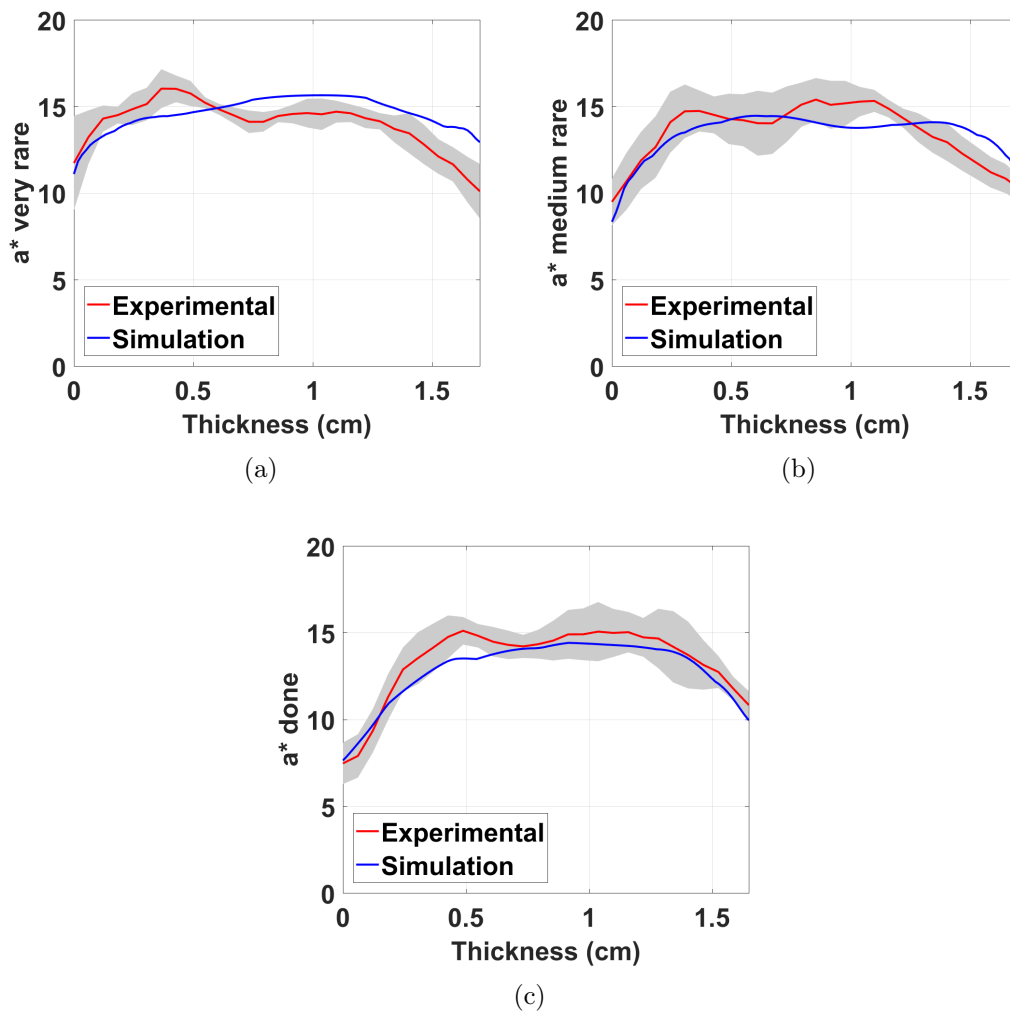
Figura 4.8: Experimental and numerical results for coordinate $a^*$ at a) very rare, b) medium rare and c) done degrees of cooking.

## 4.3.5.   Influence of the turn over time in color evolution during cooking

As in previous studies, three cooking degrees have been analysed. Fig. 4.9 shows central sections of the meet at these different cooking degrees for the final time of cooking. For shorter cooking times, two zones can be visually distinguished: a central one with slightly higher luminosity and redness than raw meat ($L^*$ around 55 and $a^*$ between 14 and 15, see Fig. 4.8 and 4.7), and another narrow area close to the surface in which the meat has lost its characteristic redness ($a^*$ lower than 13.5). For longer cooking times, the thickness of the area where the meat loses its characteristic red hue increases, acquiring more intense grayish-brownish tones (the $a^*$ coordinate in this area drops down to 8), while the luminosity of the central area reaches higher values ($L^*$ between 65 and 70).

(a)



(b)



(c)

Figura 4.9: Experimental color for the final time of cooking of a) very rare, b) medium rare and c) done degrees of cooking. Turn over at two thirds of the total cooking time.

Since the model has been validated, the evolution of the meat color over time can be known, and, thus, we can determine the turn over time of the meat for which the degree of cooking on both sides of the meat would be similar. In other words, the goal is to achieve a symmetrical distribution of the two areas that are visually appreciated throughout the thickness of the meat. In order to better appreciate the results, the conversion to RGB coordinates has been made from coordinates $L^*$ and $a^*$ and $b^*$. For the latter, a constant value equal to that of raw meat has been considered. This conversion was done using the open source ColorMine software. In this way, the color of the meat has been recreated for different instants and turn over times (Fig. 4.10) for very rare and done degrees of cooking. As it can be visually appreciated in Fig. 4.9, an

area near the surface can be distinguished in which increasingly brownish tones appear over time and also a central area with increasing luminosity over time.
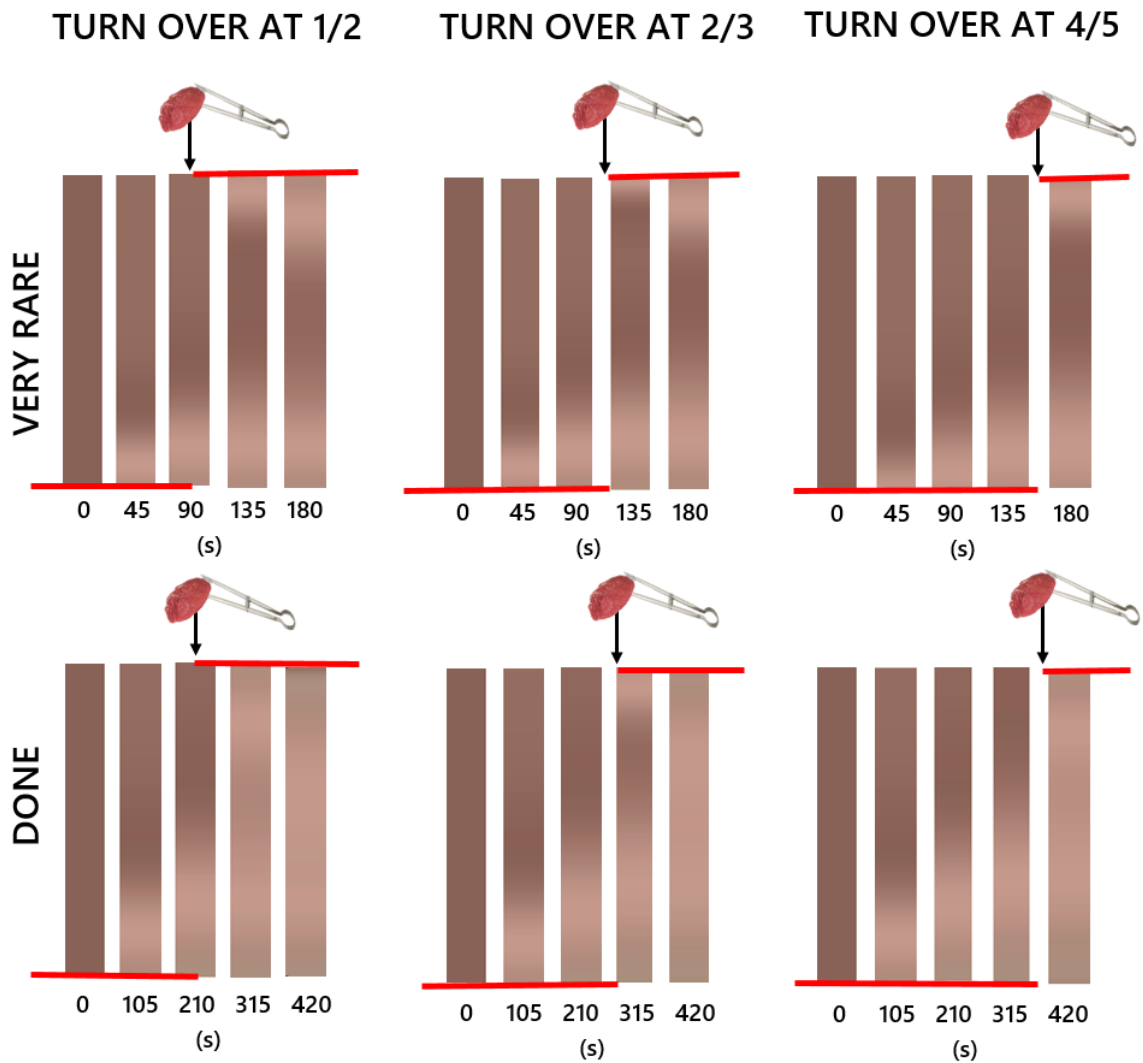


Figura 4.10: Evolution of the meat color along its thickness over time and depending on the turn over time.

The absolute color ($\Delta E^*$) at the end of the cooking process in the central zone of the meat changes from very rare degrees to done degrees: in the central zone of the meat is at a minimum for the very rare and a maximum for the done degrees of cooking.
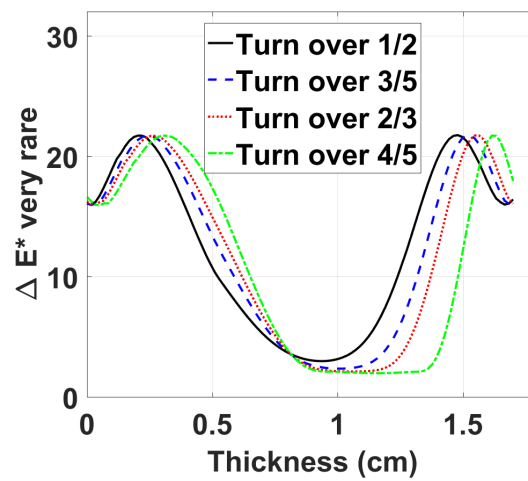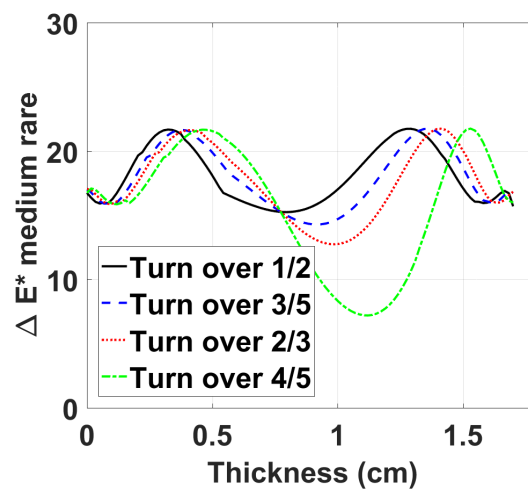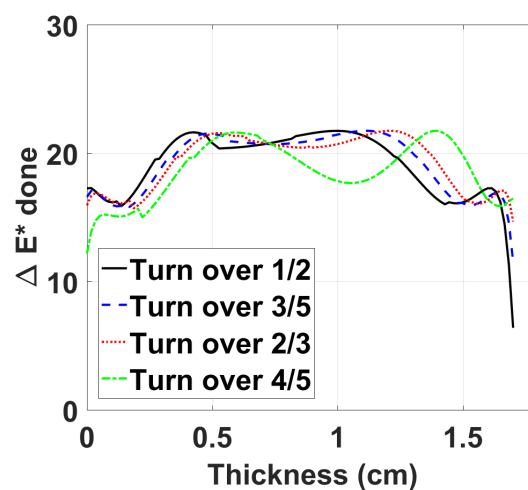
Figura 4.11: Evolution of absolute color, $E^*$, along meat thickness over time and depending on the turn over time for a) very rare, b) medium rare and c) done degrees of cooking.

In Fig. 4.11 the absolute color at the end of the cooking throughout the thickness of the meat is shown for different turning times and cooking degrees. For the very rare condition, the absolute color in the center of the meat has hardly changed with respect to the raw meat ($\Delta E^*$ around 2), while as we approach both extremes, the absolute color increases, reaching a maximum value, and then decreases sharply in the outermost area of the meat. For the medium rare and done degrees of cooking, the absolute color profile is similar, but the absolute color in the center of the meat is between 7 and 15 for medium rare and around 21 for done. The absolute color begins to decrease in every case depending on the turn over time.

As discussed above, Fig. 4.12 shows the final appearance of the color in the interior of the meat for different degrees of cooking and turn over times. From the model results, the position where the absolute color begins to decrease can be obtained, and it is indicated with a blue line, as well as the distance of those points to the edge of the meat. When the time of cooking is shorter (very rare) and the turn over occurs half way through the total cooking time, a product with a similar doneness on both sides is achieved. For longer times (medium rare and done degrees of cooking), the symmetry in color is achieved when the turn over time is three fifths and two thirds of the total cooking time, respectively.
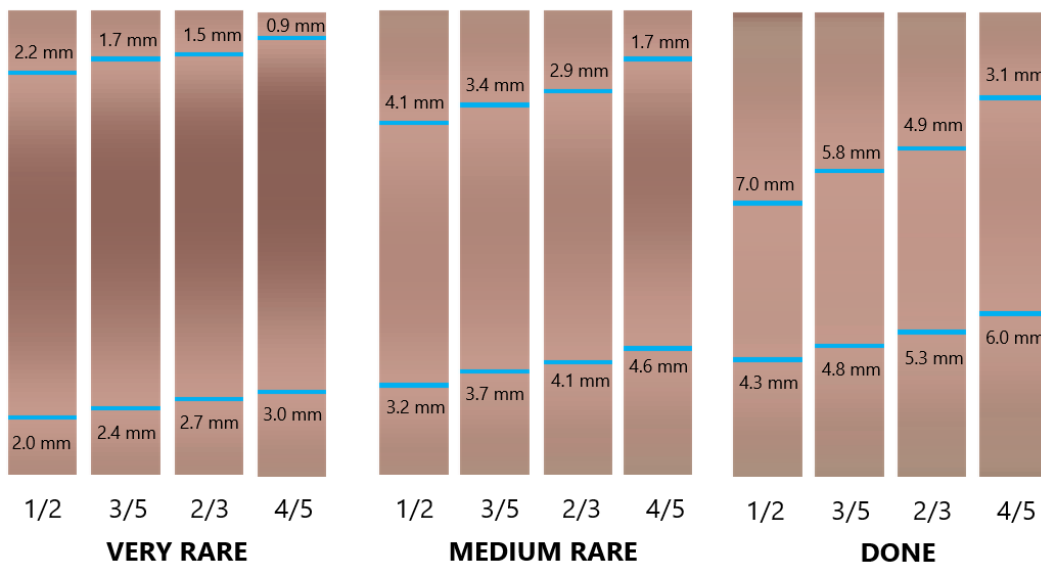


Figura 4.12: Final color of the meat for each turn over time at very rare, medium rare and done degrees of cooking. The blue lines indicate the positions in which the absolute color begins to decrease. Lower side of the meat in the figure was put in contact with the pan firstly.

## 4.4.   Conclusions

Color changes in beef meat during cooking was understood as the transition from reddish to brownish tones associated with the modifications suffered by heme proteins. However, in this study it has been demonstrated that luminosity was the color coordinate that contributed the most to the change in absolute color, confirming the importance of structural changes that modify the dispersion of light in the color of cooked meat. Using a response surface method which has allowed the implementation of beef color changes in the computational model, the evolution of the CIELab coordinates, $L^*$ and $a^*$, during beef cooking has been described. It has been observed that the different conditions of conservation (fresh, refrigerated and frozen) have no influence in the evolution of the absolute color of the meat during the heat treatment, at least not to be visually appreciated. In this way, the prediction methodology developed is valid independently of the conservation procedure.

This study completes the 3D mathematical model of meat pan cooking that includes the heat and moisture transfer phenomena, simultaneously with the meat deformation, during the two-sided pan cooking of beef, and has the kinetics of color change linked to it. This model allowed us to adequately predict the color changes of the meat as shown by the good agreement between the numerical and experimental results for the three degrees of doneness tested. According to this, it can be concluded that the profile of the luminosity along the thickness depends on the degree of doneness, being at a minimum in the center for short cooking times (very rare) and at a maximum for longer cooking times (medium rare and done). However, in all cases, a decrease in the value of the luminosity, and consequently of the absolute color, at points close to the surface has been observed. The location of these points depends on the time at which the meat has been turned over. The applicability of the model for practical cooking purposes has been illustrated by the calculation of the turn over time so that the steaks are cooked homogeneously on both sides. Depending on the degree of doneness desired, the turn over time would change.

# Chapter 5

# Conclusions and future work

This Chapter includes a brief summary of the work developed in this Thesis along with the main conclusions extracted from the fulfillment of this work. In addition, some future lines in the research field of the simulation of meat cooking are suggested.

## 5.1.   Conclusions

In recent years, Food Science has experienced a great growth in the search of healthier and better quality food but also in more efficient cooking processes. This field has been supported especially in Food Engineering. These areas of scientific activity are developed as a response to the challenges of the contemporary food market. Science advances towards the development of computational models capable of simulating different types of food treatments.

### 5.1.1.   Simulation of ohmic heating as a system for microbial inactivation in solid food

Regarding the study of simulating the ohmic heating, an axisymmetric finite element model capable of reproducing the ohmic heating suffered by cylindrical pieces of agar in a PEF treatment chamber has been developed. This model can incorporate the thermostating of the chamber electrodes. A sensitivity analysis of the main operating parameters of the PEF chamber described has been carried out, exploring every possible combinations to find an optimal one to achieve a uniform, homogeneous and efficient heating. In this study, the inactivation of the Salmonella Typhimitium 878 has been also implemented. This inactivation depends on the temperature reached by the food sample and on the times of application of the treatment. This is also a novelty with

respect to other investigations in the field. The main conclusions obtained from this research are listed below:

- The axisymmetric model adequately reproduces the experimental results of the PEF chamber prototype used for this study. Therefore we can affirm that the assumptions made regarding the boundary conditions of the model and the physics involved are correct.

- It was verified that only by applying PEF pulses by the treatment chamber, colder areas appeared near to the electrodes that were initially at room temperature. Thermostating these electrodes was proposed so that their initial temperature was higher to improve the final temperature homogeneity of the agar sample.

- A sensitivity study was carried out on the main operating parameters of the chamber, including the parameters that govern the thermostating of the electrodes. First, through an analysis of 4 variables, it was detected that the longer the time of the previous thermostation of the electrodes, the better the temperature uniformity in the agar sample. This is because a stable final temperature is achieved at the electrode. Subsequently, it was found that a uniform temperature was reached in the electrodes after 30 minutes of thermostating.

- By setting the thermostation time at 30 minutes, another sensitivity analysis was carried out, which concluded that a higher thermostation temperature of the electrodes entailed appreciable differences in the temperature homogeneity of the agar sample. The higher this temperature being the better for this homogeneity. This sensitivity analysis also provided information about the voltage of the pulses and the frequency: the higher the voltage as well as the frequency, the greater the homogeneity of temperature in the sample. However, thermostation parameters are more relevant regarding this aspect. Higher frequency and voltage mainly require shorter PEF application times. It would be necessary to make a compromise between energy requirement and temperature homogeneity.

- Once the best operating conditions were determined, the inactivation of the Salmonella Typhimitium 878 was implemented in the model, confirming that a greater homogeneity in the temperature of the sample also implied a greater homogeneity in the inactivation. Subsequently, it was numerically verified that, since the agar continued to heat up by inertia after the application of the PEF pulses, it was possible to obtain a greater inactivation than the final one after the treatment. This is a great advantage to avoid the overheating of the central

part of the sample ensuring that the necessary inactivation is reached in the most remote areas.

The main conclusions described on this section have been already presented in two international journals detailed in Appendix B.

## 5.1.2.   Simulation of beef meat pan cooking

Through this Thesis, several aspects of the simulation of beef meat has been considered. Previous works developed on the area of meat cooking had focused on baking or frying. There are little studies on pan cooking and usually they considered simplifications for both the geometry and material behavior. Although those approaches have been very useful as an starting point for this research, some aspects such as turning over the meat, the thermal contact between the pan and the meat and the evolution of color throughout the cooking have not been implemented in those models. This research is a novelty in these regards. This is one of the final objectives of this study, to describe the evolution of the color of the meat. In addition, in this model the temperature acquired by the meat during different times and for different thicknesses was adjusted taking into account experimental results, as well as the weight loss. The main conclusions extracted from this work are listed below:

- The 3D finite element model developed in this work is capable of reproducing the beef pan cooking for different thicknesses and over different cooking times. The comparison of temperature and weight loss with experimental results have allowed us to accept the hypothesis introduced in the problem, as well as the conditions and parameters of the model.

- With this model we can conclude that small deviations in the thickness of the meat can lead to appreciable changes in the temperature of the beef steaks, so that the size of the meat pieces is important when trying to predict the cooking process.

- It has been demonstrated that the weight loss in beef meat is linear with time, but it could be different in other types of meat. Thus, it would be interesting to apply this model to meat of different characteristics. A study of the water holding capacity of the new meat should be carried out, as well as the parameters of the model involved in the weight loss phenomenon.

- The evolution of the color of the meat was also implemented in the developed model, as a function of the CIELab coordinates, $a^*$ and $L^*$. These coordinates

depend especially on the temperature, so the previous good adjustment also means a good fit of the evolution of them.

- In this study, it has been shown that luminosity $L^*$, is the coordinate that most affects the change in absolute color, so we conclude that the structural changes that modify the dispersion of light in the color of cooked meat are very important and they can not be ignored.

- This study has also shown that the condition of conservation (fresh, refrigerated and frozen), did not influence the evolution of the meat color the cooking sufficiently to be visually appreciated.

- One of the applications of this study was to determine when the meat had to be turned over to achieve a symmetrical color profile throughout its thickness. The ideal moment to turn over the meat vary regarding the different cooking degrees proposed, but it can be said that the optimal moment is at two thirds of the final cooking time.

- The most determining parameters which affect the meat cooking have been obtained. Basically, these could be reduced to the initial water content and the thickness of the piece of meat.

Some of the main conclusions described on this section have been already presented in international conferences and research journals detailed in Appendix B.

## 5.2.   Future lines

The work presented in this Thesis constitutes the first but firm step towards computer aided food engineering, addressed by the AMB group of the University of Zaragoza. However, there are many open research lines to reach a full understanding and application of the developed models, both for domestic cooking and for its industrial application. As for the simulation of beef pan cooking, it has been the first step to seek the direct application of cooking guidance in domestic kitchens. The final objective would be to obtain models for all types of meat cooking, for all types of meat and for the rest of food, as well as to use these models to create an artificial intelligence tool capable of interpreting results during cooking to guide the user. Regarding the simulation of PEF ohmic heating treatment, it has been seen that it can be a very important tool to optimize these processes aimed to the inactivation of bacteria in food. Thus, it could be used to evaluate the inactivation of other bacteria, in other kind of

food or for other types of PEF chambers with other operating conditions. In addition, the possibility of applying PEF treatments to meat in an industrial environment could be studied with the aim to achieve food safety objectives, or even more, to carry out a study on the viability of bringing this type of heating to domestic kitchens. Some of these future lines are proposed here:

- The model adaptation to other geometries such as that of hamburgers. They are made of minced meat and behave differently when cooked, so its volume and shape change from that of a piece of beef steak. It would be necessary to study if the parameters and conditions applied in this study are suitable for other type of geometries.

- To extend the modeling technique to other type of cooking environments such as the oven. The boundary conditions are different in this type of cooking since the heat is not transmitted in the same way.

- To study the capacity of this model to reproduce the cooking of other types of meat and establish which of the model parameters should be modified and which remain the same.

- It would be interesting to incorporate the anisotropy of the meat during the process of protein shrinkage. This effect is determined by the orientation of the muscle fibers along the piece of meat and therefore, the model could predict in a more realistic way the deformed configuration that affect the heat transfer between the pan and the food.

- To perform the processing of the data obtained with these models evaluated in different scenarios in order to create a machine learning technique, capable of predicting the behavior of the meat when it is cooked in a real domestic environment.

- To study the inactivation of other microorganisms by applying ohmic heating by PEF systems.

- To deep into the optimization of PEF chambers, also taking into account the efficiency and not only the inactivation achieved.

- To analyze the viability of applying PEF treatments in meat, both at an industrial environment and at a domestic one.

# Chapter 6

# Bibliography

M. Abril, M. M. Campo, A. Önenç, C. Sañudo, P. Albertí, and A. I. Negueruela. Beef colour evolution as a function of ultimate pH. *Meat Science*, 2001.

S. Ahmad, M. A. Khan, and M. Kamil. Mathematical modeling of meat cylinder cooking. *LWT - Food Science and Technology*, mar 2015.

Z. T. Alkanan, A. B. Altemimi, A.R. S. Al-Hilphy, D. G. Watson, and A. Pratap-Singh. Ohmic heating in the food industry: Developments in concepts and applications during 2013–2020. *Applied Sciences*, 2021.

I. Álvarez and J. Raso. *Bacterial Inactivation for Food Preservation*. PhD thesis, Akiyama, H., Heller, R., Bioelectrics, Japan, Springer, 2017.

M.Á. Ariza-Gracia, M.P. Cabello, G. Cebrián, B. Calvo, and I. Álvarez. Experimental and computational analysis of microbial inactivation in a solid by ohmic heating using pulsed electric fields. *Innovative Food Science & Emerging Technologies*, 2020.

L. Astráin-Redín, J. Moya, M. Alejandre, E. Beitia, J. Raso, B. Calvo, G. Cebrián, and I. Álvarez. Improving the microbial inactivation uniformity of pulsed electric field ohmic heating treatments of solid products. *LWT*, 2022.

H. S. Bansal, P. S. Takhar, C. Z. Alvarado, and L. D. Thompson. Transport mechanisms and quality changes during frying of chicken nuggets-hybrid mixture theory based modeling and experimental verification. *J. Food Sci.*, pages E2759–E2773, 2015.

J. Baranyi, C. Pin, and T. Ross. Validating and comparing predictive models. *International journal of food microbiology*, 1999.

S. Barbera and S. Tassone. Meat cooking shrinkage: Measurement of a new meat quality parameter. *Meat Science*, 2006. ISSN 0309-1740.

J. A. Bernad Pérez. Simulación computacional de la retracción que se produce en el cocinado de la carne mediante modelos multifísicos. Trabajo fin de grado, Universidad de Zaragoza, 2019.

E. Bottani and Andrea Volpi. An analytical model for cooking automation in industrial steam ovens. *Journal of Food Engineering*, 90(2):153–160, 2009.

R. Buckow, Sieh Ng, and S. Toepfl. Pulsed electric field processing of orange juice: A review on microbial, enzymatic, nutritional, and sensory quality and stability. *Comprehensive Reviews in Food Science and Food Safety*, 2013.

C. Chinwuba. Timoshenko beam theory for the flexural analysis of moderately thick beams. *Department of Civil Engineering, Enugu State University of Science & Technology, Enugu State, Nigeria*, 2019.

W. Choi, Sang-Soon Kim, Sang-Hyun Park, Jun-Bae Ahn, and Dong-Hyun Kang. Numerical analysis of rectangular type batch ohmic heater to identify the cold point. *Food Science & Nutrition*, 2020.

Y. Choi and M. R. Okos. Effects of temperature and composition on thermal properties of foods. *Journal of Food Process and Applications*, 1986a.

Y. Choi and M. R. Okos. Effects of temperature and composition on thermal properties of foods.. *Journal of Food Process and Applications*, 1986b.

A.K. Datta. Porous media approaches to studying simultaneous heat and mass transfer in food processes. i: Problem formulations. *Journal of Food Engineering*, 2007a.

A.K. Datta. Porous media approaches to studying simultaneous heat and mass transfer in food processes. i: Problem formulations. *Journal of Food Engineering*, 2007b.

A.K. Datta. Toward computer-aided food engineering: Mechanistic frameworks for evolution of product, quality and safety during processing. *Journal of Food Engineering*, 2016.

A.A.P. De Alwis and P.J. Fryer. A finite-element analysis of heat generation and transfer during ohmic heating of food. *Chemical Engineering Science*, 1990.

T. Defraeye, C. Shrivastava, T. Berry, P. Verboven, D. Onwude, S. Schudel, A. Bühlmann, P. Cronje, and R. M. Rossi. Digital twins are coming: Will we need them in supply chains of fresh horticultural produce? *Trends in Food Science & Technology*, 2021.

RGM Van der Sman. Moisture transport during cooking of meat: An analysis based on flory–rehner theory. *Meat science*, 2007.

A. Dhall and A. K. Datta. Transport in deformable food materials: A poromechanics approach. *Chemical Engineering Science*, 2011.

S. Elshahat, J. V. Woodside, and M. C. McKinley. Meat thermometer usage amongst european and north american consumers: A scoping review. *Food Control*, 2019.

F. Erdogdu, F. Sarghini, and F. Marra. Mathematical modeling for virtualization in food processing. *Food Engineering Reviews*, 2017.

A. H. Feyissa, K. V. Gernaey, and J. Adler-Nissen. 3d modelling of coupled mass and heat transfer of a convection-oven roasting process. *Meat science*, 2013.

P. J. Flory. Phase changes in proteins and polypeptides. *Journal of Polymer Science*, 1961.

A.J. Fowler and A. Bejan. The effect of shrinkage on the cooking of meat. *International Journal of Heat and Fluid Flow*, 1991.

F. Gerhard. *Meat Products Handbook: Practical Science and Technology.* Woodhead Publishing Series in Food Science, Technology and Nutrition, 2011.

D. Gerlach, N. Alleborn, A. Baars, A. Delgado, J. Moritz, and D. Knorr. Numerical simulations of pulsed electric fields for food preservation: A review. *Innovative Food Science & Emerging Technologies*, 2008.

S.M. Goñi and V.O. Salvadori. Kinetic modelling of colour changes during beef roasting. *Procedia Food Science*, 2011.

T. Gulati and A. K. Datta. Mechanistic understanding of case-hardening and texture development during drying of food materials. *Journal of Food Engineering*, 2015.

J. Hughes, F. Clarke, P. Purslow, and R. Warner. High pH in beef longissimus thoracis reduces muscle fibre transverse shrinkage and light scattering which contributes to the dark colour. *Food Research International*, 2017.

J.M. Hughes, S.K. Oiseth, P.P. Purslow, and R.D. Warner. A structural approach to understanding the interactions between colour, water-holding capacity and tenderness. *Meat Science*, 2014.

F. Icier and C. Ilicali. The use of tylose as a food analog in ohmic heating studies. *Journal of Food Engineering*, 2005.

J.N. Ikediala, L.R. Correia, G.A. Fenton, and N. Ben-Abdallah. Finite element modeling of heat transfer in meat patties during single-sided pan-frying. *Journal of Food Science*, 1996.

H. Isleroglu and F. Kaymak-Ertekin. Modelling of heat and mass transfer during cooking in steam-assisted hybrid oven. *Journal of Food Engineering*, 181:50–58, 2016.

M. E. Katekawa and M. A. Silva. A review of drying models including shrinkage effects. *Drying technology*, 2006.

N. Kaur and A. K. Singh. Ohmic heating: Concept and applications-a review. *Critical reviews in food science and nutrition*, 2016.

N. King and R. Whyte. Does it look cooked? a review of factors that influence cooked meat color. *Journal of Food Science*, 2006.

A. Kondjoyan. A review on surface heat and mass transfer coefficients during air chilling and storage of food products. *International Journal of Refrigeration*, 2006.

A. Kondjoyan, S. Oillic, S. Portanguen, and J.-B. Gros. Combined heat transfer and kinetic models to predict cooking loss during heat treatment of beef meat. *Meat Science*, 95(2):336–344, 2013.

A. Kondjoyan, A. Kohler, C. E. Realini, S. Portanguen, R. Kowalski, S. Clerjon, P. Gatellier, S. Chevolleau, J. M. Bonny, and L. Debrauwer. Towards models for the prediction of beef meat quality during cooking. *Meat Science*, 2014.

K. León, D. Mery, F. Pedreschi, and J. León. Color measurement in lab units from rgb digital images. *Food Res. Int*, 2006.

B. Ling, J. Tang, F. Kong, E. J. Mitcham, and S. Wang. Kinetics of food quality changes during thermal processing: a review. *Food and Bioprocess Technology*, 2014.

M.M. López Osornio, G. Hough, A. Salvador, E. Chambers, S. McGraw, and S. Fiszman. Beef's optimum internal cooking temperature as seen by consumers from different countries using survival analysis statistics. *Food Quality and Preference*, 2008.

R.A. Mancini and M.C. Hunt. Current research in meat color. *Meat Science*, 2005.

F. Marra. Mathematical model of solid food pasteurization by ohmic heating: Influence of process parameters. *The Scientific World Journal*, 2014:1–8, 2014. doi: 10.1155/2014/236437.

H. Martens, E. Stabursvik, and M. Martens. Texture and colour changes in meat during cooking related to thermal denaturation of muscle proteins. *Journal of Texture Studies*, 1982.

L. Mayor and A. M. Sereno. Modelling shrinkage during convective drying of food materials: a review. *Journal of food engineering*, 2004.

S.M. McCurdy, V. Hillers, and S.E. Cann. Consumer reaction and interest in using food thermometers when cooking small or thin meat items. *Food Protection Trends*, 2005.

C. McLaren, C. Kopatz, N. Smith, and H. Jain. Development of highly inhomogeneous temperature profile within electrically heated alkali silicate glasses. *Scientific Reports*, 2019.

D. C. Montgomery. *Design and analysis of experiments*. John wiley & sons, 2017.

Jojo Moolayil. *Learn Keras for Deep Neural Networks*. Springer Science+Business Media New York, 2019.

J. Moya, S. Lorente-Bailo, A. Ferrer-Mairal, M. Martínez, B. Calvo, J. Grasa, and M. Salvador. Color changes in beef meat during pan cooking: kinetics, modeling and application to predict turn over time. *European Food Research and Technology*, 2021a.

J. Moya, S. Lorente-Bailo, M.L. Salvador, A. Ferrer-Mairal, M.A. Martínez, B. Calvo, and J. Grasa. Development and validation of a computational model for steak double-sided pan cooking. *Journal of Food Engineering*, 298, 2021b. ISSN 0260-8774.

J. Moya, L. Astráin-Redín, J. Grasa, G. Cebrián, B. Calvo, and I. Álvarez. A numerical approach to analyze the performance of a pef-ohmic heating system in microbial inactivation of solid food. *Frontiers in Food Science and Technology*, 2022.

N. Myhrvold. *Modernist cuisine: el arte y la ciencia de la cocina*. Taschen Benedikt, 2017.

H. Nelson, S. Deyo, S. Granzier-Nakajima, P. Puente, K. Tully, and J. Webb. A mathematical model for meat cooking. *The European Physical Journal Plus*, 2020.

P. Nesvadba. Thermal properties of unfrozen foods. In *Engineering Properties of Foods, Fourth Edition.* CRC Press, 2014.

C. Pakula and R. Stamminger.  Measuring changes in internal meat colour, colour lightness and colour opacity as predictors of cooking time. *Meat Science*, 2012.

G. Pataro, B. Senatore, G. Donsì, and G. Ferrari. Effect of electric and flow parameters on pef treatment efficiency. *Journal of Food Engineering*, 2011.

J. Peng, J. Tang, D. M. Barrett, S. S. Sablani, N. Anderson, and J. R. Powers. Thermal pasteurization of ready-to-eat foods and vegetables: Critical factors for process design and effects on quality. *Critical Reviews in Food Science and Nutrition*, 2017.

R. Pereira, J. Martins, C. Mateus, J. Teixeira, and A. Vicente.  Death kinetics of escherichia coli in goat milk and bacillus licheniformis in cloudberry jam treated by ohmic heating. *Chemical Papers- Slovak Academy of Sciences*, 2007.

P.P. Purslow, S. Oiseth, J. Hughes, and R.D. Warner. The structural basis of cooking loss in beef: Variations with temperature and ageing. *Food Research International*, 2016.

I. Pérez Salesa. Simulación numérica del cocinado de carne en plancha. Trabajo fin de grado, Universidad de Zaragoza, 2019.

F. Rabeler and A. H. Feyissa. Modelling the transport phenomena and texture changes of chicken breast meat during the roasting in a convective oven. *J. Food Eng.*, 237, 2018a.

F. Rabeler and A. H. Feyissa. Kinetic modeling of texture and color changes during thermal treatment of chicken breast meat. *Food and Bioprocess Technology*, 2018b.

F. Rabeler and A.H. Feyissa.  Kinetic modeling of texture and color changes during thermal treatment of chicken breast meat. *Food and Bioprocess Technology*, 2018b.

H. S. Ramaswamy, M. Marcotte, S. Sastry, and K. Abdelrahim. *Ohmic Heating in food processing.* CRC Press, 2014.

J. Raso and V. Heinz. Pulsed electric fields technology for the food industry. *Pulsed Electric Fields Technology for the Food Industry: Fundamentals and Applications, Food Engineering*, 2006.

R. Rocca-Poliméni, N. Zárate Vilet, S. Roux, J.-L. Bailleul, and B. Broyart. Continuous measurement of contact heat flux during minced meat grilling. *Journal of Food Engineering*, 242, 2019.

G. Saldaña, E. Puértolas, I. Álvarez, N. Meneses, D. Knorr, and J. Raso. Evaluation of a static treatment chamber to investigate kinetics of microbial inactivation by pulsed electric fields at different temperatures at quasi-isothermal conditions. *Journal of Food Engineering*, 2010.

S. Sastry. Advances in ohmic heating and moderate electric field (MEF) processing. In *Novel Food Processing Technologies*. CRC Press, 2005.

S. K. Sastry and Q. Li. Modeling the ohmic heating of food: Ohmic heating for thermal processing of foods: Government, industry, and academic perspectives. *Food technology (Chicago)*, 1996.

S. K. Sastry, B. F. Heskitt, S. S. Sarang, R. Somavat, , and K. Ayotte. *Why Ohmic Heating? Advantages, Applications, Technology, and Limitations*. CRC Press, 2014.

S. Schroeder, R. Buckow, and K. Knoerzer. Numerical simulation of pulsed electric field (pef) processing for chamber design and optimization. In *International Conference on CFD in the Minerads and Process Industries CSIRO, 17th, Australia*, 2009.

J. Shim, S. H. Lee, and S. Jun. Modeling of ohmic heating patterns of multiphase food products using computational fluid dynamics codes. *Journal of Food Engineering*, 2010.

P. G. Smith. *An Introduction to Food Process Engineering*. Springer US, Boston, MA, 2011.

R. Somavat, H. Mohamed, Yoon-Kyung Chung, A. Yousef, and S. Sastry. Accelerated inactivation of geobacillus stearothermophilus spores by ohmic heating. *Journal of Food Engineering*, 108, 2012.

S. Stella, C. Bernardi, and E. Tirloni. Influence of skin packaging on raw beef quality: A review. *Journal of Food Quality*, 2018.

J. Straub. NBS/NRC steam tables. VonL. haar, j. s. gallagher undG. s. kell. hemisphere publishing corp., washington-new york-london 1984. 1. aufl., XII, 320 s., geb., $ 34.50. *Chemie Ingenieur Technik*, 1985.

S. P. Suman, M. C. Hunt, M. N. Nair, and G. Rentfrow. Improving beef color stability: Practical strategies and underlying mechanisms. *Meat Science*, 2014.

S. Toepfl, V. Heinz, and D. Knorr. Pulsed electric field technology for the food industry. *Food Engineering Series*, 2006.

E. Tornberg. Effects of heat on meat proteins - implications on structure and quality of meat products. *Meat Sci.*, 2005.

G. R. Trout. Variation in myoglobin denaturation and color of cooked beef, pork, and turkey meat as influenced by pH, sodium chloride, sodium tripolyphosphate, and cooking temperature. *Journal of Food Science*, 1989.

R. G. M. van der Sman. Modeling cooking of chicken meat in industrial tunnel ovens with the flory–rehner theory. *Meat Science*, 2013.

R.G.M. van der Sman. Moisture transport during cooking of meat: An analysis based on flory–rehner theory. *Meat Science*, 76, 2007.

K.N. van Koerten, D. Somsen, R.M. Boom, and M.A.I. Schutyser. Modelling water evaporation during frying with an evaporation dependent heat transfer coefficient. *Journal of Food Engineering*, 197, 2017.

L. Vujosevic and V. A. Lubarda. Finite-strain thermoelasticity based on multiplicative decomposition of deformation gradient. *Theoretical and applied mechanics*, 2002a.

L Vujosevic and VA Lubarda. Finite-strain thermoelasticity based on multiplicative decomposition of deformation gradient. *Theoretical and applied mechanics*, 2002b.

Q. Wang, Y. Li, Da-Wen Sun, and Z. Zhu. Enhancing food processing by pulsed and high voltage electric fields: Principles and applications. *Critical reviews in food science and nutrition*, 2018.

Wei-Chi Wang and S. Sastry. Effects of moderate electrothermal treatments on juice yield from cellular tissue. *Innovative Food Science & Emerging Technologies*, 2002.

J.W.S. Yancey, M.D. Wharton, and J.K. Apple. Cookery method and end-point temperature can affect the warner–bratzler shear force, cooking loss, and internal cooked color of beef longissimus steaks. *Meat Science*, 2011.

G. Yildiz-Turp, I. Y. Sengun, P. Kendirci, and F. Icier. Effect of ohmic treatment on quality characteristic of meat: A review. *Meat Science*, 2013.

S. Yoon, J. Lee, Ki-Myoung Kim, and Cherl-Ho Lee. Leakage of cellular materials of yeast (saccharomyces cerevisiae) by ohmic heating. *Journal of Microbiology and Biotechnology*, 2002.

J. Zhang, A. K. Datta, and S. Mukherjee. Transport processes and large deformation during baking of bread. *AIChE Journal*, 2005.

W. Zhao, R. Yang, and H. Q. Zhang. Recent advances in the action of pulsed electric fields on enzymes and food component proteins. *Trends in Food Science & Technology*, 2012.

# Annexes

# Annex A

# Resumen en Español

El modelado de diferentes procesos de cocinado de alimentos ha experimentado un importante crecimiento en los últimos años. Inicialmente, los modelos eran fundamentamente fenomenólogicos y recimiente se han desarrollados modelos basados en la física del proceso a simular, incorporando enfoques multiescala, multifase y multifísicos (Datta, 2016). Todo esto ha sido posible al avance de las herramientas numéricas y la mayor capacidad de cálculo de los ordenadores. El modelado numérico permiten ampliar el conocimiento de estos procesos con la finalidad última de mejorarlos, establecer estrategias de ayuda al usuario o bien, fundamentalmente a nivel industrial, optimizar dichos procesos.

Esta Tesis forma parte del proyecto ARQUE, una colaboración entre el Grupo de Electrodomésticos BSH y la Universidad de Zaragoza, concretamente con el grupo AMB. Este proyecto propone abrir la línea de investigación sobre la cocina del futuro, una cocina inteligente, aprovechando el avance en la sensorización, el internet de las cosas y su combinación con el modelado de procesos de cocinado y nuevas herramientas numéricas, como la inteligencia artificial.

En este contexto, esta Tesis persigue el objetivo de encontrar una metodología numérica que permita abordar los principales fenómenos físicos que se producen en los alimentos como consecuencia de los tratamientos térmicos que sufren durante el cocinado, tanto a nivel doméstico como en futuros procesos industriales.

En concreto, a nivel doméstico, en este trabajo se ha desarrollado una metodología numérica que nos permite simular el comportamiento de la carne de ternera durante el cocinado en sartén mediante una placa de inducción. El modelo perimite obtener la evolución temporal y espacial de la temperatura, la concentracción y transporte de humedad, asi como el color. Como ejemplo industrial, la metodología se ha

utilizado para estudiar otras técnicas de calentamiento, fundamentalmente aplicables a tratamientos industriales de alimentos, como es la aplicación de calentamiento ohmico mediante campos eléctricos pulsados, PEF. Una de las aplicaciones de este proceso es mejorar de calidad y seguridad del alimento gracias a su potencia para la inactivación bacteriana.

Para comprender en su totalidad las implicaciones de esta Tesis, se requiere de una visión general de los aspectos biológicos y físicos que se producen en el alimento cuando es sometido a un proceso de calentamientos. En los apartados siguientes éstos se describen brevemente, incluyendo los pricipales trabajos publicados en el campo.

## A.1.   Aspectos teóricos

### A.1.1.   El calentamiento ohmico mediante PEF

En los últimos años se ha producido una creciente demanda de nuevas tecnologías en procesos térmicos en la industria alimentaria, como por ejemplo el calentamiento óhmico, el dieléctrico y el calentamiento inductivo. Algunas ventajas del primero, el calentamiento óhmico, es que se pueden tratar alimentos de mayor tamaño, debido a una mayor capacidad de penetración en éstos, provocando así un calentamiento más uniforme (Ramaswamy et al., 2014). El principio fundamental del calentamiento óhmico es que cuando una corriente eléctrica fluye a través de un conductor, las moléculas o átomos del material sufren una agitación debido al movimiento de cargas dentro del producto, lo que resulta en un aumento de temperatura. En los conductores metálicos, las cargas en movimiento son electrones, pero en los alimentos, las cargas suelen ser iones u otras moléculas cargadas como las proteínas. Estas cargas se mueven hacia el electrodo de polaridad opuesta (Ramaswamy et al., 2014).

Dentro de las técnicas de calentamiento óhmico, los campos eléctricos pulsados (PEF) es una tecnología que consiste en aplicar a un producto campos eléctricos de alta intensidad (0.5-50 kV/cm) de forma intermitente por periodos de tiempo del orden de microsegundos. El producto se coloca entre dos electrodos y el calentamiento se produce desde el interior hacia el exterior del alimento. Se trata de un sistema energéticamente eficiente porque permite alcanzar altas temperaturas en el producto en un corto período de tiempo. Además, los campos eléctricos de alta intensidad inducen la formación de poros en las membranas celulares del producto (electroporación) afectando a los microorganismos que pueden estar presentes en éste. Como resultado de este fenómeno, el material del interior de la célula se expulsa al entorno exterior, lo que provoca la
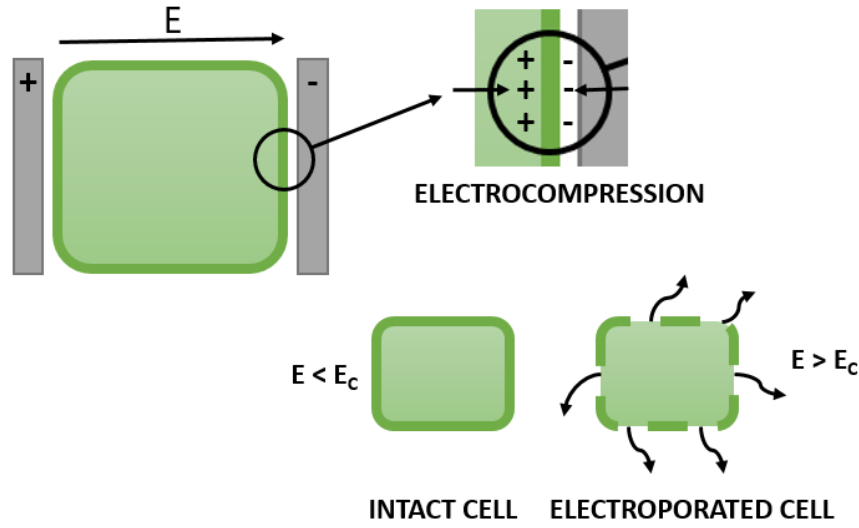
muerte celular (Figura A.1).



Figura A.1: Efecto del campo eléctrico en una celda, donde $E_c$ es el campo eléctrico límite y $E$ es el campo eléctrico en ese momento.

La generación de calor en este tipo de sistema se basa en el Efecto Joule descrito por la Ecuación A.1:

$$W = \int_0^W \chi \Xi^2 dT \qquad (A.1)$$

donde $\chi$ es la conductividad eléctrica del producto tratado en S/m, $\Xi$ es el campo eléctrico en V/m y dt es el diferencial de tiempo durante el cual el campo eléctrico se aplica en segundos (Sastry and Li, 1996).

De esta manera, al aplicar una diferencia de potencial entre los electrodos separados por el producto a pulsar, se produciría el calentamiento del mismo. Al observar esta ecuación, el campo eléctrico tiene una gran importancia en la energía transferida al producto, ya que ligeras modificaciones en su valor aumentan al cuadrado esta transmisión. Este campo eléctrico depende tanto del voltaje aplicado como de la frecuencia de los pulsos.

Sin embargo, la limitación principal de esta tecnología en productos sólidos es que, dado que el calentamiento ocurre de adentro hacia afuera, este calentamiento no es estrictamente homogéneo en todo el producto (Ariza-Gracia et al., 2020, Icier and Ilicali, 2005, Marra, 2014, Shim et al., 2010). Por ello, podrían aparecer puntos fríos en las zonas de contacto de los electrodos con el alimento, mientras que los puntos más calientes estarían ubicados en el centro de la comida. Por tanto, de cara a

conseguir la pasteurización o inactivación microbiana en todos los puntos del producto es necesario alcanzar una determinada temperatura en todo el producto, lo cual implica un sobrecalentamiento en la zona central, por lo que podrían producirse alteraciones no deseadas en las propiedades del producto en estas zonas.

La simulación numérica de este proceso de calentamiento permitirá diseñar equipos más eficaces que den lugar a incrementos de temperaturas uniformes en el producto.

## A.1.2. Cocinado doméstico de carne de ternera a la plancha

Respecto al cocinado doméstico, en esta tesis nos hemos focalizado en el cocinado de carne de ternera a la plancha en una placa de inducción. En este proceso, el calor se transmite desde la superficie de la sartén hacia el interior de la carne por contacto directo. Esta transferencia de calor, de la sartén al alimento, inicia el calentamiento de la carne, provocando cambios en sus propiedades.

Al aumentar la temperatura, se produce la desnaturalización de las proteínas, cambiando así la estructura y las propiedades de éstas. La desnaturalización consiste principalmente en la pérdida de la estructura helicoidal de las proteínas y cambios en la hidrofobicidad de su superficie, provocando la liberación del agua retenida dentro de la carne. El agua dentro de la carne, una vez que se ha producido la desnaturalización de las proteínas, tiende a moverse libremente según el gradiente de presión creado cuando el tejido conectivo se retrae, siendo expulsada hacia la superficie del trozo de carne. Dado que el calentamiento de la carne se produce más rápidamente en su superficie, la capacidad de retención de agua puede disminuir más rápidamente que la pérdida de humedad por evaporación en la superficie; en este caso, una parte del agua se perdería por goteo en estado líquido (Dhall and Datta, 2011).

También se produce la contracción de las fibras de colágeno que componen el tejido conectivo del músculo (Tornberg, 2005). Otros cambios que se producen durante el cocinado de la carne, son las variaciones de textura, tamaño y color, también provocadas por el aumento de temperatura. Siendo, éstos los principales indicadores que utilizan los usuarios para evaluar la calidad de los alimentos cocinados, ya que no es posible cuantificar parámetros como la temperatura de la pieza de carne a simple vista. La variación de color está relacionada con el fenómeno de la desnaturalización de las proteínas: la hemoglobina y la mioglobina se desnaturalizan al alcanzar ciertos valores de temperatura, cambiando su color (se vuelven más claros) (Rabeler and Feyissa, 2018b). Además, a altas temperaturas, se producen las reacciones de Maillard, que provocan el característico color marrón de la carne cocida. En la Figura A.2 se pueden

percibir diferentes tonalidades de color en la carne según el grado de cocinado.



Figura A.2: Evolución del color de la carne según el punto de cocinado.

Teniendo en cuenta todos estos efectos, podemos resumir que el aumento de temperatura conduce a la desnaturalización de las proteínas con la consiguiente liberación de agua, traducido en una pérdida de peso de la carne cocinada, y también cambios en su estructura y su color. Por tanto, las físicas involucrada en este proceso, y por lo tanto motivo de su modelado numérico, serían la transferencia de calor, la transferencia de masa, la mecánica de sólidos y la cinética del color.

## A.2.   Motivación

La principal motivación de esta Tesis radica en la necesidad de ampliar el conocimiento sobre el comportamiento de los alimentos cuando son sometidos a calentamiento, tanto a nivel doméstico como industrial, poder abordar el modelado numérico de los principales fenónemos que se producen.

En el ámbito del cocinado doméstico, esta Tesis se focaliza en el cocinado de carne de ternera en sartén utilizando una placa de inducción. Esta actividad se enmcarca dentro del proyecto ARQUE, en el que participa la Universidad de Zaragoza en colaboración con BSH. Si se conoce el comportamiento de la carne durante el cocinado, es posible crear sistemas de cocinado guiado basados en la respuesta del producto al calentamiento, siendo éste el objetivo a largo plazo de este proyecto.

El gran avance de la tecnología en los últimos años ha permitido incluirla en muchos aspectos de la vida cotidiana. Un ejemplo serían los teléfonos móviles. Por ello, las empresas buscan desarrollar sistemas que conecten estos dispositivos con todo lo que nos rodea, incluso en el ámbito doméstico. La sociedad avanza hacia el desarrollo de casas inteligentes en las que todo este conectado, por ejemplo, todos los electrodomésticos podrían gestionarse desde los smartphones. Además de la conectividad con los electrodomésticos, también se está trabajando para desarrollar

sistemas de cocinado guiados semiautónomos, que permitan al consumidor tomar decisiones acertadas en función del grado de cocinado que desea.

Debido a estas aplicaciones, el desarrollo de modelos numéricos para simular este cocinado supone un campo de estudio de mucho interés. El análisis computacional de los procesos de cocinado ahorra tiempo y dinero al recopilar los datos necesarios para caracterizar este proceso frente a las pruebas experimentales. Cocinar carne es uno de los procesos más simples para empezar, ya que es relativamente fácil agregar variabilidad tanto en el tipo de carne, como en su tamaño, como en la forma en que se cocina.

Los resultados obtenidos en las simulaciones numéricas se pueden implementar en cocinas inteligentes. Estos resultados se pueden utilizar para predecir el comportamiento de los alimentos cuando se cocinan de una determinada manera y en base a unos parámetros iniciales. De esta forma, el usuario podría ser guiado a lo largo del cocinado en función del grado de cocinado que se desee. Con la ayuda de sensores, como balanzas o sensores de temperatura, se podría crear un sistema de retroalimentación que permitiera acceder a todas las variables que intervienen en el proceso en cualquier punto de la pieza y en cualquier momento. Con la ayuda de estos sensores y la información de los modelos, la cocina de inducción también podría volver a calcular la potencia suministrada en función de cómo se estaba llevando a cabo el cocinado hasta ese momento, para garantizar la máxima calidad.

Para tener en cuenta esta calidad del cocinado, es necesario introducir en los modelos indicadores de calidad, en este caso se ha optado por trabajar con el color y la contraccióndel alimento. La contracción es el cambio de dimensiones del producto durante el proceso de calentamiento, como consecuencia de la pérdida de humedad. El consumidor suele asociar que una elevada contracción de la carne puede ser un indicador de baja calidad, por exceso de agua o por efecto de tratamientos hormonales en el animal. El usuario puede hacerse una idea del grado de cocinado que está adquiriendo la carne en función de cuánto se ha encogido la pieza. El contenido de agua en la carne y el encogimiento están relacionados. Ambos tienen que ver con el proceso de desnaturalización que sufren las proteínas cuando se calientan. Desde una perspectiva culinaria, las proteínas actina y miosina tienen el mayor interés. Cuando se desnaturaliza la actina, la carne parece más seca. Por eso la mayoría de la gente prefiere aquellos grados de cocción en los que la miosina ya está desnaturalizada pero aún no la actina, es decir, los grados de cocción menos hechos.

Otras cualidades que indican la calidad del cocinado de la carne son su textura y

su color. La textura no es apreciada por el usuario hasta el momento del consumo, pero sí el color que adquiere durante el cocinado. A través del color, el consumidor juzga si la carne está suficientemente hecha y aceptable para el consumo. También hay diferencias en las preferencias de cada consumidor: estudios como el de López Osornio et al. (2008) muestran las diferencias entre individuos de distintos países y rangos de edad. La *American Meat Science Association* ha desarrollado una guía, *Beef Steak Color Guide*, en la que clasifica el grado de cocinado según el color, como podemos ver en la Figura A.3.
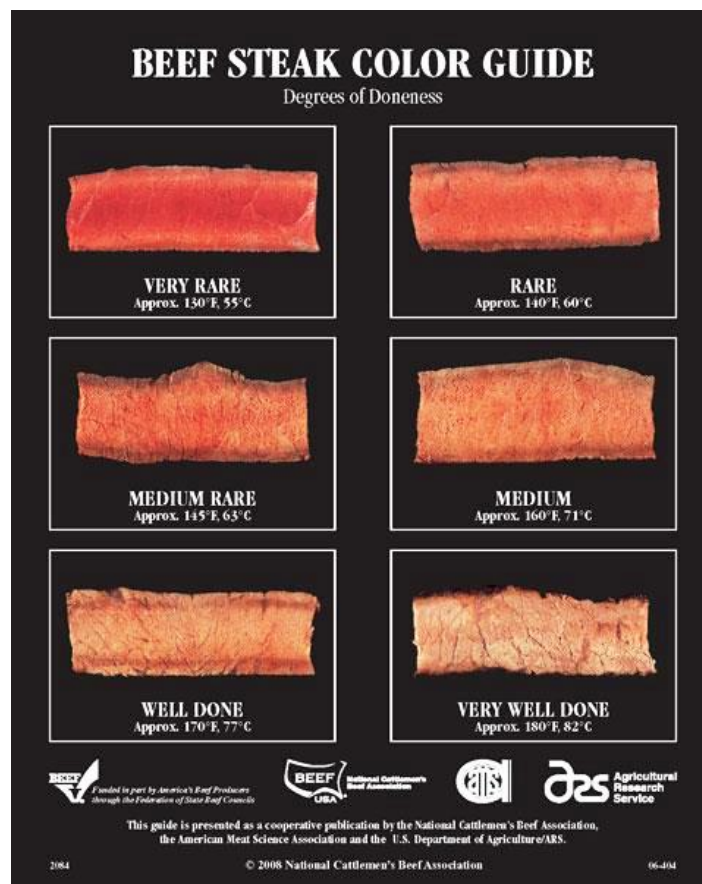


Figura A.3: Color de la carne de ternera para diferentes puntos de cocinado según la Beef Steak Color Guide descrita por la American Meat Science Association, AMSA (1995).

En cuanto al tratamiento térmico de alimentos en el ámbito industrial, en esta tesis nos hemos focalizado en los sistemas PEF, una tecnología de alto interés en el campo de la inactivación microbiana y calentamiento ohmico, y como se ha observado en otros estudios (Ariza-Gracia et al., 2020). El calentamiento producido con esta metodología en Agar en una cámara de electrodos paralela, provocó un gradiente de temperatura entre el punto más frío y el más caliente (alrededor de 10 °C), lo que provocó un grado de inactivación microbiana no uniforme. Como este hecho no es deseable, sería

interesante explorar diferentes formas de evitarlo, ya sea analizando los parámetros involucrados en el funcionamiento de estas camaras así como con nuevos diseños para éstas. En este estudio, la cámara PEF que se utiliza para el análisis experimental y numérico es una cámara de electrodos huecos y paralelos compuesta por dos cilindros de acero inoxidable de 20 mm de diámetro con un espacio entre ellos de 20 mm donde se coloca la muestra de agar, basándonos en el diseño de Saldaña et al. (2010). Esta cámara se muestran en la Figura A.4. Con este diseño, el aceite caliente se recicla dentro de los electrodos los cuales están vacíos en su interior, permitiendo de esta manera termostatar los electrodos logrando un precalentamiento de los mismos, lo que favorece temperaturas más altas en los puntos de la superficie del Agar en contacto con ellos, reduciendo así la diferencia de temperatura mencionada.



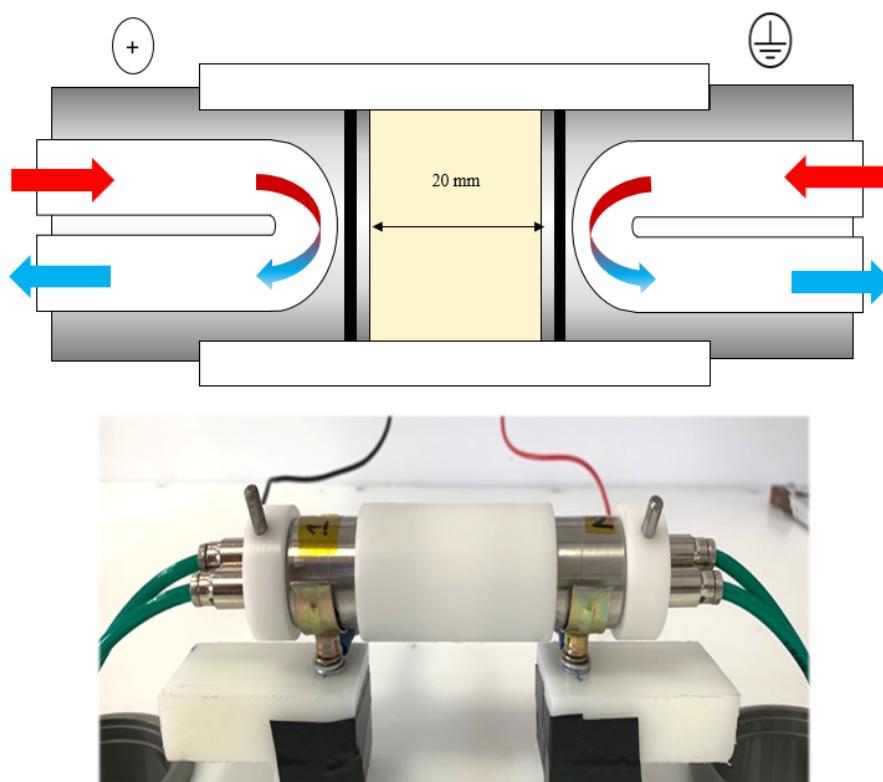Figura A.4: Cámara de tratamiento PEF con electrodos huecos y paralelos.

## A.3. Objetivos

El objetivo principal de esta Tesis es diseñar una metodología numérica que permita abordar los principales fenómenos físicos que se producen en los alimentos como consecuencia de la aplicación de tratamientos térmicos, bien a nivel doméstico como industrial. En el cocinado doméstico, la idea futura en el marco del proyecto ARQUE, es

poder aplicar esta metodología en el diseño de cocinas inteligentes que puedan ayudar al usuario durante el cocinado de los alimentos, de cara a mejorar la calidad de los productos cocinados. La aplicación a nivel industrial, es poder utilizar la simulación numérica para diseñar prototipos a nivel de planta piloto que optimicen los parámetros del proceso industrial, como el campo eléctrico, la frecuencia o los parámetros de termostatación, con el fin de alcanzar niveles adecuados de seguridad alimentaria en productos sólidos asegurando la inactivación de microorganismos en todo el producto, en este caso se ha seleccionado como producto sólido el agar.

Para simular numéricamente el proceso de cocinado de la carne, se debe resolver un problema multifísico acoplado de transferencia de calor, transferencia de masa y mecánica de sólidos. Con respecto al proceso PEF, se debe resolver un problema multifísico acoplado de transferencia de calor y campo eléctrico. Se ha utilizado el software comercial *COMSOL Multiphysics 5.2a* para simular ambos procesos.

Para alcanzar el objetivo principal de la Tesis, se han establecido los siguientes objetivos específicos que se han ido consiguiendo a lo largo del desarrollo de esta Tesis:

- Comprensión de los principales fenómenos físicos que aparecen en los alimentos cuando se aplica una fuente de calor y estudio de los diferentes modelos matemáticos propuestos en la literatura, tanto para simular el cocinado de la carne como para simular el calentamiento óhmico y la muerte de microorganismos en alimentos sólidos en los sistemas PEF.

- Implementación en el software de elementos finitos *COMSOL* de las diferentes ecuaciones que rigen ambos problemas, tales como las de transferencia de calor, transferencia de masa, mecánica sólida deformable y la fuente de calor, ya sea para el tratamiento de la carne como para la aplicación de PEF.

- Desarrollo de modelos numéricos que pueden ayudar al usuario a establecer los grados de cocinado deseados a través del color y la pérdida de peso del alimento.

- Desarrollo de modelos numéricos que puedan ayudar a explorar nuevas formas de mejorar la metodología PEF para lograr la muerte de microorganismos en alimentos sólidos sin alterar las propiedades del producto.

- Análisis de los resultados numéricos obtenidos y su validación por comparación con resultados experimentales. Para llevar a cabo la parte experimental de esta Tesis se ha colaborado estrechamente con dos grupos de la Universidad de Zaragoza: el grupo T07-24R de Alimentación de Origen Vegetal, dirigido por Marisa Salvador en el caso del cocinado de carne, y con el grupo A03 -17R de

Nuevas Tecnologías de Procesado de Alimentos, dirigido por Ignacio Álvarez en el caso de tratamientos PEF de alimentos sólidos.

- Obtención de soluciones orientadas a la cocina semi-guiada o semi-dirigida que, a partir de un mayor conocimiento del comportamiento de los alimentos, con la información obtenida del propio sistema así como de fuentes de información externas (sensores, sistemas con inteligencia artificial), permitan asegurar las propiedades de los alimentos cocinados y mejorar la eficiencia y seguridad.

- Incrementar la experiencia del usuario durante el cocinado, a través de la interactividad entre el asistema y el usuario (conectividad, inteligencia artificial).

## A.4. Contribuciones originales

En este apartado se incluyen los resultados de la tesis, es decir las contribuciones originales, que han sido publicadas en revistas incluidas en la base de datos Web of Science y difundidas en congresos.

### A.4.1. Publicaciones

Los siguientes artículos hacen referencia a trabajos publicados en revistas científicas internacionales, cuyo contenido está total o parcialmente recogido en esta tesis.

- J. Moya, S. Lorente-Bailo, M.L. Salvador, A. Ferrer-Mairal, M.A. Martínez, B. Calvo, J. Grasa. Development and validation of a computational model for steak double-sided pan cooking. *Journal of Food Engineering*, vol 298 (2021). doi: 10.1016/j.jfoodeng.2021.110498.

- J. Moya, S. Lorente-Bailo, A. Ferrer-Mairal, M.A. Martínez, B. Calvo, J. Grasa, M.L. Salvador. Color changes in beef meat during pan cooking: kinetics, modeling and application to predict turn over time. *European Food Research Technology*, vol 247, (2021). doi: 10.1007/s00217-021-03821-y

- J. Moya, L. Astráin-Redín, J. Grasa, G. Cebrián, B. Calvo and I. Álvarez. A numerical approach to analyze the performance of a PEF system in microbial inactivation of solid food. *Frontiers in Food Science and Technology*, (2022), doi: 10.3389/frfst.2022.880688.

Por último, se incluye el trabajo experimental que se ha desarrollado paralelamente al desarrollo de esta tesis, y que ha permitido obtener los parámetros del modelo

correspondiente al producto sólido tratado (agar) asi como verificar la capacidad de la simulación numérica para desarrollar un equipo industrial a nivel de planta piloto.

- L. Astráin-Redín, J. Moya, M. Alejandrez, E. Beitia, J. Raso, B. Calvo, G. Cebrián, I. Álvarez. Improving the microbial inactivation uniformity of pulsed electric field ohmic heating treatments of solid products. *LWT*, vol 154 (2021). doi: 10.1016/j.lwt.2021.112709.

### A.4.2.    Congresos

A cotinuación se detallan las ponencias en reuniones y congresos nacionales e internacionales.

- J. Moya, S. Lorente-Bailo, J.A. Bernard. Computational Simulation of Steak Pan Cooking. 11th biennial FOODSIM2020 Conference. University of Leuven – Ghent Campus, Ghent, Belgium from September 6-10, 2020.

- J. Moya, B. Calvo, J. Grasa. Hacia la ingeniería alimenticia asistida por ordenador. Aplicación al cocinado doméstico de carne y tratamientos térmicos mediante pulsos eléctricos. VII Jornada de Doctorandos del Programa de Doctorado en Ingenería mecánica. Zaragoza (Spain), 2020.

- J. Moya, B. Calvo, J. Grasa. Hacia la ingeniería alimenticia asistida por ordenador. Aplicación al cocinado doméstico de carne y tratamientos térmicos mediante pulsos eléctricos. IX Jornada Jóvenes Investigadores Instituto de Investigación en Ingeniería de Aragón. Zaragoza (Spain), 2020.

- J. Moya, L. Astrain, B. Calvo, I. Álvarez, J.A. Bernard. Optimization by Finite Element Analysis of the uniformity of the ohmic heating generated by the application of PEF in solid food. 7th School on PEF applications in food and biotechnology. Zaragoza (Spain), 2021.

## A.5.    Conclusiones

Esta sección incluye un breve resumen del trabajo desarrollado en esta Tesis. Se va a hacer una división según la línea de investigación.

## A.5.1. Simulación del tratamiento mediante PEF como sistema de inactivación microbiana en alimentos sólidos

Respecto al estudio del tratamiento mediante PEF, se ha desarrollado un modelo de elementos finitos aximétrico capaz de reproducir el calentamiento óhmico que sufren las piezas cilíndricas de agar en una cámara de tratamiento PEF. Este modelo puede incorporar la termostatización de los electrodos de la cámara, aspecto que también ha sido verificado experimentalmente. Se ha realizado un análisis de sensibilidad de los principales parámetros de funcionamiento de estas cámaras, explorando todas las combinaciones posibles para encontrar la óptima para conseguir un calentamiento uniforme, homogéneo y eficiente. En este estudio también se ha implementado la inactivación de la Salmonella Typhimitium 878. Esta inactivación depende de la temperatura que alcanza la muestra de alimento y de los tiempos de aplicación. Esto también supone una novedad con respecto a otras investigaciones en el campo. Las principales conclusiones obtenidas en esta línea de investigación se enumeran a continuación:

- El modelo axisimétrico desarrollado reproduce adecuadamente los resultados experimentales del prototipo de cámara PEF utilizado para este estudio. Por lo tanto, podemos afirmar que los supuestos realizados con respecto a las condiciones de contorno del modelo y la física involucrada son correctos.

- Se verificó que solo aplicando pulsos PEF en la cámara de tratamiento, aparecieron áreas más frías cerca de los electrodos que inicialmente estaban a temperatura ambiente. Se propuso termostatar previamente los electrodos para que su temperatura inicial fuera mayor, para así mejorar la homogeneidad de la temperatura final de la muestra de agar. La homogeneidad en la temperatura del producto asegura la efectividad de inactivación de microorganismos, evitando zonas sobrecalentadas que pueden afectar a la calidad del mismo.

- Se realizó un estudio de sensibilidad sobre los principales parámetros de funcionamiento de la cámara, incluyendo los parámetros de termostización de los electrodos. Primero, mediante un análisis de 4 variables, se detectó que cuanto mayor es el tiempo de la termostatización previa de los electrodos, mejor es la uniformidad de temperatura en la muestra de agar. Esto se debe a que se logra una temperatura final estable en el electrodo. Posteriormente, se encontró que se alcanzaba una temperatura uniforme en los electrodos después de 30 minutos de termostatización.

- Al fijar el tiempo de termostatización en 30 minutos, se realizó otro análisis de sensibilidad, que concluyó que una mayor temperatura de termostatización de los electrodos conllevaba menores diferencias en la homogeneidad de temperatura de la muestra de agar. Cuanto mayor sea esta temperatura, mejor para esta homogeneidad. Este análisis de sensibilidad también proporcionó información sobre el voltaje de los pulsos y la frecuencia: cuanto mayor es el voltaje y la frecuencia, mayor es la homogeneidad de la temperatura en la muestra. Sin embargo, los parámetros de termostatización son más relevantes en este aspecto. La frecuencia y el voltaje más altos requieren principalmente tiempos de aplicación de PEF más cortos. Sería necesario un compromiso entre el requisito energético y la homogeneidad de la temperatura.

- Una vez determinada la combinación más óptima de los parámetros evaluados, se implementó la inactivación de Salmonella Typhimitium 878 en el modelo, constatándose que una mayor homogeneidad en la temperatura de la muestra implicaba también una mayor homogeneidad en la inactivación. Posteriormente, se verificó numéricamente que, dado que el agar continua calentándose por inercia tiempo después de la aplicación de los pulsos PEF, se puede obtener una inactivación mayor. Esta es una gran ventaja para evitar el sobrecalentamiento de la parte central de la muestra asegurando que se alcanza la inactivación necesaria también en las zonas más alejadas.

## A.5.2.   Simulación del cocinado a la plancha de carne de ternera

A lo largo de esta Tesis se han considerado varios aspectos de la simulación del cocinado a la plancha de carne de ternera. Respecto a la simulación del cocinado de carne, la mayoría de los trabajos en la literatura se habían centrado en el cocinado mediante horno o mediante frituras. Hay pocos estudios sobre el cocinado en sartén y por lo general consideran simplificaciones tanto para la geometría como para el comportamiento del material. Aunque estos enfoques han sido muy útiles como base para nuestra investigación, algunos aspectos como el hecho de darle la vuelta a a la carne, el contacto térmico entre la sartén y el filete, la retracción y la evolución de color a lo largo del cocinado no se han implementado en esos modelos. Por ello, este trabajo supone una novedad en este sentido. Uno de los objetivos de este estudio es describir la evolución del color de la carne al ser uno de los parámetros de referencia para el usuario a la hora de establecer el punto de cocción. Además, en este modelo se ajustó la temperatura adquirida por la carne en diferentes tiempos y para diferentes espesores de

filetes, teniendo en cuenta los resultados experimentales, así como su pérdida de peso. A continuación se enumeran las principales conclusiones extraídas de este trabajo:

- El modelo 3D de elementos finitos desarrollado en este trabajo es capaz de reproducir el cocinado de carne de ternera en sartén para diferentes espesores y para diferentes tiempos de cocinado o grados de cocción. La comparación de la temperatura y la pérdida de peso con los resultados experimentales nos ha permitido aceptar como correctos os fenómenos e hipótesis introducidas en el problema, así como las condiciones y parámetros del modelo.

- Con este modelo hemos podido concluir que pequeñas desviaciones en el grosor de la carne pueden provocar cambios apreciables en la temperatura de los filetes de ternera, por lo que el tamaño de los trozos de carne es importante a la hora de predecir el proceso de cocinado.

- Se ha demostrado que la pérdida de peso en la carne de ternera es lineal con el tiempo, pero esto puede ser distinto para otros tipos de carne. Por ello sería interesante aplicar este modelo a otras carnes de otras caracteristicas. Se tendría que realizar un estudio de la capacidad de retención de agua de la nueva carne utilizada, así como obtener nuevamente los parámetros del modelo involucrados en el fenómeno de la pérdida de peso.

- La evolución del color de la carne se ha implementado en este modelo en función de las coordenadas CIELab, $a^*$ y $L^*$. Estas dependen especialmente de la temperatura, por lo que el buen ajuste previo del modelo supuso también un buen ajuste de la evolución de estos dos parámetros.

- En este estudio se ha demostrado que la luminosidad, $L^*$, es la coordenada que más afecta al cambio de color absoluto de la carne, por lo que concluimos que los cambios estructurales que modifican la dispersión de la luz durante el cocinado de la carne son muy importantes y no se pueden ignorar. Además se comprobó que la coordenada $b^*$ no cambiaba.

- Este estudio también ha demostrado que el estado de conservación de la carne (fresco, refrigerado y congelado), no influyó lo suficiente en la evolución del color de la carne durante el cocinado de ésta para ser apreciado visualmente.

- Una de las aplicaciones de este estudio ha sido determinar cuándo era necesario dar la vuelta a la carne para lograr un perfil de color simétrico en todo el grosor de la carne. El momento ideal para dar la vuelta a la carne varía en función de los diferentes grados de cocinado propuestos, pero se puede decir que el momento

óptimo es dos tercios del tiempo de cocinado final.

- Se han obtenido los principales parámetros que afectan en el cocinado de la carne mediante plancha. Básicamente, éstos podrían reducirse a la capacidad de retención de agua de la carne y el espesor del filete.

## A.6.  Líneas futuras

El trabajo presentado en esta Tesis constituye los primeros, aunque firmes, pasos hacia la ingeniería alimentaria asistida por ordenador, abordados por el grupo AMB de la Universidad de Zaragoza. Por ello, existen bastante líneas de investigación abiertas para poder ampliar y mejorar los modelos numéricos desarrollados, tanto para la cocina doméstica como para su aplicación industrial.

En cuanto a la simulación del cocinado de carne de ternera en sartén, este trabajo ha supuesto el primer paso en la búsqueda de un sistema de cocinado guiado. El objetivo final sería obtener modelos para otro tipo de carnes, y posteriormente para otros alimentos. Una vez validados los modelos, éstos podría ser utilizados para generar una amplia base de datos correspondiente a cocinados de múltiples usuarios, para posteriormente crear una herramienta de inteligencia artificial capaz de proporcionar en tiempo real los resultados durante la cocción para orientar al usuario. En cuanto a la simulación del tratamiento de calentamiento óhmico mediante PEF, se ha visto que puede ser una herramienta importante para optimizar estos procesos dirigidos a la inactivación de bacterias en los alimentos. Por ello, podría emplearse para evaluar la inactivación de otras bacterias, en otro tipo de alimentos, o para otros tipos de cámaras PEF con otras condiciones de funcionamiento. Además, la posibilidad de aplicar tratamientos PEF a la carne en un entorno industrial podría ser estudiada para cumplir con los objetivos de seguridad alimentaria, o más allá aún, se podría realizar un estudio sobre la viabilidad de llevar este tipo de tratamientos PEF a las cocinas domésticas.

Algunas de las posibles líneas futuras se resumen a continuación:

- La adaptación del modelo de simulado del cocinado de carne a otros tipos de carne o geometrías, como la de las hamburguesas. Están hechas de carne picada y su comportamiento puede ser diferente cuando se cocina, por lo que su volumen y forma cambian con respecto al de los filetes de ternera. Actualmete estamos analizando si los parámetros y condiciones aplicadas en el estudio de los filetes de ternera, son extrapolables a este nuevo producto.

- Generalizar el estudio de carne de ternera a otros tipos de cocinado, como el cocinado en horno. Las condiciones de contorno son diferentes en este tipo de cocinado ya que la transferencia de calor se produce por convección en lugar de conducción. Los primeros resultados ya han sido obtenidos, verificando la robustez del modelo.

- Estudiar la capacidad de este modelo para reproducir el cocinado de otros tipos de carne, e indetificar los parámetros del modelos claves a modicar.

- Sería interesante incorporar la anisotropía de la carne, asociada a la orientación de las fibras muscukares, durante el proceso de encogimiento de las proteínas. El modelo podría predecir de una manera más realista la configuración deformada del producto con el incremento de temperatura, que a su vez afecta la transferencia de calor entre la sartén y la comida.

- Una limitación de los modelos numéricos es que los resultados no se optienen en tiempo real, por lo que para que estas simulaciones sean de utilidad al usuario durante el cocinado es necesario combinarlas con otras herramientas. Por ejemplo, se pueden utilizar para crear bases de datos sintéticas, que alimenten una herramienta de inteligencia artificial, como las redes neuronales, capaz de predecir el comportamiento de la carne cuando se cocina en un entorno doméstico en tiepo real.

- Estudiar la inactivación de otros microorganismos mediante la aplicación de calentamiento óhmico mediante sistemas PEF. Por ejemplo, el próximo estudio será la inactivación de anisakis en el pescado.

- Profundizar en la optimización de las cámaras PEF, teniendo en cuenta también la eficiencia energética y no solo la inactivación conseguida.

- Analizar la viabilidad de aplicar tratamientos PEF en la carne, tanto a nivel industrial como a nivel doméstico, como técnica de calentamiento complementaria con el cocinado tipo plancha.

# Annex B

# Original contributions

The original contributions carried out during the period of this Thesis as well as the financial support are detailed in this section.

## B.1.   Financial support

## B.2.   Publications

The following publications directly related to the topics of this work are shown below:

- J. Moya, S. Lorente-Bailo, M.L. Salvador, A. Ferrer-Mairal, M.A. Martínez, B. Calvo, J. Grasa. Development and validation of a computational model for steak

double-sided pan cooking. *Journal of Food Engineering*, vol 298 (2021). doi: 10.1016/j.jfoodeng.2021.110498.

- J. Moya, S. Lorente-Bailo, A. Ferrer-Mairal, M.A. Martínez, B. Calvo, J. Grasa, M.L. Salvador. Color changes in beef meat during pan cooking: kinetics, modeling and application to predict turn over time. *European Food Research Technology*, vol 247, (2021). doi: 10.1007/s00217-021-03821-y.

- J. Moya, L., Astráin-Redín, J. Grasa, G. Cebrián, B. Calvo, I. Álvarez. A numerical approach to analyze the performance of a PEF system in microbial inactivation of solid food. *Frontiers in Food Science and Technology*. (2022). doi: 10.3389/frfst.2022.880688.

On the other hand, another additional publication that has been made in parallel to the development of this Thesis is also detailed. Its preparation has definitely contributed to improving its content.

- L. Astráin-Redín, J. Moya, M. Alejandrez, E. Beitia, J. Raso, B. Calvo, G. Cebrián, I. Álvarez. Improving the microbial inactivation uniformity of pulsed electric field ohmic heating treatments of solid products. *LWT*, vol 154 (2021). doi: 10.1016/j.lwt.2021.112709.

## B.3. Conferences

The presentations at national and international meetings and congresses related to the field of study of this Thesis are shown below:

- J. Moya, S. Lorente-Bailo, J.A. Bernard. Computational Simulation of Steak Pan Cooking. 11th biennial FOODSIM2020 Conference. University of Leuven – Ghent Campus, Ghent, Belgium from September 6-10, 2020.

- J. Moya, B. Calvo, J. Grasa. Hacia la ingeniería alimenticia asistida por ordenador. Aplicación al cocinado doméstico de carne y tratamientos térmicos mediante pulsos eléctricos. VII Jornada de Doctorandos del Programa de Doctorado en Ingenería mecánica. Zaragoza (Spain), 2020.

- J. Moya, B. Calvo, J. Grasa. Hacia la ingeniería alimenticia asistida por ordenador. Aplicación al cocinado doméstico de carne y tratamientos térmicos mediante pulsos eléctricos. IX Jornada Jóvenes Investigadores Instituto de Investigación en Ingeniería de Aragón. Zaragoza (Spain), 2020.

- J. Moya, L. Astrain, B. Calvo, I. Álvarez, J.A. Bernard. Optimization by Finite Element Analysis of the uniformity of the ohmic heating generated by the application of PEF in solid food. 7th School on PEF applications in food and biotechnology. Zaragoza (Spain), 2021.

## B.4.  Research stay

During the development of this Thesis, a research stay of three months has been carried out in BSH Home Appliances Group.

# Annex C

# Publications

# Development and validation of a computational model for steak double-sided pan cooking

J. Moya [a], S. Lorente-Bailo [b], M.L. Salvador [b], A. Ferrer-Mairal [b], M.A. Martínez [a,c], B. Calvo [a,c], J. Grasa [a,c,*]

[a] *Aragón Institute of Engineering Research (i3A), Universidad de Zaragoza, Spain*
[b] *Plant Foods Research Group, Instituto Agroalimentario de Aragon IA2, Universidad de Zaragoza-CITA, Miguel Servet 177, 50013, Zaragoza, Spain*
[c] *Centro de Investigación Biomédica en Red en Bioingeniería, Biomateriales y Nanomedicina (CIBER-BBN), Spain*

## ARTICLE INFO

## ABSTRACT

The objective of this study was to develop and validate a numerical model to adequately simulate the double-sided pan cooking of beef in a domestic environment. The proposed model takes into account the heat flow from the pan to the meat and the moisture transfer, simultaneously with the meat deformation. The model considers the swelling pressure gradient caused by the shrinkage of the meat fibers and connective tissue due to the denaturation of proteins and the loss of the water holding capacity during cooking. The model results were successfully verified with experimental data of the central temperature and weight loss recorded during cooking for three degrees of doneness. The measured experimental temperatures at the center of the meat were $30 \pm 3$ °C (very rare), $44 \pm 3$ °C (rare) and $57 \pm 2$ °C (done) for a 19 mm steak thickness. Meanwhile, their water losses were $4 \pm 2$ %, $8 \pm 1$ % and $11 \pm 2$ %, respectively. The root mean squared errors of the model predictions were 2.16 °C (very rare), 3.56 °C (rare) and 4.57 °C (done) for the central temperature and 1.48 %, 2.08 % and 2.40 %, respectively for the water loss. The model also correctly predicts cooking times for steaks of different thicknesses, taking weight loss as a reference to set this time. The proposed model is postulated as a useful cooking assistance tool to estimate the optimal cooking time according to consumer preferences.

## 1. Introduction

There is increasing interest in developing accurate numerical models of meat cooking processes with the aim of achieving a high degree of knowledge and control of the complex heat and mass transfer phenomena involved. Knowledge of meat behavior during cooking is very important for optimizing and controlling the final quality of the product. The physical phenomena that underlie the meat cooking process can basically be considered by the coupling of heat and moisture transfer in a deforming porous medium (Datta, 2007). The state of the art models differ in their degrees of approximation and therefore in their complexity. Some exclusively consider conductive heat transfer and the diffusive transport of matter. Other models incorporate the convective heat transport by the liquid moisture flow and also describe the moisture transport by the Flory-Rehner theory (van der Sman, 2015; Feyissa et al., 2013; Ahmad et al., 2015; Nelson et al., 2020). However, little information has been provided on meat deformation during cooking as a solid mechanics problem, with some exceptions such as the research

conducted by Dhall and Datta (2011), Feyissa et al. (2013) and Blikra et al. (2019). When meat is heated, water migrates through the surface either in the form of liquid or in the form of vapor whilst the temperature and water content inside the meat vary in space and time at the same time that the meat volume changes. During cooking, meat proteins denature and cause structural changes, such as the shrinkage of muscle fibers and connective tissue, and the formation of larger pores in parts closer to the surface, being smaller in parts closer to the center (Feyissa et al., 2013). These changes in porosity lead to an increase in water permeability in the outer parts of the meat and consequently in the water transport. Not considering this shrinkage could lead to errors in the estimation of the weight loss of the meat (Datta, 2016). These structural changes also decrease the water holding capacity of the meat. The mechanical force exerted by the contracting protein network on the interstitial fluid, denoted swelling pressure, leads to the expulsion of the moisture from the meat (Tornberg, 2005). In water loss, swelling pressure is a more important mechanism than surface evaporation, accounting for up to 80% of the water losses during double-sided pan

---

**ORIGINAL PAPER**

# Color changes in beef meat during pan cooking: kinetics, modeling and application to predict turn over time

Jara Moya[1] · Silvia Lorente-Bailo[2] · Ana Ferrer-Mairal[2] · Miguel A. Martínez[1,3] · Begoña Calvo[1,3] · Jorge Grasa[1,3] · María L. Salvador[2]

## Abstract

The kinetics of heat-induced color changes in beef meat was determined and implemented in a numerical model for double-sided pan cooking of steak. The CIELab color space was used to obtain the lightness (coordinate $L^*$) and the reddish tone (coordinate $a^*$) of the cooked meat. $L^*$ was the CIELab coordinate that contributed the most to the change in the absolute color. Two response surfaces were found to describe the evolution with time and temperature of both color coordinates, $L^*$ and $a^*$. The model results were successfully verified with experimental data of the two coordinates along the thickness of the meat for three degrees of cooking. The Root-Mean-Squared Errors (RMSE) for coordinate $L^*$ were 5.17 (very rare), 2.02 (medium rare) and 3.83 (done), and for coordinate $a^*$ 1.44 (very rare), 1.26 (medium rare) and 0.89 (done). The applicability of the model for practical cooking purposes was illustrated by determining the optimum turn over time to achieve a similar color profile on both sides of the meat. The turn over time depended on the desired degrees of cooking, and were comprised between one-half and two-thirds of the final cooking time, increasing from very rare cooking degree to done cooking degree.

## Introduction

The color of beef as a parameter to establish the final time of cooking is highly questioned, since color depends on many factors. For example, high pH, modified atmosphere packaging, rapid thawing and low fat content can prolong the characteristic redness of raw meat; in contrast, brownish hues may appear prematurely in meat which has been frozen in bulk, thawed for a long time or packed in oxygen-rich packaging [1, 2]. To guarantee microbiological safety, the cooking times for meat should be based on temperature. The United States Department of Agriculture, USDA, recommends a temperature of at least 62.8 °C for steaks and a rest time of three minutes before eating. However, preferences from the point of view of consumer sensory perception may not coincide with safe temperatures [3]. In a domestic environment, meat color is still used to define the degree of doneness. Thermometers are usually employed when the meat is baked, but not when cooking by contact with a hot surface [4, 5]. In this type of cooking, it is not easy to accurately measure the temperature in the center of the meat. A deviation of ± 1 mm in the temperature sensor position can cause temperature changes of 3°–5 °C [6, 7]. For practical domestic cooking purposes, it would be very interesting to know the evolution of color inside the meat. This information, as a complement to the temperature data, would allow a better approximation to the degree of doneness desired by the consumer. The relationship between cooking time, temperature and color of the meat depends on many factors such as the pH [8, 9], the source of the meat [10], the water holding capacity [11], the packaging conditions [2] or the cooking method [12]. Those factors influencing the internal color of cooked meats have been recently reviewed by [13]. Despite the difficulties posed by these factors, color changes caused by heating can be quantified by chemical reaction

✉ Jara Moya
jaram@unizar.es

1 Aragón Institute of Engineering Research (i3A), Universidad de Zaragoza, Zaragoza, Spain

2 Plant Foods Research Group, Instituto Agroalimentario de Aragon IA2, Universidad de Zaragoza-CITA, Miguel Servet 177, 50013 Zaragoza, Spain

3 Centro de Investigación Biomédica en Red en Bioingeniería, Biomateriales y Nanomedicina (CIBER-BBN), Zaragoza, Spain

# A Numerical Approach to Analyze the Performance of a PEF-Ohmic Heating System in Microbial Inactivation of Solid Food

J. Moya[1], L. Astráin-Redín[2], J. Grasa[1,3], G. Cebrián[2], B. Calvo[1,3] and I. Álvarez[2]*

[1]Instituto de Investigación en Ingeniería de Aragón (I3A), Universidad de Zaragoza, Zaragoza, Spain, [2]Departamento de Producción Animal y Ciencia de los Alimentos, Tecnología de los Alimentos, Facultad de Veterinaria, Instituto Agroalimentario de Aragón (IA2), Universidad de Zaragoza, Zaragoza, Spain, [3]Centro de Investigación Biomédica en Red en Bioingeniería, Biomateriales y Nanomedicina (CIBER-BBN), Zaragoza, Spain

Pulsed Electric Fields (PEF) technology has been recently proposed as a new ohmic-heating system for the heat treatment of solid products in short periods (less than 1 min). However, similar to traditional ohmic heating, non-homogeneous distribution of temperature has been observed and cold points appeared in the interphase between the solid treated product and the electrodes, which can limit the technology for assuring food safety for treated solid products. In this investigation, a computational axisymmetric model of a lab-scale PEF system for a solid product (agar cylinder) was developed. This model was used to predict the temperature and the electric field distribution, treatment time, and the microbial inactivation (*Salmonella* Typhimurium 878) in the solid product after a PEF-ohmic treatment. Using a factorial analysis, a total of 8 process conditions with different settings of applied field strength levels (2.5–3.75 kV/cm), frequencies (100–200 Hz), and initial agar and electrode temperature (40–50°C) were simulated for the agar cylinder in order to identify the effect and optimal values of these parameters, which offer the most temperature homogeneity. The results showed that the initial temperature of the agar and the electrodes was of great importance in achieving the best temperature uniformity, limiting the occurrence of cold points, and therefore, improving the homogeneity in the level of inactivation of *Salmonella* Typhimurium 878 all over the agar cylinder. A treatment of 2.3 s would be enough at 3.75 kV/cm, 200 Hz with an initial temperature of 50°C of the agar and the electrodes, for a 5-Log$_{10}$ reduction of *Salmonella* Typhimurium 878 in the whole product with a deviation of 9°C between the coldest and hottest point of the solid.

Keywords: microbial inactivation, ohmic heating, *Salmonella*, numerical simulation, pulsed electric fields

## INTRODUCTION

Numerical simulation is a useful and complementary method for solving physical processes described by differential equations. It is a helpful tool for evaluating scenarios that sometimes are difficult or impossible to carry out experimentally (Wölken et al., 2017), such as the evaluation of microbial inactivation by thermal treatment in a solid food product, as in the pasteurization process. In this case, all parts of the product have to be treated with at least the minimum process criteria (a

# Improving the microbial inactivation uniformity of pulsed electric field ohmic heating treatments of solid products

L. Astráin-Redín [a], J. Moya [b,c], M. Alejandre [a], E. Beitia [a], J. Raso [a], B. Calvo [b,c], G. Cebrián [a], I. Álvarez [a,*]

[a] Departamento de Producción Animal y Ciencia de los Alimentos, Tecnología de los Alimentos, Facultad de Veterinaria, Instituto Agroalimentario de Aragón (IA2), Universidad de Zaragoza, Zaragoza, Spain
[b] Aragón Institute for Engineering Research (I3A), University of Zaragoza, Zaragoza, Spain
[c] Centro de Investigación Biomédica en Red en Bioingeniería, Biomateriales y Nanomedicina (CIBER-BBN), Spain

## ABSTRACT

The application of Pulsed Electric Fields (PEF) at high frequencies leads to rapid and volumetric ohmic heating. Its application in solid foods could avoid the problem of conventional systems in which the external areas are over-treated in order to apply the desired heat treatment in the center. In this study it was evaluated the heating of technical agar cylinders by applying PEF (2.5 kV/cm, 50 Hz) by warming the electrodes to 25, 32 and 39 °C. Results showed that PEF heating without control of the electrode temperature showed temperature differences of 10.5 °C after 50 s. However, regulation of the electrodes at 39 °C reduced the gradient to 1.7 °C achieving 73.4 °C at the coldest point after 28 s. To evaluate the impact of the electrode temperature regulation on the uniformity of microbial inactivation, the inactivation of *Listeria monocytogenes* STCC 5672 ($D_{60°C} = 0.63$ min, $z$-value = 5.4 °C) was evaluated. Results showed that to inactivate 5-$Log_{10}$ at the coldest spot of the cylinder, 68 s were necessary when electrode temperatures were not regulated, and 26 s when they were tempered to 39 °C, reaching a temperature of 71 °C.

## 1. Introduction

Consumer demand for long-life products that maintain the organoleptic and nutritional characteristics of fresh foods has been increasing. Therefore, ever since the late 20th century, research has been carried out on non-thermal processing technologies that achieve the inactivation of microorganisms with only a minimal increase of food temperature, thereby preserving heat-sensitive food compounds (Smith, 2011). Pulsed Electric Fields (PEF) belong to this group of novel technologies. The process consists in the application of electric fields of high intensity (>0.1 kV/cm) and short duration (from milliseconds to microseconds) to a product placed between two electrodes (Barbosa-Cánovas et al., 2001). The application of PEF causes the permeabilization of cell membranes, a phenomenon called electroporation. This technology has been widely investigated for the pasteurization of liquid foods, mainly juices, as well as for improving the extraction of intracellular compounds such as betalanin from red beets, polyphenols from grape skins, and carotenoids from microalgae, among others (Buckow et al., 2013; Wang et al., 2018; Álvarez & Raso, 2017).

However, although PEF is considered a non-thermal technology, the flow of electric current through a material causes it to heat due to the Joule effect described with the following equation:

$$W = \int_0^{\omega} \sigma E^2 dt \tag{1}$$

where $\sigma$ is the electrical conductivity of the treated medium or product (S/m), $E$ is the electric field strength (V/m); and $dt$ is the time (s) during which the field strength is applied (Sastry & Li, 1996). PEF causes ohmic heating, since solid as well as liquid foodstuffs behave as an electrical resistance that is internally heated (Imai et al., 1995; Sastry & Barach, 2000). This type of heating from the inside of the product to the outside is known as volumetric heating (Sastry & Li, 1996). It allows not only for the food to be heated, but also for the heating to spread more homogeneously and rapidly (from minutes to seconds), similarly to other systems such as microwaves and radiowaves, but with a greater penetration capacity (Sastry, 2005; Sastry et al., 2014). This aspect of ohmic